Particulate Trace Metals & Iron Availability to Phytoplankton in a Changing Arctic Ocean

by

Jingxuan Li

B.Sc., Xiamen University, 2010

A DISSERTATION SUBMITTED IN PARTIAL FULFILLMENT OF

The REQUIREMENTS FOR THE DEGREE OF

MASTER OF SCIENCE

in

THE FACULTY OF GRADUATE AND POSTDOCTORAL STUDIES

(Oceanography)

THE UNIVERSITY OF BRITISH COLUMBIA

(Vancouver)

June 2017

Abstract

This thesis, focusing on the Canadian Arctic Ocean, investigates the cycling of particulate trace metals, and the bioavailability of iron to phytoplankton in this rapidly changing ocean. Full depth profiles of particulate Al, Cd, Pb, P, V, Mn, Fe, Co, Cu, Zn and Ba were determined. Trace elements displayed various vertical distributions. Firstly, some elements had a strong lithogenic component (Al, Fe and V), and were characterized by a maximum at the surface. Indeed, their concentrations strongly correlated with each other across basins. Secondly, elements with a significant biogenic component (Cd and Cu) were characterized by a decrease in concentration with depth. Furthermore, preferential remineralization of P over Cd at shallow depths in numerous stations is reported. In some stations across basins, the molar ratio of particulate Cu and P approached a plateau at the meso- or bathy-pelagic zone, suggesting the presence of ammonium oxidizing archaea, which require Cu-dependent enzymes. Thirdly, Mn, a trace metal with a predominant redox cycle, showed a spike in concentration between 100-200 m, as well as a bottom enrichment. In the Canada Basin, we suggest interactions between the production of manganese oxide, cobalt oxide and barite by manganese oxidizing bacteria.

The Arctic Ocean is experiencing the greatest decrease in seawater pH, as well as rapid ice melting which elevates light intensity in surface waters. To examine changes in Fe bioavailability to Arctic phytoplankton under a varying environment, two incubation experiments were conducted. After natural phytoplankton assemblages were acclimated to different light/CO_2 treatments for one week, short-term Fe uptake assays were performed to assess the capability of phytoplankton to access Fe. Generally, Fe uptake capability was positively influenced by CO_2 level, and negatively impacted by light level in the incubations. These observations imply that high CO_2 has a significant negative effect on Fe bioavailability, while high light has a positive effect. Furthermore, when comparing future scenario (higher atmospheric CO_2 and underwater irradiance) with present-day conditions, the bioavailability of Fe to phytoplankton appeared to be similar.

Lay Summary

Marine phytoplankton account for about half of the Earth's primary productivity (CO_2 consumption and O_2 production), exerting a critical influence on global climate. Trace metals (Fe, Cu, Co, Zn, etc.) play an important role in the growth and production of marine phytoplankton, either as limiting resources or toxins. Particles exert a significant impact on the distributions of dissolved trace metals, the latter are normally the available species to phytoplankton. This study investigates the distribution of particulate trace elements in the changing Canadian Arctic Ocean, which is subject to temperature rise, ice melting and ocean acidification. The present study aims to reveal how trace metals interact with phytoplankton, how climate change affects their bioavailability to phytoplankton, and how phytoplankton cope with these changes.

Preface

The data in Chapter 2 were collected during the 2015 Canadian GEOTRACES Arctic Expedition (Leg 2 and Leg 3b). I was responsible for trace metal sampling and filtration on board, digestion and measurement back in the lab, under the training of Maite Maldonado, David Semeniuk and Nari Sim. David Semeniuk, Nina Schuback, Clara Hoppe and Richard Nixon performed the POC filtrations. Maureen Soon trained me on POC measurements. All collaborators in the expedition provided background knowledge on the Canadian Arctic Ocean. Jay Cullen's group shared dissolved metal data, which significantly improve the interpretation of my data in this Chapter. Roberta Hamme's group shared N* data, and Manuel Colombo provided the insights on anthropogenic Cu enrichment from Arctic rivers. Lindsay Fenwick shared N_2O data, Jean-Eric Tremblay's group provided nutrients data, and Markus Kienast's group shared $\delta^{15}NO_3^-$ data. I analyzed the data and wrote this chapter. Roger Francois provided important comments and ideas. Maite Maldonado provided helpful discussions and also edited the chapter.

Chapter 3 describes an *in situ* experiment conducted during Leg 2. Maite Maldonado and David Semeniuk designed the experiments. David Semeniuk performed the experiment on board, in collaboration with Clara Hoppe, Nina Schuback and Philippe Tortell. Jay Cullen's group analyzed the dissolved Fe samples from the incubation experiments. I have been responsible for sample processing back in the lab, data analysis and interpretation. David Semeniuk and Maite Maldonado provided valuable discussion in the writing process. Maite Maldonado also edited the chapter.

Table of Contents

Abstract----ii
Lay Summary----iii
Preface----iv
Table of Contents----v
List of Tables----vi
List of Figures----viii
Glossary and Abbreviations----xi
Acknowledgement----xii
Chapter 1: Introduction----1
1.1 Phytoplankton and metal limitation----1
1.2 Particulate trace metal----2
1.3 Fe bioavailability to phytoplankton under climate change----2
1.4 Phytoplankton physiological response to low Fe concentrations----3
1.5 Objectives----4
Chapter 2: Particulate Trace Metals in the Canadian Arctic Ocean----5
2.1 Introduction----5
2.2 Material and methods----7
2.2.1 Particulate trace metal sampling----8
2.2.2 Analytical technique----9
2.2.3 POC sampling and analysis----10
2.3 Results and discussion----11
2.3.1 Particulate organic matter: barren Canada Basin and N-fixation in Labrador Sea----11
2.3.2 At a glance: spatial distributions and principal component analysis----16
2.3.3 Vertical distributions of pTM----21
2.3.4 Canada Basin: connections among pBa, pMn, pCo and pCu----34
2.3.5 Canadian Arctic Archipelago: pTM behaviors under strong lithogenic input----38
2.4 Summary----42
Chapter 3: Physiological Response on Iron Uptake by Subarctic and Arctic Phytoplankton Assemblages under Ocean Acidification and High Irradiance----44
3.1 Introduction----44
3.2 Materials and methods----46
3.2.1 Experimental setup----46
3.2.2 Short-term Fe uptake assays----46
3.2.3 Calculations and statistics----47
3.3 Results----49
3.3.1 Phytoplankton community Chl *a* and composition during incubations----50
3.3.2 Fe uptake rate constants in short-term assays----50
3.3.3 An index of Fe uptake physiology for comparison among treatments----53
3.4 Discussion----56
3.4.1 What was the substrate for uptake during short-term Fe uptake assays?----56
3.4.2 CO_2 and light effects on phytoplankton Fe uptake capability----57
3.4.3 Present-day vs. future Arctic waters----59
3.5 Summary----61
Chapter 4: Conclusion----63
4.1 Significance and major findings----63
4.2 Caveats and limitations----64
4.3 Future outlook----65
Bibliography----67
Appendices (Supplementary tables)----80

List of Tables

Table 2.1: CRM BCR-414 (n=4) was digested and measured prior to sample processing. The recovery for each element are listed, accompanied by RSD of certification. C: certified value; I: indicative value of BCR-414; GR: consensus provided by Database on geochemical, environmental and biological reference materials. NA denotes not applicable. Sample measurements were accomplished in four days (D1-D4). Detection limits were determined by 8 to 11 runs of 1% HNO_3 per measurement day. The standard deviation (ppt) was derived from these runs, and detection limit (DL, ppt) equals three times the standard deviation. For each sample, the relative standard deviation (RSD, %) of various elements was calculated. The median RSDs per measurement day are reported for each element. ----------10

Table 2.2: Ratios between PON and pP in surface Canadian Arctic Ocean, average, standard deviation and median are reported, n denotes sample number. ----------15

Table 2.3: Principal component analysis (PC) loading of particulate elements and biological parameters. The percentage in bracket is the explained contribution of principal components to the total variance. pP, POC, PON and AOU constitute a firmly related group (bolded in PC1), while another group is composed of Al, Fe and V (bolded in PC2). Cu and Zn are associated within PC3 (bolded), which accounts for 10% of total variance. ----------17

Table 2.4: A compilation of metal:Al molar ratios in crustal materials. Taylor and McLennan (1995) and Wedepohl (1995) reported composition of the upper continental crust; Taylor (1964) introduced average composition of continental crust; while Shaw et al. (1976) reported continental surface Precambrian shield composition in Canada. Given the location, the values in the latter study are used for the lithogenic correction in our study. For phosphorus, given that no P:Al data are available in Shaw et al. (1976), we applied the average of the values reported by the other three studies (8.7×10^{-3}). ----------19

Table 3.1: Average pH on the total scale and temperature (±SD of triplicates), as well as irradiance during the short-term assays in OA1 (Davis Strait, Subarctic) and OA2 (Baffin Bay, Arctic). Irradiance was calculated based on surface PAR and percentage of penetration, indicating the light experienced by phytoplankton, standard deviation of irradiance during the short-term assays are also reported. K_d'(dark), K_{hv}, and K_d' are the FeEDTA dissociation constants used for the Fe′ calculations in various environmental conditions. The Fe′ concentrations under these specific incubation conditions were calculated using 0.4 nM and 200 nM Fe additions as examples. Fe′ concentrations under 0.4 nM Fe addition were calculated as 0.5% of dissolved Fe after addition. These illustrate the range of [Fe′] in a given CO_2/light condition during short-term assays. LL and HL denote 15% and 35% of surface PAR, respectively, while LC and HC denote 380 ppm and 1000 ppm of CO_2. ----------49

Table 3.2: $Uptake_{100/20}$=(Fe uptake rates under 100 nM Fe addition)/(Fe uptake rates under 20 nM Fe addition) for the two phytoplankton size fractions SSF (0.6-5 µm) and LSF (>5 µm). LL and HL denote 15% and 35% of surface PAR, respectively, while LC and HC denote 380 ppm and 1000 ppm of CO_2. Mean ± SD is derived from triplicates, except for 1) OA2 low light/high CO_2, where both SSF and LSF data are derived from duplicates; and 2) OA2 low light/high CO_2, where one of the SSF replicates is a potential outlier, the value in brackets is derived after excluding the putative outlier.----------54

Table 3.3: Results from two-way ANOVAs of Fe uptake rate constants k_{in}^{20} (20 nM Fe:10 µM EDTA addition) for OA1 and OA2 for the two phytoplankton size fractions SSF (0.6-5 µm) and LSF (>5 µm). LL and HL denote 15% and 35% of surface PAR, respectively, while LC and HC denote 380 ppm and 1000 ppm of CO_2. Kolmogorov-Smirnov normality tests were performed and passed prior to ANOVA. Significance level was set to p=0.05, significant effects are bolded, and NA denotes not applicable. The statistical results are then interpreted in combination with Figure 3.3. ----------56

List of Figures

Figure 2.1: Oceanographic stations from the CCGS Amundsen cruise Canadian GEOTRACES Arctic Expedition in July-October 2015, where particulate samples were collected. Seventeen stations across four basins were investigated, including Labrador Sea (K1 and LS2), Baffin Bay (BB1-3), Canadian Arctic Archipelago (CAA1, 3-9) and Canada Basin (CB1-4). ----------9

Figure 2.2: Depth profiles of POC in the upper 500 m at 16 stations. K1 and LS2 locate in the Labrador Sea; BB, CAA and CB denote Baffin Bay, Canadian Arctic Archipelago and Canada Basin, respectively. Station CAA9 is omitted due to the lack of POC samples. Note the scale of x-axis in the Canada Basin is distinct from that of other basins. ----------12

Figure 2.3: Relationship between POC and PON in the Canadian Arctic Ocean, including Labrador Sea and Baffin Bay (a), CAA (b), and Canada Basin (c). In panel a and b, the solid black line represents the linear regression of the data. In panel c, the red data points denote potential outliers with low C:N ratios (CB1, 75 and 400 m; CB4, 10 and 25 m). The dotted line is the regression including those 4 potential outliers, and the solid line is the regression excluding those 4 outliers. Note the scale in panel c is different from that in a and b. ----------13

Figure 2.4: Values of N* ($N^*=[NO_3^-]-16[PO_4^{3-}]$) in the Canadian Arctic Ocean. Labrador Sea (K1 and LS2), Baffin Bay (BB), Canadian Arctic Archipelago (CAA). Data source: J. Tremblay; plot by R. Hamme. ----------16

Figure 2.5: Particulate elements median (blue dot) and range (black bar) of all water column samples for each station. Each panel denotes an element and each bar represents a station. Missing blue dots indicates that the median was below detection limit. Basins are divided by the red dotted lines, from left to right, Labrador Sea, Baffin Bay, CAA and Canada Basin. ----------17

Figure 2.6: Relationship between pFe and pAl for samples across four basins examined in the Canadian Arctic Ocean (a); and between pV and pAl (b). Data from all 17 stations and full depth are included. Solid line denotes linear regression, while dotted lines denote 95% confidence interval of regression. ----------18

Figure 2.7: Relationship between total pTM and non-lithogenic pTM in the Labrador Sea and Baffin Bay (red dots) and in the Canada Basin (blue dots). For example, for Cu, non-lithogenic $pCu=pCu-pAl\times[Cu/Al]_{crust}$. Dotted lines denote y=x, thus the lithogenic pTM contribution is negligible. Aluminum is omitted as it was used for the lithogenic correction. This method does not apply to pV and pFe, as the linear regression slopes in Figure 2.6 are lower than crustal ratios in Table 2.4. Therefore, lithogenic corrections might yield negative value for non-lithogenic pV or pFe. ----------20

Figure 2.8: Relationship between total pTM and non-lithogenic pTM in the CAA. Dotted lines denote y=x, thus data points on the line indicate that the lithogenic pTM contribution is negligible (Cd and P); while data points significantly deviating from the line indicate a strong lithogenic contribution (Pb, Mn, Co, Cu, Zn and Ba). --------21

Figure 2.9: Vertical distributions of pFe at the upper 200 m of Canadian Arctic Ocean (blue square), supplemented by vertical distributions of pAl (red square), which are scaled down by multiplying 0.173. The value of 0.173 is derived from the regression coefficient of pFe-pAl plot in Figure 2.6a. ----------22

Figure 2.10: Depth profiles of salinity (upper panels) and pAl (lower panels) at stations where surface pAl enrichment was observed. Only data from the upper 500 m are shown. Low salinity (~25) at the surface indicates strong freshwater input. ----------23

Figure 2.11: Depth profiles of pFe at deep stations across Canadian Arctic Ocean. Note the different scales among stations. ----------24

Figure 2.12: Vertical distribution of pCd:pP ratio in the Canadian Arctic Ocean. Data from station CAA5 (few depths were sampled) and CB4 (pCd at depth were below detect limitation) are omitted. Blue vertical bars indicate phytoplankton cellular Cd:P stoichiometry (Ho et al., 2003). Note the scale of y-axis is different in the upper panels. ----------26

Figure 2.13: Vertical profiles of non-lithogenic pCu:pP across the Canadian Arctic Ocean. Lithogenic correction was applied before calculating pCu:pP. Magenta bars denote a fixed molar stoichiometry of 5 mmol Cu $(mol\ P)^{-1}$, which often describes the plateau in non-lithogenic pCu:pP at depth. Data from station CAA4 are omitted due to few sampling depths. Note the scale of y-axis is different in the upper panels. ----------28

Figure 2.14: Vertical distribution of particulate Mn in the Canadian Arctic Ocean. Data from station CAA4 (few depths were sampled) are omitted. Blue box indicates the depth interval of 100-200 m. Note the scale of x-axis is different among panels. Only data from the upper 500 m of the water column are shown. ----------30

Figure 2.15: Depth profiles of dissolved Mn in the Canada Basin (a, c, e, g, data from M. Colombo), along depth profiles of the fraction of Upper Halocline Water (b, d, f, h, data from A. Beaupré-Laperriere). Only data from upper 500 m of water column are shown. ----------31

Figure 2.16: Depth profiles of pMn at stations where bottom input is evident (a-e), supplemented by depth profiles of pAl (f-j). Grey boxes indicate marine sediments. pMn:pAl ratio at the deepest depth of each station (k); the continental surface Precambrian Canadian shield composition (Shaw et al., 1976) is indicated with a dotted horizontal line. ----------32

Figure 2.17: Depth profiles of pBa (green squares) and AOU (red dots) at 4 stations in the Canada Basin (a-d); At CB2, CB3 and CB4, samples at 100-200 m depth with maxima values of pBa are enclosed in purple boxes, which include concomitant AOU peaks. ----------34

Figure 2.18: Correlation between pBa and pCu in the Canada Basin for samples collected between 100 m and the bottom depths. Data above 100 m are excluded due to photo-reduction of pMn. ----------36

Figure 2.19: Trace metal correlations in the CAA, where lithogenic inputs are significant, between pCd-pP below 100 m (a), between pMn-pAl below 100 m (b), and between non-lithogenic pZn-pP at all depths (c). In panel a and c, potential outliers are in red, and are excluded from the regression; In panel b, the dotted line describes data in red, presumably indicating the influence by MnO_x; samples above 100 m are excluded, due to photo-reduction of pMn. ----------40

Figure 3.1: Fe uptake rate constants (mean ± SD) in short-term Fe uptake assays for the small size fraction of the phytoplankton (SSF; 0.6-5 µm) in the incubation treatments of OA1 (a-d) and OA2 (e-h). LL and HL denote 15% and 35% of surface PAR, respectively, while LC and HC denote 380 ppm and 1000 ppm of CO_2. The dashed line

denotes the empirical k_{in} calculated for Fe´ uptake of *Micromonas pusilla*-like cells (which dominated SSF community in both OA1 and OA2), with a cell radium of 0.8 µm. ----------52

Figure 3.2: Fe uptake rate constants (mean ± SD) in short-term Fe uptake assays for the large size fraction of the phytoplankton (LSF; >5 µm) in the incubation treatments of OA1 (a-d) and OA2 (e-h). LL and HL denote 15% and 35% of surface PAR, respectively, while LC and HC denote 380 ppm and 1000 ppm of CO_2. The dashed line denotes the empirical k_{in} for Fe´ uptake of those representative diatom species. In OA1, volume and SA are represented by averaging those of *Pseudo-nitzschia* cf. *delicatissima* and *Fragilariopsis* cf. *cylindrus*, which dominated the LSF phytoplankton in all treatments. In OA2, volume and SA applied are those of *Chaetoceros socialis*, which dominated the LSF phytoplankton in all treatments. ----------53

Figure 3.3: Fe uptake rate constants k_{in}^{20} (mean ± SD) from short-term assays (20 nM Fe:10 µM EDTA addition) for OA1 (a, b) and OA2 (c, d), under different CO_2 and light levels for the two phytoplankton size fractions SSF (0.6-5 µm) and LSF (>5 µm). LL and HL denote 15% and 35% of surface PAR, respectively, while LC and HC denote 380 ppm and 1000 ppm of CO_2. ----------55

Figure 3.4: POC-normalized Fe uptake rates of the size-fractionated phytoplankton assemblage, versus calculated Fe´ concentrations for two treatments in each experiment. The two treatments mimic present-day (15% of surface PAR, 380 ppm CO_2), and future conditions (35% of surface PAR, 1000 ppm CO_2) in surface Arctic waters. Mean + SD of triplicates is reported. ----------60

Figure 3.5: In the present-day scenario (a), atmospheric CO_2 level is 380 µatm, resulting in a surface seawater pH of ~8.1. Fe´ is produced by both photo-dissociation and dark dissociation of FeL. In the future scenario (b), atmospheric CO_2 level is 1000 µatm, resulting in a surface seawater pH of ~7.7. This pH decline impacts the dark dissociation of FeL, thus decreasing Fe´ concentration. In addition, the ice melting leads to a shallower mixed layer and enhanced light penetration, hence promoting photo-dissociation of FeL and increasing Fe´ concentration. Consequently, Fe´ concentration in future Arctic Ocean could remain similar as that of present-day value, and phytoplankton might not show obvious physiological response in Fe uptake. ----------61

Glossary and Abbreviations

FeL: complex of Fe bound to *in situ* organic ligands

OA: ocean acidification

PAR: photosynthetic active irradiance

Fe´: dissolved inorganic iron, primarily of $Fe(OH)_x$ complexes

EDTA: ethylenediamine tetraacetic acid

DFB: desferri-ferrioxamine B

SCM: subsurface chlorophyll maximum

PC: polycarbonate

k_{in}: Fe uptake rate constant

ANOVA: analyses of variance

SA: surface area

HAFeTS: high-affinity Fe transport system

CAA: Canadian Arctic Archipelago

LS: Labrador Sea

CB: Canada Basin

BB: Baffin Bay

SD: standard deviation

RSD: relative standard deviation

UCYN-A: unicellular cyanobacteria group A

N*: nitrate concentration minus sixteen times of phosphate concentration

$\delta^{15}NO_3^-$: nitrogen isotope ratio of nitrate

PCA: principal component analysis

AOU: apparent oxygen utilization

POC: particulate organic matter

pTM: particulate trace metals

AOA: ammonium oxidizing archaea

Acknowledgement

I would like to thank my supervisor, Maite Maldonado for elevating my maximum uptake rate to overcome numerous limitations; My committee members, Urs Hafeli and Kristin Orians for promoting my growth; David Semeniuk and Nari Sim for installing me with various transporters; Roger Francois, Philippe Tortell, Jay Cullen and Maureen Soon for showing me how to function properly at sea; Manuel Colombo for being a self-certified king in the upper layer and Chen Zeng for forming a colony together. I thank all Tornado lab friends for the knowledge and concerns, which provide me with nutrients and PAR, respectively. I thank Trimborn group at AWI for the infinite amount of clean tubes, and hosting me for 2 months. I thank crew members, scientists, and Zhiyuan Gao on board Amundsen, for creating a diligently photosynthesizing community. I also thank IsoSiM program for inoculating me into UBC. Finally, I thank my parents for their relentless love.

Chapter 1: Introduction

1.1 Phytoplankton and metal limitation

Marine phytoplankton account for about half of the Earth's primary productivity (Field et al., 1998), exerting a critical influence on global climate. At times, marine phytoplankton growth and production can be limited, or co-limited by trace metal deficiency. Cobalt (Co) limitation of the cyanobacteria *Prochlorococcus* has been reported (Saito et al., 2002), and attributed to their high cellular demand for carbonic anhydrase (a key component of their carbon-concentrating mechanism), which could not be satisfied by zinc (Zn). Similarly, co-limitation by Zn and carbon has been documented for the diatom *Thalassiosira weissflogii*, though the cellular Zn requirement for synthesizing carbonic anhydrase can be replaced with Co or cadmium (Cd) (Morel et al., 1994). In marine diatoms, the copper (Cu) containing enzyme plastocyanin has been shown to replace its iron (Fe) containing counterpart cytochrome c_6 in photosynthesis (Peers and Price, 2006). Copper is also involved in the high-affinity Fe transport system of some Fe-limited diatoms (Maldonado and Price, 2001; Maldonado et al., 2006). These uses of Cu imply an interaction between Fe and Cu nutrition in diatoms, which has been documented in lab (Annett et al., 2008; Guo et al., 2012), and field studies (Semeniuk et al., 2016).

Fe is the most essential micronutrient for phytoplankton growth (Ho et al., 2003) and has been shown to limit plankton productivity in 30% of the world's oceans. Fe is involved in fundamental cellular processes, such as photosynthesis (Raven et al., 1999), nitrogen fixation (Mills et al., 2004) and nitrate assimilation (Maldonado and Price, 1996). Other metabolisms relying on Fe include respiration, vitamin synthesis, fatty acid metabolism using dehydrogenases and oxygenases, and oxygen detoxification via superoxide dismutases (for a review see Marchetti and Maldonado, 2016).

In contrast to deficiency and limitation, excessive trace metals have also been shown to impact phytoplankton growth, including Cu, Cd and Zn (Rueter et al., 1979; Brand et al., 1986; Sunda and Huntsman, 1998). Therefore, understanding how trace metals control marine phytoplankton, and ultimately the ocean's biological pump, is a prerequisite for predicting how marine productivity will change in the future and how in turn this activity will impact global climate.

1.2 Particulate trace metal

Particles—operationally defined as materials collected onto filters with pore sizes of 0.2 or 0.4 μm—are an important reservoir of trace metals, exceeding the dissolved pool by 1000 times in some shelf regions (e.g., Fe in the Bering Strait, Cid et al., 2011). Particles exert a significant impact on the distributions of dissolved trace metals, by serving as a source (via dissolution or remineralization) or a sink (via active uptake or scavenging) (Ohnumus, 2014). Particles are delivered to the ocean by aeolian deposition, river discharge, sediment re-suspension, hydrothermal vents, etc. In addition, particles are generated *in situ* by plankton activity, detrital processes and authigenic Fe/Mn oxidation. Given their respective delivery or formation processes, some particulate trace metals can be used as tracers of biogeochemical processes. For example, Al and Ti are used as proxies for lithogenic particles (Ohnemus and Lam, 2015), Fe for hydrothermal inputs (Revels et al., 2015), Mn for redox cycle (Brujevicz, 1938), Ba for paleoproductivity (Francois et al., 1995), Cd and Zn for planktonic paleoecology (Boyle, 1981), and V for fossil fuel combustion (Duce and Hoffman, 1976).

The Arctic Ocean is experiencing rapid changes, originated from anthropogenic activities (see section 1.3 for details). For example, the Arctic's sea ice wintertime maximum extent has been declining, on average, at a speed of 2.8% per decade since 1979. The summertime minimum extent losses are five times faster, at 13.3% per decade (https://climate.nasa.gov). Predicting future biogeochemical conditions in the rapidly changing Arctic is extremely difficult, because we presently lack basic knowledge in many biological, physical and chemical processes in the Arctic Ocean. For example, due to seasonal ice cover and harsh weather, our knowledge of particulate trace metals' cycling is very limited. Studying particulate trace metals in the Arctic Ocean would help us elucidate biotic and abiotic processes affecting trace metals distributions and concentrations, as well as, how trace metal bioavailability (toxic and essential) may control plankton productivity and community composition in this polar region. This study will ultimately contribute to a better understanding of the biogeochemical cycles of trace metals in the global ocean.

1.3 Fe bioavailability to phytoplankton under climate change

The Arctic Ocean, currently accounting for 5 to 14% of the total ocean CO_2 uptake (Bates and Mathis, 2009), is undergoing rapid climate-driven changes, including acidification and sea

ice cover decline (Pachauri et al., IPCC 2014). These changes would lead to increasing levels of CO_2 and irradiance in the surface ocean, which could consequently alter Fe bioavailability to phytoplankton. Taylor et al. (2013) investigated the potential for nitrate, light, and Fe co-limitation of Beaufort Sea phytoplankton, and concluded that given the seasonal cycles of light, nitrate and Fe availability in the Arctic, Fe could play an important role in regulating phytoplankton production, especially during late summer and early fall.

Carbon dioxide and light levels may modulate the concentrations of various Fe substrates for phytoplankton uptake. The most bioavailable Fe species to phytoplankton is dissolved inorganic iron (Fe´), comprising primarily $Fe(OH)_x$ complexes, and accounting for less than 0.1% of the dissolved Fe (Gledhill and Buck, 2012). In the ocean, the vast majority of dissolved Fe is bound to strong organic ligands (FeL). Iron within these organic complexes is bioavailable to phytoplankton, but at slower rates than Fe´. The relative pools of Fe´ and FeL in the surface ocean are influenced by both pH (as the thermal conditional stability constant of FeL are pH sensitive), and light intensity (as light can mediate the photo-degradation of FeL complexes). Indeed, high CO_2, which induces lower pH, has been shown to lower Fe bioavailability to phytoplankton in the presence of organic complexes that either release protons during dissociation (e.g., FeEDTA, ethylenediamine tetraacetic acid) or need to be reduced at the cell surface before internalization of the free Fe (e.g., FeDFB, desferri-ferrioxamine B) (Shi et al., 2010). In addition, Fe bound to some organic ligands is subject to photo-reduction (Gledhill and Buck, 2012 and references therein), so that elevated light intensities can enhance the pool of Fe´ in the presence of both synthetic (Sunda and Huntsman, 2003) and natural organic ligands (Kuma et al., 1992; Waite et al., 1995).

1.4 Phytoplankton physiological response to low Fe concentrations

Under low Fe concentrations, phytoplankton are able to increase the number of cell surface Fe transporters in order to enhance Fe´ uptake and maintain maximal growth (Hudson and Morel, 1990). For example, phytoplankton preconditioned in Fe-limiting medium could possess 20-fold higher maximum uptake rates, relative to those cultured in Fe-replete medium (Harrison and Morel, 1986). However, the potential of this strategy is ultimately limited by the available surface area for Fe transporters. Under extremely low Fe´ concentrations, phytoplankton might be Fe-limited, and their growth rate may drop substantially. Under these conditions, they may

access Fe bound to organic ligands by up-regulating a high-affinity Fe transport system, which involves the coupling of ferrireductases with multi-Cu ferroxidase permease complexes at the cell surface (Maldonado et al., 2006). Indeed, phytoplankton preconditioned in Fe-limiting medium may possess both low and high-affinity Fe transport system (Maldonado and Price 2001), as previously shown for Cu (Guo et al., 2010).

1.5 Objectives

The present study focuses on the Canadian Arctic Ocean, an understudied and quickly changing oceanic region. My investigation included two distinct but related projects. Firstly, I determined the spatial and vertical distributions of particulate trace metals in the Canada Basin, Canadian Arctic Archipelago, Baffin Bay, and Labrador Sea during the 2015 Canadian GEOTRACES Expedition. Secondly, using *in situ* experiments, I investigated Fe bioavailability to Arctic phytoplankton assemblages under present and future conditions, focusing on the predicted effects of enhanced light and CO_2 concentrations in surface waters. This thesis elucidates biotic and abiotic processes affecting the cycling of trace elements in the Arctic, and in turn highlights how future changes in trace metals speciation will affect plankton productivity and ecology in the Arctic Ocean.

Chapter 2: Particulate Trace Metals in the Canadian Arctic Ocean

2.1 Introduction

Particles are an important reservoir of trace metals, exceeding the dissolved pool by 1000 times in some shelf regions (e.g. Fe in the Bering Strait, Cid et al., 2011). Particles exert a significant impact on the distributions of dissolved trace metals, by serving as a source (via dissolution or remineralization) or a sink (via active uptake or scavenging). Particulate matter in the ocean is operationally defined as material collected onto filters with pore sizes of 0.2 or 0.4 μm.

Particulate trace metals (pTM, whereas dissolved trace metals are hereafter referred to as dMe) can be classified based on three criteria: 1) their source of origin; 2) their solubility under acidic condition and 3) their research applicability. Firstly, according to their sources, pTM can be broadly classified as biogenic, lithogenic and authigenic. Biogenic particles include living and dead organic matter and mineral skeletons (Ohnemus et al., 2015). In addition, particles for which the formation processes are mediated by organisms—such as barite (Dehairs et al., 1980) and manganese oxide crust (Tebo et al., 2005)—are also considered biogenic. Lithogenic particles originate from the weathering of terrestrial rock, and are delivered to the ocean by aeolian dust (Jickells et al., 2005), river discharge (Nair and Ittekkot, 1991), and lateral transport of continental margin sediments (Lam et al., 2006). Authigenic particles are abiotically generated *in situ*, such as Fe/Mn oxyhydroxides. Diffusion of dFe and dMn from reducing sediment, and subsequent precipitation of these metals near the sediment-water interface or in the overlying water column leads to authigenic formation of Fe/Mn oxyhydroxides (Ohnemus et al, 2015). In addition, along the pathway of hydrothermal plumes, the abundant Fe within the fluid rapidly precipitates as sulfides, oxides and oxyhydroxides, which set another example for authigenic particles (Sherrell et al., 1999). Secondly, pTM are reported, depending on the effectiveness of the acidic digestion during sample processing, as labile pTM (or leachable, determined as total dissolvable metal minus dissolved metal) or total pTM (or bulk, determined after presumably complete digestion). Thirdly, based on the research interest, bioactive metals and tracers are two sets of pTM being frequently investigated. Bioactive trace metals, such as Mn, Fe, Co, Ni, Cu, Zn, Cd, Al, Pb and Hg, are essential to organisms and/or toxic at high concentrations. Some pTM can be used as tracers of biogeochemical processes. For example, pAl and pTi are used as

proxies of lithogenic particles (Ohnemus et al., 2015), pBa for paleoproductivity (Francois et al., 1995), and pV for fossil fuel combustion (Duce and Hoffman, 1976).

The Canadian Arctic Ocean includes the Beaufort Sea of the Canada Basin, Canadian Arctic Archipelago (CAA) and Baffin Bay. By linking the Pacific and the Atlantic oceans, the Canadian Arctic exerts an impact on ocean circulation, nutrients dynamics and global climate. Pacific water enters the Arctic Ocean exclusively through Bering Strait, then it splits near the Chukchi Plateau. One branch flows northwards, the other branch flows eastwards, along Alaska, through CAA towards Greenland, and exiting via the CAA and Fram Strait (Beszczynska-Möller et al., 2011). During this pathway across the Canadian Arctic Ocean, the Pacific water is modified by river discharge (Dery and Wood, 2005), heat exchange, ice formation and melting, biological production and by its interaction with sediments (McLaughlin et al., 2005). Atlantic waters enter the Arctic Ocean through the eastern side of the Fram Strait, into the Barents Sea. These waters flow counter-clockwise around the Arctic Basin, before exiting via the western side of the Fram Strait and the Nares Strait (Jones et al., 2003; Rudels et al., 2004).

In the high Arctic, our knowledge of pTM is still limited, due to seasonal ice cover and harsh weather. Cid at al. (2012) estimated the concentrations of labile pTM in the shelf region of the Beaufort Sea. They suggested that the distributions of Ni, Cu and Zn in this area were dominated by physical transport and chemical reactions—such as redox cycling and scavenging—while biogeochemical processes were less important. In the Russian Lena River estuary, Martin et al. (1993) investigated total pTM, and suggested that pCu and pNi were preferentially associated with organic matter and clay minerals, respectively. Similarly, relatively high content of pCu, pZn and pCd were reported in the Lena River basin by Rachold et al. (1996), and were explained by high levels of organic matter.

Though datasets on pTM in the Arctic Ocean are very limited, distributions of pTM have been documented in other northern latitudes. For example, in the Bering Sea, measurements of labile pTM in shelf seawater suggested that pAl and pCd were dominated by terrigenous clay and organic matter, respectively, whereas particulate Mn, Fe, Co, Ni, and Cu were dominated by Fe-Mn oxides (Cid et al., 2011). In the Bering Sea, others have observed elevated labile particulate Fe in shelf bottom waters (~70 m), accounting for 81% of the total particulate Fe; and equivalent to ~23 times the concentration of dissolved Fe (Hurst et al., 2010). This high labile particulate Fe content was attributed to Fe reduction in surficial sediments, and was proposed to

be an important Fe source for phytoplankton in these surface waters (~25 m). In a glacial fjord in the Norwegian Svalbard Islands, Al, Co, Fe, Ti and V were shown to enter the fjord onto/in lithogenic particles from the glaciers, whereas Cd, Cr, Cu, Mo, Ni and Zn were mainly introduced through the intrusion of Atlantic waters (Ardini et al., 2016). Even though these studies are starting to reveal some patterns of pTM in these northern latitudes, they also highlight our limited understanding of the factors that control the distributions and cycling of pTM in the Arctic Ocean.

The present study reports for the first time spatial and vertical distributions of total pTM in four basins: the Canada Basin/Beaufort Sea, CAA, Baffin Bay, and Labrador Sea. One common factor controlling biogenic particle dynamics (i.e. phytoplankton productivity) across the Canadian Arctic is low solar radiation. Although the Arctic sea ice can be biologically productive (Arrigo et al., 2012), ice cover limits primary productivity by hindering light penetration (Arrigo et al., 2008). However, the basins investigated in our study are characterized by distinct features. For example, in the perennially ice covered central Canada Basin, the Beaufort Sea, stratification (McLaughlin and Carmack, 2010) and downwelling (Yang, 2009) reduce nutrient availability, rendering it an oligotrophic system with low terrestrial particulate inputs. In contrast, in the shallow CAA, discharge from rivers both enhances primary production by supplying extra nutrients, and inhibits it by limiting light transmission through lithogenic particle loading. Baffin Bay is one of the most productive regions of the Arctic (Michel et al., 2015), receiving no major river draining but considerable fresh water input from icebergs (Campbell and Yeats, 1982), which could be enriched in terrigenous material (Smith et al., 2007). We also collected samples from the Labrador Sea, an ice-free productive area that links the Arctic and North Atlantic oceans (note that when we refer to the Canadian Arctic Ocean hereinafter, we include the Labrador Sea). In addition to depth profiles of total pTM in these basins, we also determined the contributions of lithogenic and biogenic particles using proxies as particulate Al and P, respectively.

2.2 Material and methods

This section focuses on the sampling, handling and processing of particulate samples. Oceanographic parameters were obtained with a CTD (SBE 911) fitted with a dissolved oxygen

sensor (SBE 43), a transmissometer (CST-558DR) and a fluorometer (Seapoint). Nutrient samples were collected according to Tremblay et al. (2008).

2.2.1 Particulate trace metal sampling

pTM samples were collected during the 2015 Canadian GEOTRACES Arctic Expedition (Leg 2, July 10 to August 20, 2015, from Quebec City to Kugluktuk; Leg 3b, September 4 to October 2, 215, from Sachs Harbour to Resolute) on board CCGS Amundsen (Figure 2.1). The dataset described herein involves samples collected between 10 and 3500 m (near bottom), at 17 stations located in the Labrador Sea, Baffin Bay, CAA and Canada Basin. Twelve 12 L GO-FLO bottles (General Oceanics) were mounted on the GEOTRACES trace metal-clean rosette system and deployed on a Kevlar cable with a dedicated custom designed winch (Christopher et al., 2008). Upon recovery, GO-FLO bottles were transferred to a portable trace metal clean sampling van, and ~10 L of seawater were collected into LDPE cubitainers, using a piece of C-flex tubing (Masterflex) together with a Teflon straw. Seawater was then filtered through a 0.45 µm Supor filter (47 mm diameter) inside a HEPA-filtered clean air bubble. The filtration system included a cubitainer placed inside a milk crate, a spigot, a C-flex tubing, a peristaltic pump (Cole-Palmer), a 47 mm filter holder (Millipore) with customized screws, a waste tubing and a waste container for volume recording. After filtration, the filters were dried on top of a trace metal clean plastic egg grid inside a laminar flow hood, folded in half, and stored in clean poly bags until further analysis. Containers and apparatus were cleaned according to GEOTRACES protocols (Cutter et al., 2010).

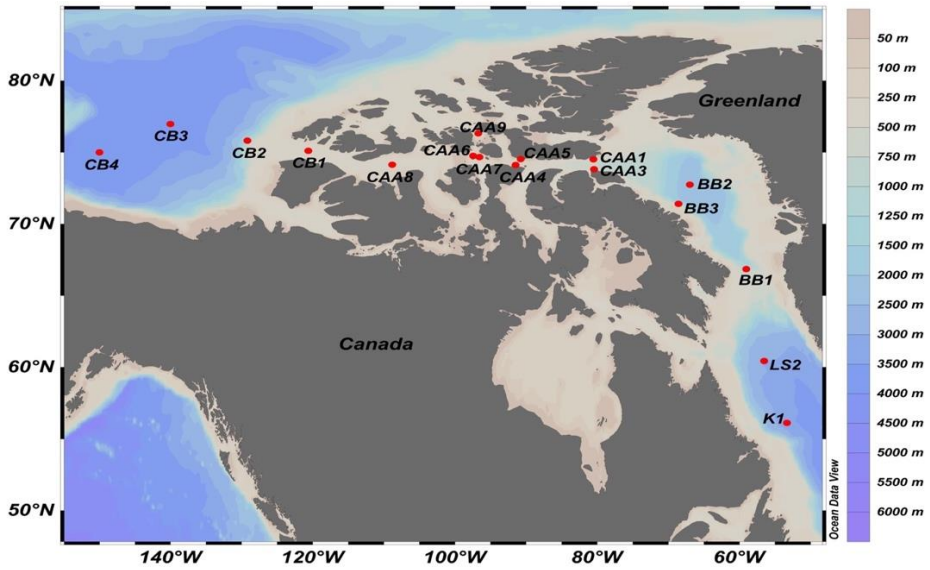

Figure 2.1: Oceanographic stations from the CCGS Amundsen cruise Canadian GEOTRACES Arctic Expedition in July-October 2015, where particulate samples were collected. Seventeen stations across four basins were investigated, including Labrador Sea (K1 and LS2), Baffin Bay (BB1-3), Canadian Arctic Archipelago (CAA1, 3-9) and Canada Basin (CB1-4).

2.2.2 Analytical technique

Filters were completely digested at UBC in a HEPA-filtered fume hood, class 100 cleanroom, using the 'Piranha' procedure (Ohnemus et al., 2014). Briefly, filters were placed in 15 mL Teflon vials (Savillex), and digested using a mixture of concentrated H_2SO_4 and concentrated H_2O_2 (1.2 mL and 0.4 mL, respectively) at high heat, to digest organic matter and filter matrix. Depending on the particle loading and composition, for total digestion, 0.4 mL of concentrated H_2O_2 might be added multiple times (5 times in this study, with 2-hour reflux at 200°C and slight drying, between additions). The vials were then placed in a heated Teflon block and the solution was dried at 245°C, which generated a solid black deposit. To wash off H_2SO_4 drops from the inner wall of the vials, 0.1 mL of 8N HNO_3 were added, refluxed (245°C, 2 h) and dried. The remaining materials were digested using a concentrated acid mixture of HNO_3-HCl-HF (453 µL H_2O, 506 µL HNO_3, 687 µL HCl and 354 µL HF) at 110°C for 4 h. After complete drying, 1 mL of concentrated HNO_3 and 1 mL of concentrated H_2O_2 were added to the vials, and taken to dryness again. At this stage, the complete digest looked like either gel-like material or a pellet and was transparent or white in color. If the digest was yellow—which was extremely rare—remaining organic matter was suspected, and another 1 mL of concentrated

HNO_3 and 1 mL of concentrated H_2O_2 were added, refluxed, and dried. Afterwards, to the ideal pellet, 0.1 mL of concentrated HNO_3 were added and taken to dryness. All reagents used in the digestion and subsequent sample preparation, including the four acids and H_2O_2, were Optima grade (Fisher Scientific). For analysis in the ICP-MS at UBC (Element2, Thermo Scientific), the final digest was re-suspended in 1% HNO_3 with 10 ppb Indium, as an internal standard. The elements measured were Al, Cd, Pb (low resolution), P, V, Mn, Fe, Co, Cu, Zn and Ba (medium resolution). Instrumental blanks were monitored every 6 samples by measuring 1% HNO_3 with Indium, and the detection limit is reported as 3σ of instrumental blank (Table 2.1). Before processing our samples, we conducted a trial batch of certified reference material BCR-414 for validation of the digestion method. The recovery is listed in Table 2.1. We also participated in the GEOTRACES inter-calibration on particulate trace metals, and have successfully submitted the data.

Table 2.1: CRM BCR-414 (n=4) was digested and measured prior to sample processing. The recovery for each element are listed, accompanied by RSD of certification. C: certified value; I: indicative value of BCR-414; GR: consensus provided by Database on geochemical, environmental and biological reference materials. NA denotes not applicable. Sample measurements were accomplished in four days (D1-D4). Detection limits were determined by 8 to 11 runs of 1% HNO_3 per measurement day. The standard deviation (ppt) was derived from these runs, and detection limit (DL, ppt) equals three times the standard deviation. For each sample, the relative standard deviation (RSD, %) of various elements was calculated. The median RSDs per measurement day are reported for each element.

		Al	Cd	Pb	P	V	Mn	Fe	Co	Cu	Zn	Ba
CRM	Recovery (%)	138	96		119	129	97	106	82	103	81	89
	CRM RSD (%)	37	4		39	2	4	10	4	4	2	16
	Certification	GR	C		GR	C	C	I	I	C	C	GR
D1	DL(ppt)	1045	22	35	52	12	10	49	20	8	6	28
RSD(%)	Med	7	10	8	5	6	6	6	8	6	8	6
D2	DL(ppt)	184	6	19	25	21	40	126	21	6	3	13
RSD(%)	Med	3	6	5	3	4	2	3	5	4	4	4
D3	DL(ppt)	1014	10	7	117	60	31	19	17	12	7	53
RSD(%)	Med	6	8	8	4	5	5	4	10	5	7	4
D4	DL(ppt)	109	1	2	86	24	21	11	5	4	4	14
RSD(%)	Med	5	14	13	5	7	5	6	12	7	9	6

2.2.3 POC sampling and analysis

POC samples were collected at all locations to match the pTM samples. Between 2 and 9 L of seawater were filtered through 25 mm pre-combusted (450°C for 4 h) GF/F filters (Whatman,

0.7 μm). Filters were stored at -20°C and later oven dried at 60°C for 24 h. To remove particulate inorganic carbon, filters were acid fumed with concentrated HCl for 3 days, and then dried at 50°C for 24 h (Brown et al., 2014). Samples were analyzed for POC and particulate nitrogen (PON), by a CNS vario MICRO cube (Elementar). Detection limits are determined by measuring pre-combusted blank GF/F filters, and reported as three times standard deviation of replicates (0.009 mg for PON, n=8; 0.012 mg for POC, n=10).

2.3 Results and discussion

Our dataset covers 4 basins across Canadian Arctic Ocean, namely Labrador Sea (stations K1 and LS2), Baffin Bay (stations BB1, 2, and 3), Canadian Arctic Archipelago (stations CAA1, 3, 4, 5, 6, 7, 8 and 9) and Canada Basin (stations CB1, 2, 3, and 4), containing 154 particulate trace metal samples (10-3500 m) from 17 stations. The elements we measured include P, Al, Cd, Pb, V, Mn, Fe, Co, Cu, Zn, and Ba. Section 2.3.1 reports the distribution of POC and PON, as well as C:N:P stoichiometry across the Canadian Arctic Ocean. Section 2.3.2 is a preview of our pTM dataset, where we introduce their spatial distributions and the contribution of lithogenic particles to the total pTM. Section 2.3.3 focuses on several interesting pTM depth profiles from our dataset. Section 2.3.4 is a detailed study of pTM in the Canada Basin, where we suggest interactions between biogenic production of manganese oxide, cobalt oxide and barite. Section 2.3.5 presents data from the CAA, where pTM is strongly influenced by lithogenic materials.

2.3.1 Particulate organic matter: barren Canada Basin and N-fixation in Labrador Sea

Spatial and vertical distribution of POM

In our full-depth dataset (Table SI1-4), the maximum POC and PON are 27.8 μmol L^{-1} and 3.3 μmol L^{-1}, respectively. The depth profiles of both POC and PON demonstrate a decline with depth (see Figure 2.2, for POC as an example). Above 100 m, our POC values span from 1.2 to 27.8 μmol L^{-1}, and are in good agreement with previous studies in the Chukchi and Beaufort Seas (ranging from 1.5 to 28.3 μmol POC L^{-1} above 100 m, Zhang et al., 2015).

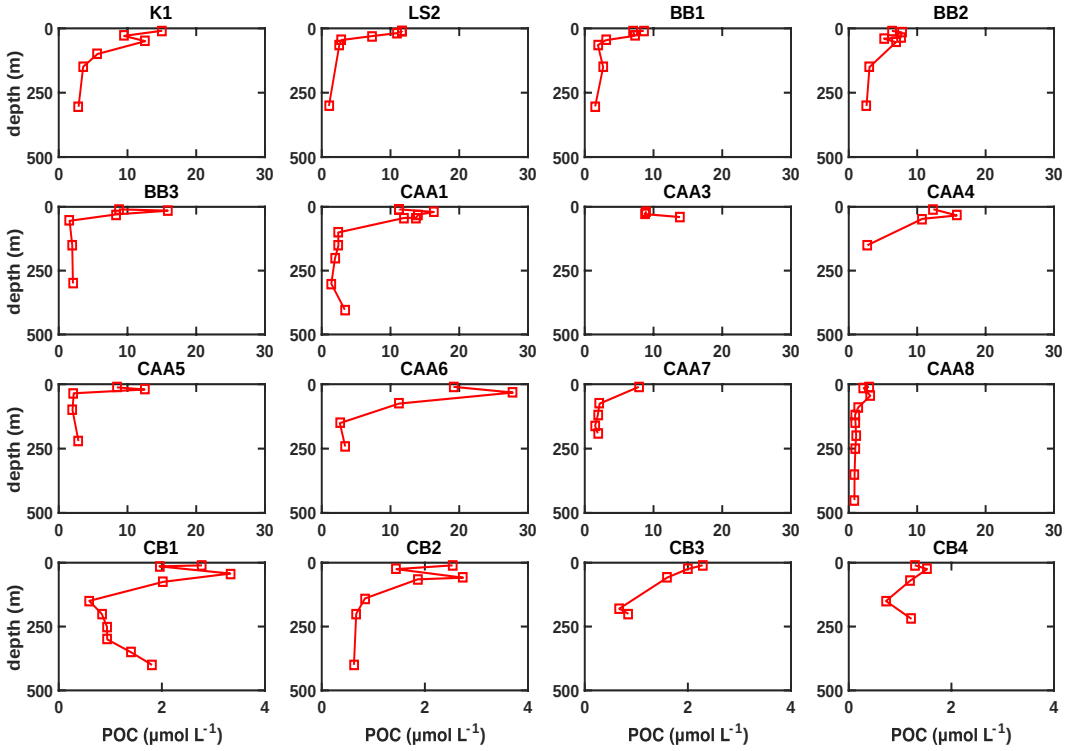

Figure 2.2: Depth profiles of POC in the upper 500 m at 16 stations. K1 and LS2 locate in the Labrador Sea; BB, CAA and CB denote Baffin Bay, Canadian Arctic Archipelago and Canada Basin, respectively. Station CAA9 is omitted due to the lack of POC samples. Note the scale of x-axis in the Canada Basin is distinct from that of other basins.

In the present study, in the 13 stations where both POC and PON were detectable, POC:PON molar ratios at the bottom depth average at 6.6±2.8. In the Canada Basin, particles with a molar C:N ratio exceeding 10, at depth lower than 2000 m, has been considered to be river-delivered and refractory (Trimble and Baskaran, 2005). The average of 6.6 suggests that the sediment's POM in these 13 stations is dominated by marine sources.

POM in the Canada Basin

The Canada Basin is unique among the four basins investigated here, in showing low POC and PON concentrations, as well as a deviation of POC:PON ratio from the classic Redfield ratio (Figure 2.3c).

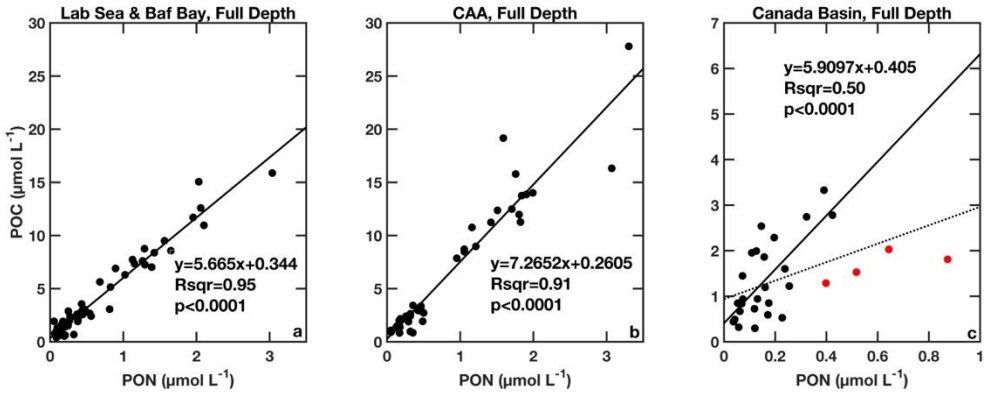

Figure 2.3: Relationship between POC and PON in the Canadian Arctic Ocean, including Labrador Sea and Baffin Bay (a), CAA (b), and Canada Basin (c). In panel a and b, the solid black line represents the linear regression of the data. In panel c, the red data points denote potential outliers with low C:N ratios (CB1, 75 and 400 m; CB4, 10 and 25 m). The dotted line is the regression including those 4 potential outliers, and the solid line is the regression excluding those 4 outliers. Note the scale in panel c is different from that in a and b.

In the Canada Basin, the maximum POC (3.3 µmol L^{-1} at 40 m of CB1) and PON concentrations (0.9 µmol L^{-1} at 400 m of CB1) are quite low compared with those in other basins (up to 27.8 µmol L^{-1} POC and 3.3 µmol L^{-1} PON, Figure 2.3a and 2.3b). Furthermore, for the two central Canada Basin stations (CB 3 and 4, with 3500 m depths), the POC and PON concentrations showed even lower maxima, with values of 2.3 and 0.5 µmol L^{-1}, respectively. Previous studies in the Canada Basin have shown similarly low POC and PON values at deep stations (>2500 m). For example, Brown et al. (2014) reported POC spanning 1.2-2.8 µmol L^{-1} at the surface mixed layer (~10 m). In the upper 200 m of central Canada Basin, Trimble and Baskaran (2005) reported maxima of 3.1 µmol L^{-1} POC and 0.3 µmol L^{-1} PON, while Moran and Smith (2000) documented a maximum of 1.0 µmol L^{-1} POC and 0.1 µmol L^{-1} PON. Low POC and PON in the Canada Basin have been attributed to extremely low levels of primary productivity (Varela et al., 2013; Crawford et al., 2015), resulting from limitation by light and nitrate (Tremblay et al., 2008; Tremblay and Gagnon, 2009). In addition, a recent study argued that in addition to nitrate and light, Fe availability might control primary productivity in late summer of the Beaufort Sea (Taylor et al., 2013).

Another phenomenon in the Canada Basin is the deviation of POC:PON from the Redfield ratio of 6.6 (Figure 2.3c). When all the data are included, the POC-PON ratio is 2.1, which is significantly lower than 6.6. However, when 4 outlier data points are removed, the slope is identical to that for the data from the Labrador Sea and Baffin Bay (Figure 2.3a). Those 4

outliers correspond to 75 and 400 m at CB1 (shelf); plus 10 and 25 m at CB4 (central basin). Low POC:PON ratios in the Canada Basin have been observed (Crawford et al., 2015), and attributed to 1) the small contribution of phytoplankton C to the total particulate organic C pool; and 2) the dominance of heterotrophic bacteria which have low C:N ratios (4.5-6.7 by Bratbak, 1985; 3.2–4.2 by Lee and Fuhrman, 1987; and 3 by Banchetti et al., 1989); relative to phytoplankton (6.6 for eukaryotic and >5 for prokaryotic, Finkel et al., 2009; and references therein). Thus, the low POC:PON ratios of those four samples could be accounted for by the abundance of heterotrophic bacteria, possibly relying on allochthonous lateral supply of DOC (Kirchman et al., 2009), which uncouples bacterial and primary production in time and space.

N:P stoichiometry

As a macronutrient, phosphorus in particles and its relative abundance to C and N is of interest. We calculated the PON:pP ratios of the surface water samples, and compared ratios among the four basins (Table 2.2). Surprisingly, the PON:pP value in surface water of each basin exceeds that of Redfield ratio, and this anomaly could not be explained by insufficient collection of pP. Indeed, POC/PON samples were collected on GF/F filters (nominal pore size 0.7 μm), while pP was collected on Supor filters (0.45 μm). Martiny et al. (2014) compiled a dataset of PON:POP ratio in the global ocean, with a mean value of 22, higher than the classical Redfield ratio of 16. This global mean PON:POP ratio is close to our measured PON:pP ratio in upper BB, CAA and CB (21-29, Table 2.2). However, whether data from the 0-50 m or 0-100 m depths are used, the average PON:pP ratio is significantly higher in the Labrador Sea (~40, Table 2.2). Martiny et al. (2014) compiled 27 dataset (cruises or time-series) where PON:POP ratios were available. Only three of them display average PON:POP ratios higher than 40, which is similar to our observed value in upper Labrador Sea. Two of theses three dataset were collected in North Atlantic, where N-fixation was expected. The other was collected in central Pacific, where N-fixation was identified during the same expedition (Wilson et al., 2013). We suggest that N-fixation in the Labrador Sea may account for its higher PON:pP in surface waters, which is supported by five independent lines of evidence.

Table 2.2: Ratios between PON and pP in surface Canadian Arctic Ocean, average, standard deviation and median are reported, n denotes sample number.

Depth	N:P (mol mol^{-1})	Labrador Sea	Baffin Bay	CAA	Canada Basin
0-50 m	Average±SD	38±21 (n=8)	23±5 (n=11)	29±12 (n=21)	21±16 (n=9)
	Median	32	24	27	17
0-100 m	Average±SD	38±20 (n=10)	24±9 (n=14)	29±15 (n=26)	24±17 (n=14)
	Median	33	23	26	20

First, in the Labrador Sea, POM data within the upper 100 m show C:N ratios of 6.4±0.9, indicating the dominance of phytoplankton. Second, N-fixation at high latitudes has been revealed and attributed to unicellular cyanobacteria group A (UCYN-A, Diez et al., 2012 and Perez et al., 2016). These organisms display a cosmopolitan distribution in the global ocean, and rival the contribution to N-fixation by *Trichodesmium* in the tropical North Atlantic (Luo et al., 2012), subtropical North Pacific (Zehr et al., 2001) and oligotrophic Pacific Ocean (Montoya et al., 2004). Some N-fixers have been reported to have abnormally high cellular N:P ratios (e.g. *Trichodesmium* N:P is up to 45, Letelier and Karl, 1996; or even 125, Karl et al., 1992), though the N:P stoichiometry of UCYN-A is unknown, as these organisms have never been successfully cultivated. Third, sixteen percent of N-fixation in the North Atlantic is supported by excess phosphate from the Arctic flow into the Atlantic through the CAA (Yamamoto-Kawai et al., 2006). Fourth, during our cruise, the N* ($N^*=[NO_3^-]-16[PO_4^{3-}]$) measured in surface waters of the Labrador Sea was much higher than that in the other Arctic basins (Figure 2.4, J. Tremblay and R. Hamme). This high N* was accompanied by a lower $\delta^{15}NO_3^-$ (4.5-5‰ at LS2, versus 6-12‰ in other basins, N. Lehman and M. Kienast, same expedition, data not shown), suggesting N-fixation ($\delta^{15}NO_3^-$=0‰). The concomitant high N* and low $\delta^{15}NO_3^-$, indicates N-fixation in the Labrador Sea or its sourced water. Fifth, gross primary production in the mixed layer of Labrador Sea stations was roughly three times higher than that in Baffin Bay and CAA (~3 vs. ~1 mmol C m^{-3} d^{-1}, Timmerman et al., in prep.), supposedly supported by excess nitrogen in the Labrador Sea. Presumably, this nitrogen fixation is fueled by the P-rich Labrador Current, which is a combination of West Greenland Current and Baffin Island Current, both exiting the Arctic Ocean. We acknowledge that direct evidence of N-fixation in the Labrador Sea is still lacking. However, significant N-fixation in the Canadian Arctic Ocean has been recently documented (Blais et al., 2012). Given the abnormally high N:P value within the particles, concomitant high

N* and low $\delta^{15}NO_3^-$, and high primary production, we suggest that N-fixation does occur in the Labrador Sea.

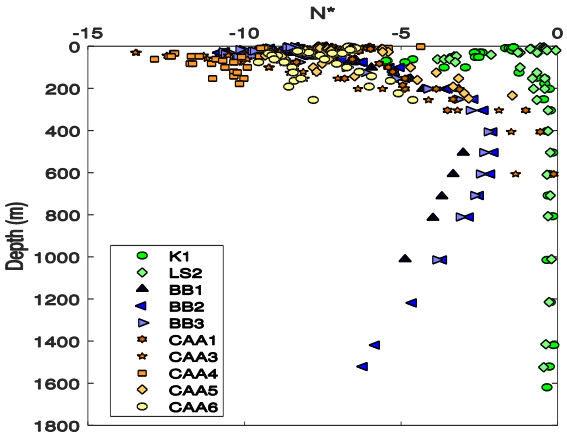

Figure 2.4: Values of N* (N*=[NO_3^-]-16[PO_4^{3-}]) in the Canadian Arctic Ocean. Labrador Sea (K1 and LS2), Baffin Bay (BB), Canadian Arctic Archipelago (CAA). Data source: J. Tremblay; plot by R. Hamme.

2.3.2 At a glance: spatial distributions and principal component analysis

In order to investigate trends in the spatial distribution of the particulate elements in the studied basins, we plotted station-specific concentration ranges and medians for each element (Figure 2.5). Cobalt was omitted, as pCo was too low to be detected with pAl, for which intensive dilution of final digest was usually required. We only successfully detected pCo concentrations for the Canada Basin, ranging from 3-70 pM (Table SI1-4). These pCo values are comparable to those in Antarctic waters (<10 pM, Noble et al., 2013).

As expected, pAl, a tracer of lithogenic inputs, was generally low in the Labrador Sea and Canada Basin, and high in the CAA. In contrast, pP, a proxy of biogenic particles was only low in the Canada Basin, consistent with low POC and PON in this region.

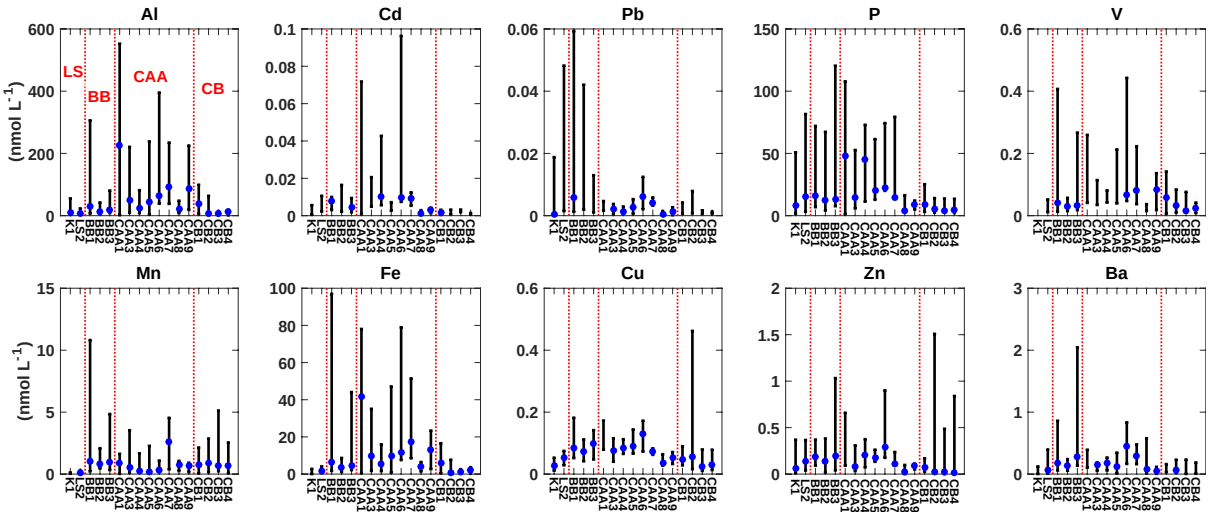

Figure 2.5: Particulate elements median (blue dot) and range (black bar) of all water column samples for each station. Each panel denotes an element and each bar represents a station. Missing blue dots indicates that the median was below detection limit. Basins are divided by the red dotted lines, from left to right, Labrador Sea, Baffin Bay, CAA and Canada Basin.

Principal component analysis (PCA) was conducted on a subset of the data, using IBM SPSS Statistics 2015. PCA is an analytical tool applied to assess metal behavior in aquatic systems (Liu et al., 2003). Particulate Pb and Co were excluded, because numerous values were below detection limit. PON, POC and apparent oxygen utilization (AOU) were also incorporated into the PCA, generating a subset of 91 samples and 12 parameters (Table 2.3).

Table 2.3: Principal component analysis (PC) loading of particulate elements and biological parameters. The percentage in bracket is the explained contribution of principal components to the total variance. pP, POC, PON and AOU constitute a firmly related group (bolded in PC1), while another group is composed of Al, Fe and V (bolded in PC2). Cu and Zn are associated within PC3 (bolded), which accounts for 10% of total variance.

	PC 1 (37.5%)	PC 2 (29.8%)	PC 3 (10.0%)
pAl	0.095	**0.853**	0.269
pCd	0.613	0.227	0.410
pP	**0.925**	0.057	0.127
pV	-0.053	**0.943**	0.175
pMn	-0.374	0.626	-0.028
pFe	0.012	**0.937**	0.234
pCu	0.113	0.272	**0.866**
pZn	0.294	0.047	**0.884**
pBa	0.356	0.487	-0.166
PON	**0.947**	0.004	0.133
POC	**0.933**	0.016	0.191
AOU	**-0.740**	0.365	-0.088

Three principal components explained ~80% of total variance of the dataset. The first component is associated with biological parameters (POC, PON, pP and AOU), showing a negative correlation between AOU and the POC-PON-pP set, due to the coupling of oxygen consumption (increasing AOU) and remineralization of nutrients within particles (decreasing POC, PON and pP).

The second component is associated with lithogenic material, grouping pAl, pFe and pV together. To further illustrate the relationship between these elements, pFe and pV were plotted versus pAl (Figure 2.6), and showed robust correlations. Similarly, strong positive correlations between pFe and pAl have been reported for the North Atlantic, due to considerable aeolian deposition that results in the prevalence of lithogenic materials throughout the entire basin (Ohnemus and Lam, 2015). Covariance between non-HAc-leachable pV and pAl has also been shown in the sediments of Baffin Bay, indicating the presence of V in fine-grained alumino-phyllosilicate minerals in Arctic sediments (Loring,1984). In the deep Atlantic, fine suspended particles (Buat-Menard and Chesselet, 1979) and sediment trap materials (Brewer et al., 1980) also displayed strong correlations between pV and pAl, with ratios similar to those in continental crust.

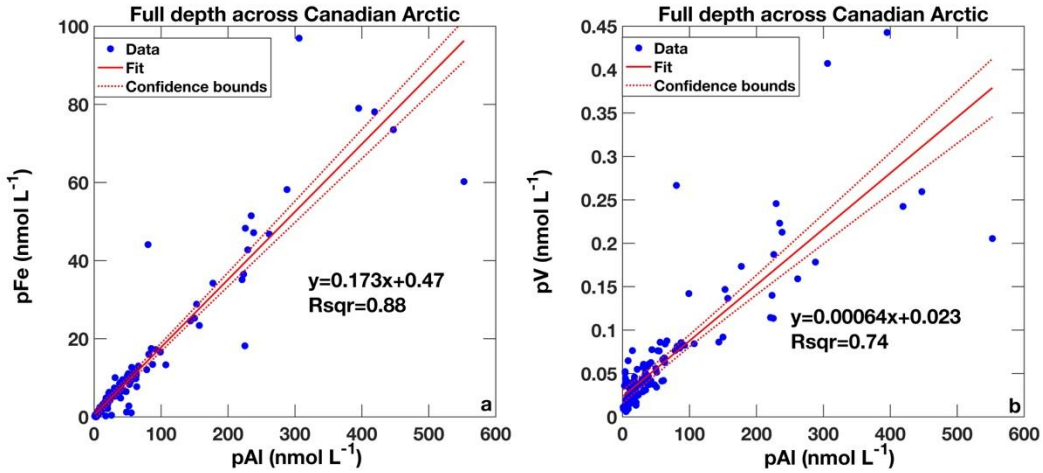

Figure 2.6: Relationship between pFe and pAl for samples across four basins examined in the Canadian Arctic Ocean (a); and between pV and pAl (b). Data from all 17 stations and full depth are included. Solid line denotes linear regression, while dotted lines denote 95% confidence interval of regression.

Since pAl exists mainly in lithogenic particles (Ho et al., 2007), the correlations above indicate that lithogenic materials dominate pFe and pV across the Canadian Arctic Ocean.

Consequently, the pFe associated with biological particles is completely masked by its lithogenic component, despite that Fe is the most abundant trace metal in phytoplankton (Ho et al., 2003). Furthermore, the robust correlation between pFe and pAl suggests that the vast majority of lithogenic particles in the water column are of a homogenous composition. Indeed, the pFe-pAl slope is 0.17 (Figure 2.6a), and likely reflects the regional crustal composition, which falls at the lower end of crustal ratios in the literature (0.19-0.33, Table 2.4). The regression slope for pV versus pAl is 6×10^{-4} (Figure 2.6b), falling within the range of published studies ($3.6\text{-}8.7\times10^{-4}$, Table 2.4). In the PCA, pCu and pZn are grouped with each other in PC3. It is surprising that pCu and pZn show no association with parameters in PC1 or PC2, given that, both POM and lithogenic materials, contain substantial amount of these two metals. Interestingly, the pZn:pCu ratios seem similar within phytoplankton cells (~2, average of 15 species, Ho et al., 2003) and continental crust (1.2-3.5, see below and Table 2.4). Thus, we attribute the pCu-pZn association to their relatively constant ratio in the different particle types.

Table 2.4: A compilation of metal:Al molar ratios in crustal materials. Taylor and McLennan (1995) and Wedepohl (1995) reported composition of the upper continental crust; Taylor (1964) introduced average composition of continental crust; while Shaw et al. (1976) reported continental surface Precambrian shield composition in Canada. Given the location, the values in the latter study are used for the lithogenic correction in our study. For phosphorus, given that no P:Al data are available in Shaw et al. (1976), we applied the average of the values reported by the other three studies (8.7×10^{-3}).

Study	Cd:Al $\times10^{-6}$	Pb:Al $\times10^{-6}$	P:Al $\times10^{-3}$	V:Al $\times10^{-3}$	Mn:Al $\times10^{-3}$	Fe:Al $\times10^{-3}$	Co:Al $\times10^{-6}$	Cu:Al $\times10^{-6}$	Zn:Al $\times10^{-3}$	Ba:Al $\times10^{-3}$
T&M 1995	0.29	32	7.6	0.40	3.7	210	57	130	0.36	1.3
W 1995	0.31	28	7.5	0.36	3.3	190	69	79	0.27	1.7
T 1964	0.58	20	11	0.87	5.7	330	140	290	0.35	1.0
S 1976	0.23	28	NA	0.36	3.3	190	71	77	0.27	2.7

In studies on pTM, lithogenic corrections are frequently applied in order to examine the contribution of lithogenic particles to pTM; and to uncover the relationship among trace metals in non-lithogenic particles. This section focuses on the former application, and the latter application is discussed in sections 2.3.4 and 2.3.5. Lithogenic correction is based on measured pAl concentrations and published crustal ratios of Metal:Al (compiled in Table 2.4). For each sample, the pAl concentration is multiplied by the crustal ratio. The product is then subtracted from the total pTM, yielding a non-lithogenic pTM (e.g., non-lithogenic pCu=pCu-pAl$\times$[Cu/Al]$_{crust}$). Here we used the crustal ratios of the Canadian continental surface

Precambrian shield (Shaw et al., 1976). For validation, these ratios were compared with several frequently-cited global average crustal ratios (Table 2.4). Subsequently, the total pTM were plotted versus non-lithogenic pTM for each element. In the Labrador Sea, Canada Basin and Baffin Bay (Figure 2.7), particulate Cd, Pb, P, Mn, Co, Cu, Zn and Ba show negligible influence by lithogenic particles, even if pTM concentrations span a few orders of magnitude. In contrast, in the CAA (Figure 2.8), pTM seem to be strongly affected by lithogenic particles. This is reflected in substantial deviation from the y=x line, with the exception of pCd and pP. As expected for the micronutrient Cd (Cullen et al., 1999), its concentration across the entire Canadian Arctic Ocean is dominated by biogenic particles.

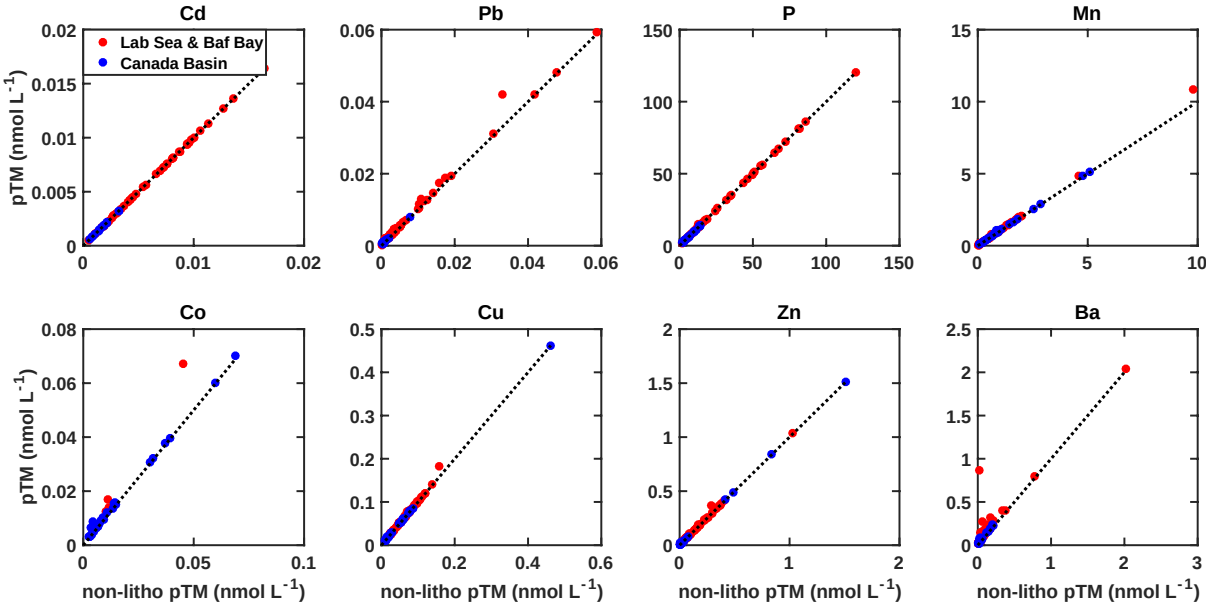

Figure 2.7: Relationship between total pTM and non-lithogenic pTM in the Labrador Sea and Baffin Bay (red dots) and in the Canada Basin (blue dots). For example, for Cu, non-lithogenic pCu=pCu-pAl×$[Cu/Al]_{crust}$. Dotted lines denote y=x, thus the lithogenic pTM contribution is negligible. Aluminum is omitted as it was used for the lithogenic correction. This method does not apply to pV and pFe, as the linear regression slopes in Figure 2.6 are lower than crustal ratios in Table 2.4. Therefore, lithogenic corrections might yield negative value for non-lithogenic pV or pFe.

Notably, the Labrador Sea and Baffin Bay are characterized by high pPb concentrations, compared to other two basins (Figure 2.7 and 2.8). Moreover, these high pPb do not originate from lithogenic particles. Lead concentrations in Greenland snow have fluctuated upon usage and prohibition of leaded petrol (Murozumi et al., 1969; Rosman et al., 1993). Boyle et al. (2014)

argued that dissolved Pb levels in surface waters have been changing in line with regional emissions, with North Atlantic dissolved Pb increasing from 1830 to 1975 and decreasing afterwards. We suggest that the high pPb concentration is due to regional anthropogenic input, as Labrador Sea and Baffin Bay are close to intense human activity.

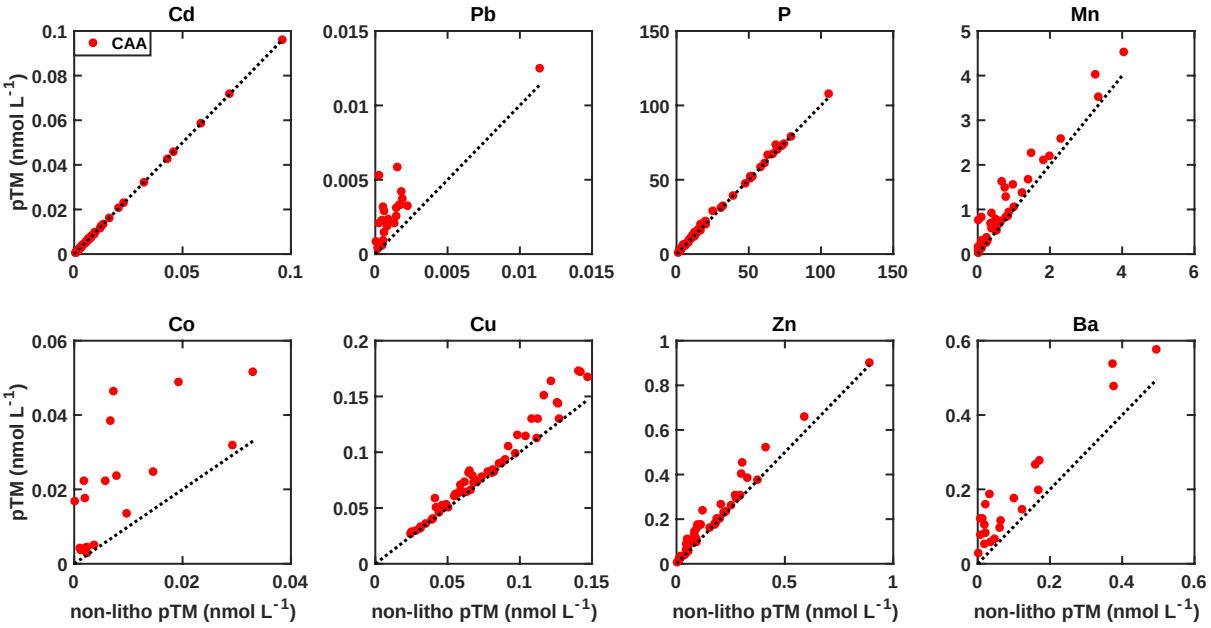

Figure 2.8: Relationship between total pTM and non-lithogenic pTM in the CAA. Dotted lines denote y=x, thus data points on the line indicate that the lithogenic pTM contribution is negligible (Cd and P); while data points significantly deviating from the line indicate a strong lithogenic contribution (Pb, Mn, Co, Cu, Zn and Ba).

2.3.3 Vertical distributions of pTM

In this section, we report the vertical distributions of particulate trace metals, focusing on three distinct depth profile types: particulate elements with a strong lithogenic component (Al, Fe and V), with a significant biogenic component (Cd and Cu), and with a predominant redox cycle (Mn).

Elements with a strong lithogenic component: Al, Fe and V

Surface enrichment of pAl, pFe and pV due to sediments released from melting sea ice

The vertical distributions of pFe and pV resemble that of pAl (Figure 2.9 for pFe and pAl as an example). For these elements, eight out of seventeen stations are characterized by a surface enrichment, defined by at least a three-fold difference in concentration between the mixed layer

sample (~10 m) and the second shallowest sample (10~30 m). In the Canada Basin, Giesbrecht et al. (2013) observed a maximum in low salinity surface waters (S=26-30) for dissolved and total dissolvable Al, and attributed this enrichment to sediments released from the melting sea ice. Previous studies have highlighted sediments within the sea ice as an important source of some trace metals to Arctic surface waters (Measures, 1999).

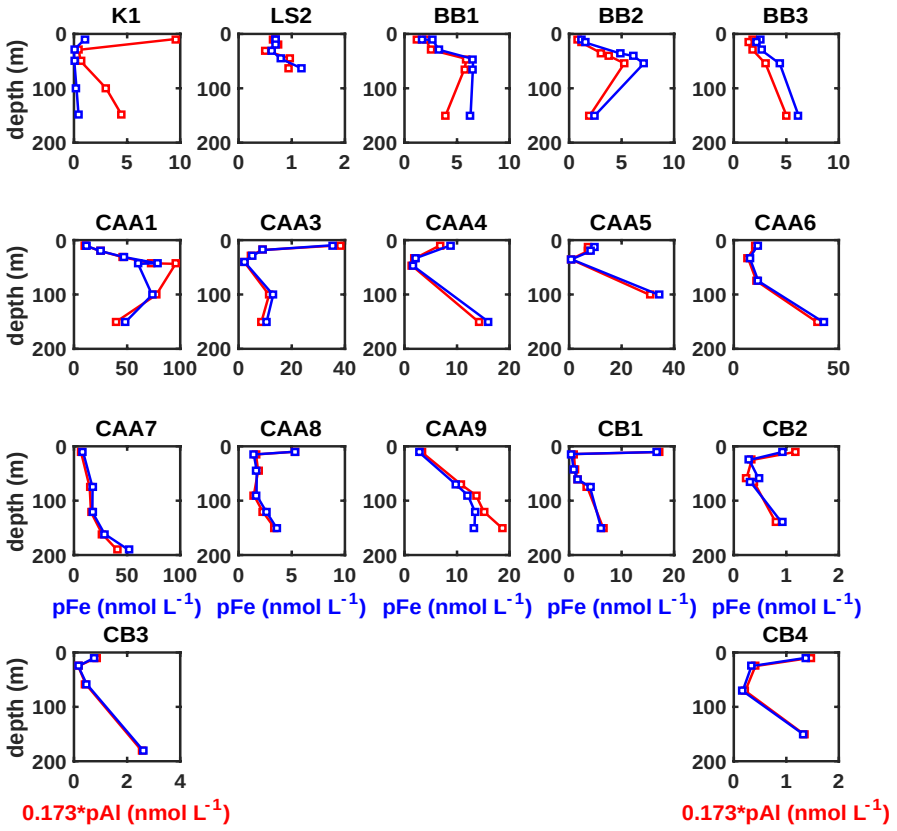

Figure 2.9: Vertical distributions of pFe at the upper 200 m of Canadian Arctic Ocean (blue square), supplemented by vertical distributions of pAl (red square), which are scaled down by multiplying 0.173. The value of 0.173 is derived from the regression coefficient of pFe-pAl plot in Figure 2.6a.

We believe that sediments released from the sea ice also account for the high surface pAl and pFe we measured. Two lines of evidence support this conclusion. For 7 out of 8 surface samples where pAl enrichments were observed, the calculated pFe:pAl molar ratio is 0.17±0.03 (excluding one data at station K1 with pFe:pAl=0.02, Figure 2.9), which is very similar to the local crustal pFe:pAl ratio (0.17, Figure 2.6a and Table 2.4). Furthermore, at the stations where surface pAl were enriched, the mixed layers were often characterized by salinity lower than 30,

indicating substantial freshwater input (Figure 2.10). Low salinity at the surface suggests that pAl and pFe enrichments were due to sediments entrained into the sea ice, which melted and released pTM into the water column. Sediment might be embedded into sea ice after aeolian deposition, and sediment re-suspension, the later implying the formation of sea ice in shallower shelf regions. For example, in the deep Canada Basin, surface enrichment is prevalent for pAl (Figure 2.10), confirming that this sea ice was originally formed in the shallower Chukchi Sea (Lippsett, 2005; Rosen, 2017). In K1 (Subarctic) and CAA3—where surface enrichment of pAl were observed—salinity at the surface was above 30, indicating a negligible input of pAl from melting ice.

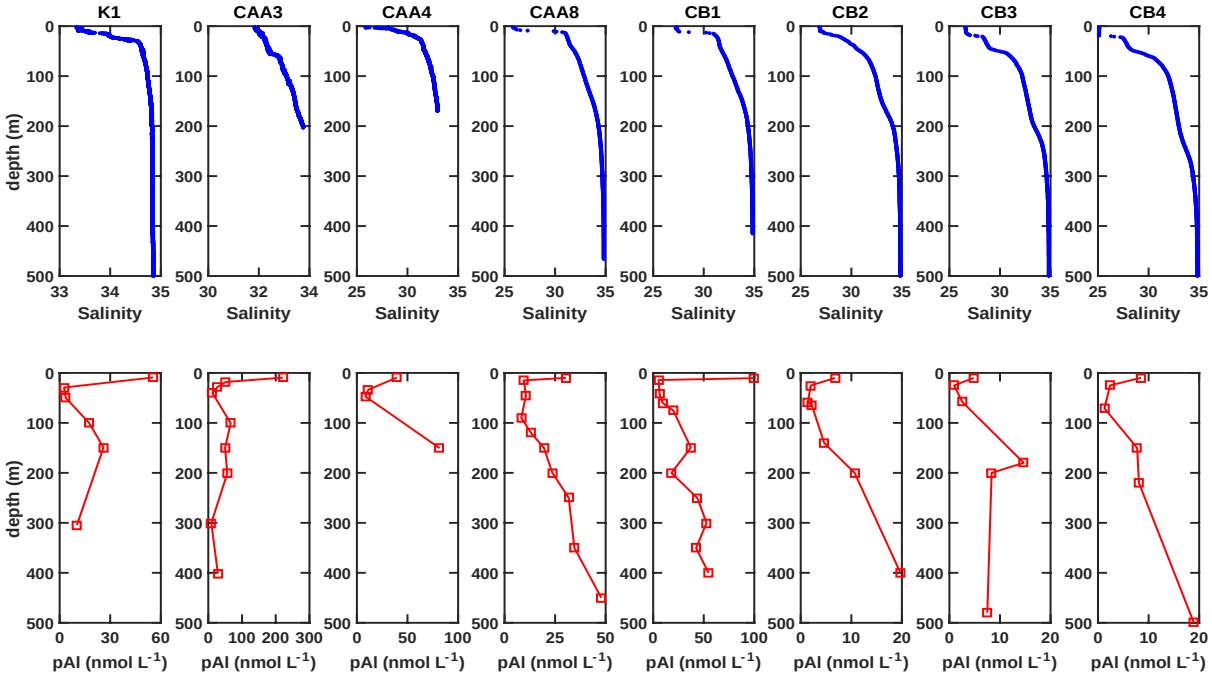

Figure 2.10: Depth profiles of salinity (upper panels) and pAl (lower panels) at stations where surface pAl enrichment was observed. Only data from the upper 500 m are shown. Low salinity (~25) at the surface indicates strong freshwater input.

pAl and pFe are strongly influenced by lateral transport of re-suspended sediments

Figure 2.11 presents the vertical distributions of pFe in some deep stations. The shallow CAA stations are not the focus, where pFe and pAl at the bottom reach up to 100 nM and 400 nM, respectively (Table SI3). On the Chukchi shelf, the pAl concentration could exceed 10000 nM at the bottom depth (A. Aguilar-Islas, pers. comm.). This abundant pAl was attributed to

sediment input, which similarly explained our high value at the bottom of shallow stations. As pFe strongly correlates to pAl, this section will focus on pFe in deep stations only.

In most of these stations (Figure 2.11), pFe concentrations display an increase with depth, or a mid-depth maximum. As particle-reactive metals, the distribution of Al and Fe and their partitioning between dissolved and particulate phases are strongly influenced by scavenging (Orians and Bruland, 1986; Boyd and Ellwood, 2010). However, given the low concentrations of dAl (generally <5 nM in the Beaufort Sea, Giesbrecht et al., 2013), and dFe (<1.5 nM, same investigation as the present study, Jackson et al., in prep.), we expect that scavenging at depth would not likely result in an increase of particulate Al and Fe, of 50 and 5 nM, respectively (Figure 2.11). More specifically, scavenging rate of Fe has recently been refined in the deep Canada Basin (0.0024 nM yr^{-1}, J. Cullen, in prep.). As this region is relatively less influenced by external dFe input (which could mask the signal of scavenging), the dFe-based scavenging rate derived from the deep Canada Basin is more realistic than the global mean, for the present study.

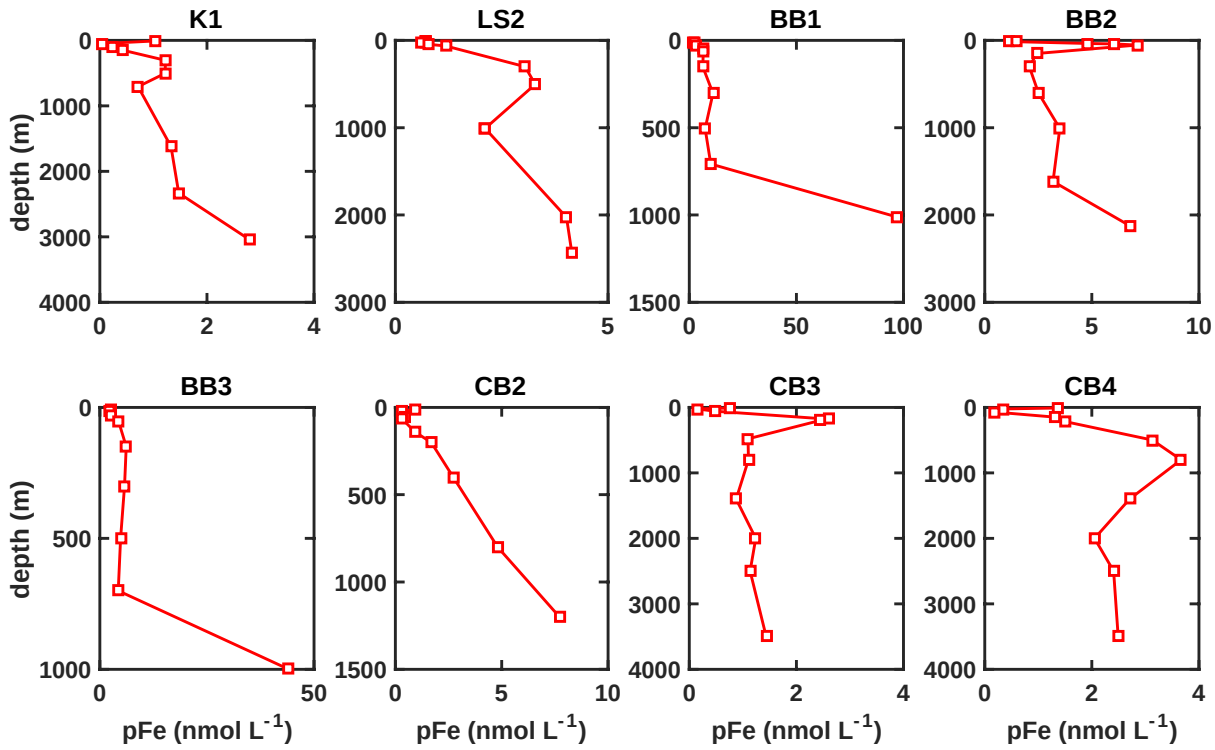

Figure 2.11: Depth profiles of pFe at deep stations across Canadian Arctic Ocean. Note the different scales among stations.

In addition, Fitzsimmons et al. (2017) reported extremely slow sinking rate of 5–10 m yr^{-1} of hydrothermal plume particles, in which pFe occurred within low-density organic matrices. This speed is much slower than typical settling rates for marine aggregates (~17–200 m d^{-1}; Honjo et al., 2008). To examine the importance of scavenging on the vertical distribution of pFe, we apply the recently available particle sinking speed and Fe scavenging rate on station CB2 as an example. The bottom depth of 1200 m converts to 120-240 yr of particle sinking through the water column. Assuming steady state of dFe and pFe, during particle sinking, the increase in pFe concentration caused by scavenging is 0.3-0.6 nM, which is ~10 times lower than our observed increase in CB2 (Figure 2.11). Thus, we conclude that the steady increase with depth or mid-depth maxima of pFe concentration was not due to scavenging. Instead, this features may be caused by lateral transport of re-suspended sediments. For example, station BB1 displays a spike at 300 m in the depth profile of pFe (Figure 2.11). This is attributed to lateral transport of re-suspended sediment from an adjacent sill, the depth of which is approximately 300 m (Figure 2.1).

Lateral transport of re-suspended sediments, containing both redox-mobilized and mechanically re-suspended pFe, has been documented as a significant source of Fe to Ocean Station Papa (900 km off the BC coast in the Subarctic Pacific, Lam et al., 2006), and to the Western Subarctic Pacific (Lam and Bishop, 2008). At two slope stations in the Canada Basin, pAl increases with depth, reaching 50 nM and 100 nM pAl, respectively (Giesbrecht et al., 2013). Our observation suggests that shelf sediment re-suspension and subsequent lateral transport can be a significant source of pAl and pFe in the Canadian Arctic Ocean.

Elements with a significant biogenic component: Cd and Cu

Preferential regeneration of P over Cd at shallow depths

As a phytoplankton nutrient, Cd may serve as the cofactor in carbonic anhydrase, a component in the carbon concentrating mechanism (Xu et al., 2008). Near Bermuda, depth profiles of pCd show great enrichments in surface waters and a monotonic decrease down to 1000 m, resembling the vertical distribution of pP (Sherrell and Boyle, 1992). Similar pCd profiles have been observed in the Weddell Sea (Westerlund and Ohman, 1991) and the central North Pacific (Bruland et al., 1994). In the present study, we also found a prevalent decreasing trend of pCd below the photic zone, suggesting gradual POM remineralization (data not shown).

A well-documented behavior of dCd in the ocean is its positive, linear correlation with phosphate, though with a 'kink' at [PO_4^{3-}] ~1.3 µM (Boyle et al., 1976; Cullen et al., 1999). Different explanations have been proposed for the kink, including preferential algal uptake of Cd over phosphate under Fe limitation (Cullen, 2006) and deeper regeneration of pCd than pP (Frew, 1992). To examine the latter, ratios of pCd:pP are plotted versus depth. Lithogenic correction is not exercised here due to its negligible contribution to pCd and pP in all basins (Figure 2.7 and 2.8). At numerous stations (Figure 2.12), the pCd:pP ratios display an increase with depth to a maximum at 100-200 m, followed by a gradual decrease with depth down to the bottom. This trend indicates preferential remineralization of pP within 0-200 m, and a deeper pCd regeneration. In waters off Southern Morocco, increases in pCd:pP ratios were observed from 30 to 60 m, and were attributed to preferential release of P from decaying organic matter (Waeles et al., 2016). Our findings support this observation, confirming the decoupling of these two elements during remineralization processes.

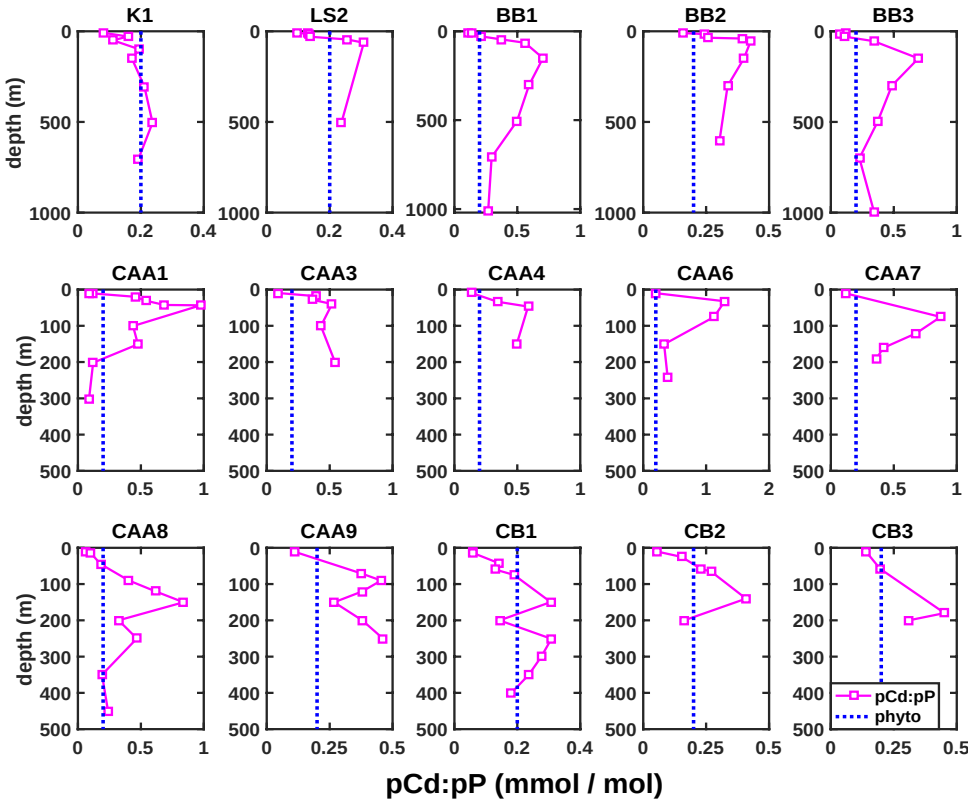

Figure 2.12: Vertical distribution of pCd:pP ratio in the Canadian Arctic Ocean. Data from station CAA5 (few depths were sampled) and CB4 (pCd at depth were below detect limitation) are omitted. Blue vertical bars indicate phytoplankton cellular Cd:P stoichiometry (Ho et al., 2003). Note the scale of y-axis is different in the upper panels.

Cd is considered to be taken up by phytoplankton via non-specific divalent metal transporters (Zn^{2+}, Mn^{2+} and Co^{2+}, Horner et al., 2013). To avoid toxicity, cellular Cd homeostasis is managed by binding imported Cd to cysteine-rich peptides (Grill et al., 1987). The complexes are then transported to a vacuole, or ejected from the cell (Lee et al., 1996; Silver and Phung, 2005). As the membrane-associated phospholipids represent a major biochemical reservoir of phosphorus (Geider and La Roche, 2002), the preferential remineralization of P over Cd (presumably located in vacuoles or cytosols) is somewhat expected. In HNLC surface waters, low dissolved Cd:P ratios have been published and attributed to preferential accumulation of Cd over P by phytoplankton (Saager and de Baar, 1993; Loscher et al., 1998; Elderfield and Rickaby, 2000). The present study suggests that preferential regeneration of P over Cd could occur in the photic zone and should not be ruled out when studying low dissolved Cd:P ratios at surface.

High and constant pCu:pP value at depth due to the presence of ammonium oxidizing archaea

Another micronutrient of interest is copper. A prevalent trend among stations is the approach of non-lithogenic pCu:pP ratio at depth, to a constant molar ratio of 5 mmol Cu (mol $P)^{-1}$ (Figure 2.13). Crustal materials could not account for the constant plateau value across stations, as the pCu:pP was calculated after lithogenic correction.

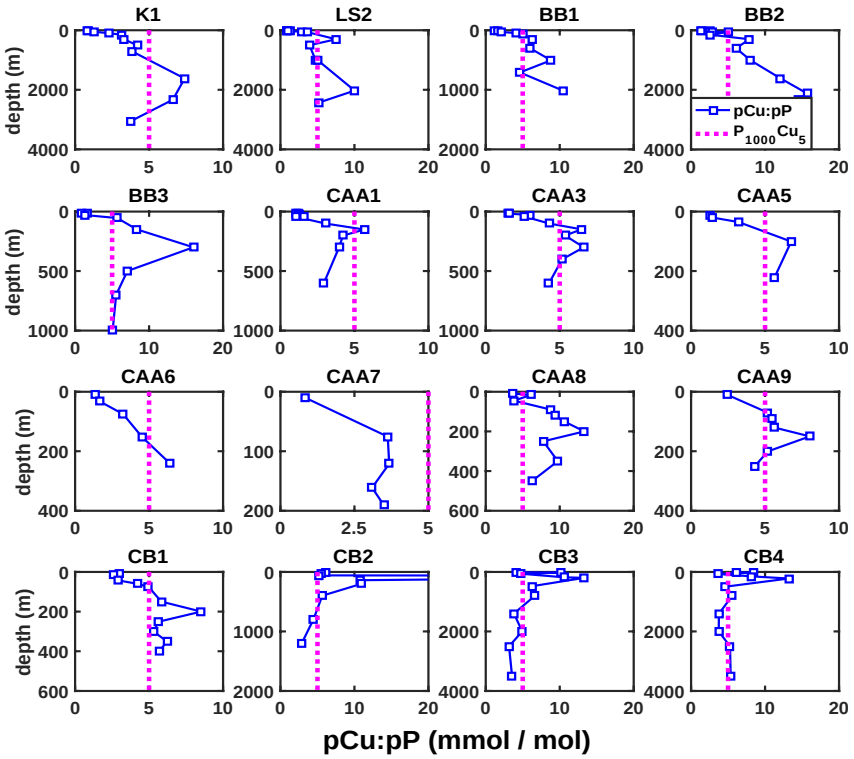

Figure 2.13: Vertical profiles of non-lithogenic pCu:pP across the Canadian Arctic Ocean. Lithogenic correction was applied before calculating pCu:pP. Magenta bars denote a fixed molar stoichiometry of 5 mmol Cu (mol P)$^{-1}$, which often describes the plateau in non-lithogenic pCu:pP at depth. Data from station CAA4 are omitted due to few sampling depths. Note the scale of y-axis is different in the upper panels.

Published phytoplankton Cu quotas range from 0.2-2.1 mmol Cu (mol P)$^{-1}$, derived from lab culture, bulk marine particles and depth profiles of dissolved Cu and P (Twining and Baines, 2013). This range encloses the average Cu quota of 15 phytoplankton species grown under non-limiting conditions, $Cu_{0.4}P_{1000}$ (Ho et al., 2003). Thus, the pCu:pP ratio we measured is 2.4 to 25 times higher than the average phytoplankton Cu quota. The relative constant pCu:pP value at depth across the Canadian Arctic Ocean led us to speculate that the plateau was caused by the dominance of ammonium oxidizing archaea (AOA) at depth. Furthermore, non-lithogenic pCu:pP ratios display a downward increase between surface and 100 or 200 m, depending on stations (Figure 2.13). We attribute this increase to the shallower recycling of P relative to Cu, as shown for Cd.

Four lines of evidence support the influence of AOA on pCu at depth. Firstly, AOA are ubiquitous throughout the global oceans, with strains affiliated with Crenarchaeota accounting for up to 39% of the microbial plankton in meso- and bathypelagic zones (Martens-Habbena et

al., 2009 and references therein). Secondly, many AOA are extremophiles (Konneke et al., 2005), thriving in harsh environments, including polar regions. For example, in the upper halocline of the central Arctic Ocean (55-235 m), polar-specific Crenarchaeota are ubiquitous and abundant (Kalanetra et al., 2009). Moreover, AOA are large enough (sub-micron size, Hatzenpichler, 2012) to be captured on Supor filters. Thirdly, AOA possess a cellular Cu demand 10 times higher than phytoplankton (Amin et al., 2013). Specifically, growth rate of AOA *Nitrosopumilus maritimus* equals 76% of its maximum growth rate under $[Cu^{2+}]$ of 10^{-13} mol L^{-1}, whereas the oceanic diatom *Thalassiosira oceanica* achieves 65% of its maximum growth rate at $[Cu^{2+}]$ of ~10^{-14} mol L^{-1} (Peers et al., 2005). The high Cu requirement of AOA is due to numerous Cu-dependent enzymes involved in both ammonia oxidation and electron transfer. This large quota could account for the high pCu:pP ratios we measured at depth. Fourthly, ammonia was usually depleted below 100 m in our dataset, suggesting intense nitrification at depth where photo-inhibition is absent (Guerrero and Jones, 1996). For example, for the Labrador Sea, Baffin Bay and CAA data combined, only 44 out of 622 samples below 100 m showed NH_4^+ higher than 1 nM (J. Tremblay, in prep.). Similarly, O_2, which is required for nitrification by AOA, constantly exceeded 200 µM in water columns across the Canadian Arctic Ocean, suggesting potential for nitrification. In summary, we suggest that AOA are abundant below 100 m, where nitrification is not photo-inhibited. Their nitrifying activity results in low NH_4^+ at depth and high pCu:pP, associated with their biomass.

Elements with a predominant redox cycle: Mn

Spike of pMn concentration at 100-200 m due to manganese oxidizing bacteria

Depth profiles of pMn concentration are characterized by a maximum at 100-200 m, which is prevalent across the entire Canadian Arctic Ocean (Figure 2.14). A peak of pMn concentration typically occurs below the photic zone, due to a combination of Mn (II) oxidation to MnO_x, and Mn scavenging onto particles (reviewed by Hansel, 2017). In support of our findings, Morton et al. (in prep.) also observed a maximum of pMn at 100-200 m in the Chukchi Sea. Similarly, Cid et al. (2012) reported a maximum of total dissolvable Mn (dMn and MnO_x) at ~200 m in waters on the slope and in the center of the Beaufort Sea. In McMurdo Sound in the Ross Sea, Noble et al. (2013) also detected a pMn concentration spike at ~150-300 m. We attribute the peak in pMn

concentration at 100-200 m across the Canadian Arctic Ocean to the presence of Mn-oxidizing bacteria.

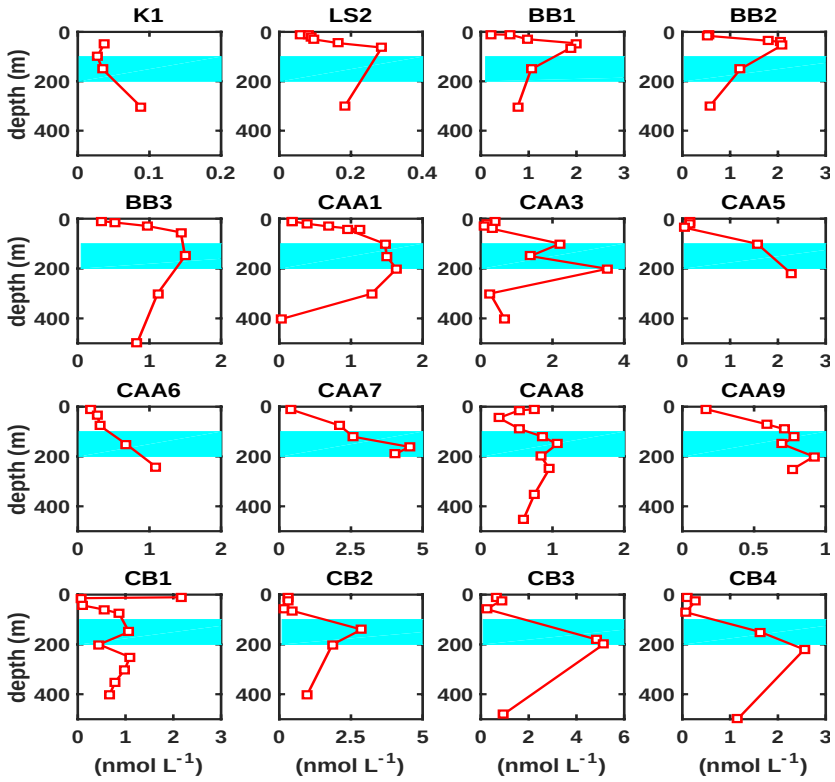

Figure 2.14: Vertical distribution of particulate Mn in the Canadian Arctic Ocean. Data from station CAA4 (few depths were sampled) are omitted. Blue box indicates the depth interval of 100-200 m. Note the scale of x-axis is different among panels. Only data from the upper 500 m of the water column are shown.

The concentration of pMn in the Canada Basin is higher than at numerous CAA stations (Figure 2.5). In contrast, the concentrations of pAl and pP—proxies for lithogenic and biogenic particles, respectively—in the Canada Basin are considerably lower than those in the CAA (Figure 2.5). Therefore, in the Canada Basin, abundant pMn in the scarcity of lithogenic and biogenic particles indicates authigenic pMn via oxidation, instead of scavenging. In the presence of O_2, Mn (II) oxidation rates are five orders of magnitude faster by Mn-oxidizing bacteria than by abiotic processes (Nealson et al., 1988; Tebo, 1991). Therefore, we attribute the spike of pMn at 100-200 m in the Canada Basin to the activity of Mn-oxidizing bacteria, which supposedly thrive in waters with higher dMn (Tebo et al., 2005). Indeed, complementary data on dMn depth profiles at our stations (Figure 2.15, data source: M. Colombo) confirm a peak of dMn at depths

where we observed a peak in pMn. The peak of dMn occurs on the top 250 m, and is associated with the Upper Halocline Water (UHW, data source: A. Beaupré-Laperriere).

The UHW originates in the Pacific, and shoals up along its path from CB4, via CB3 and CB2, to CB1 (Figure 2.15). The core of the UHW corresponds to a peak in the depth profile of dMn in CB2, CB3 and CB4 (Figure 2.15). Remarkably, the spike of pMn also occurs at the UHW core in CB2, CB3 and CB4 (Figure 2.14). Thus, in these 3 stations, Mn-oxidizing bacteria are fueled by a dMn input, during the transition of Pacific water along 100-200 m depth. In CB1, the core of UHW is present at ~100 m, whereas the spike of pMn occurs at ~150 m. The deeper occurrence of these putative Mn-oxidizing bacteria possibly results from photo-lability of MnO_x.

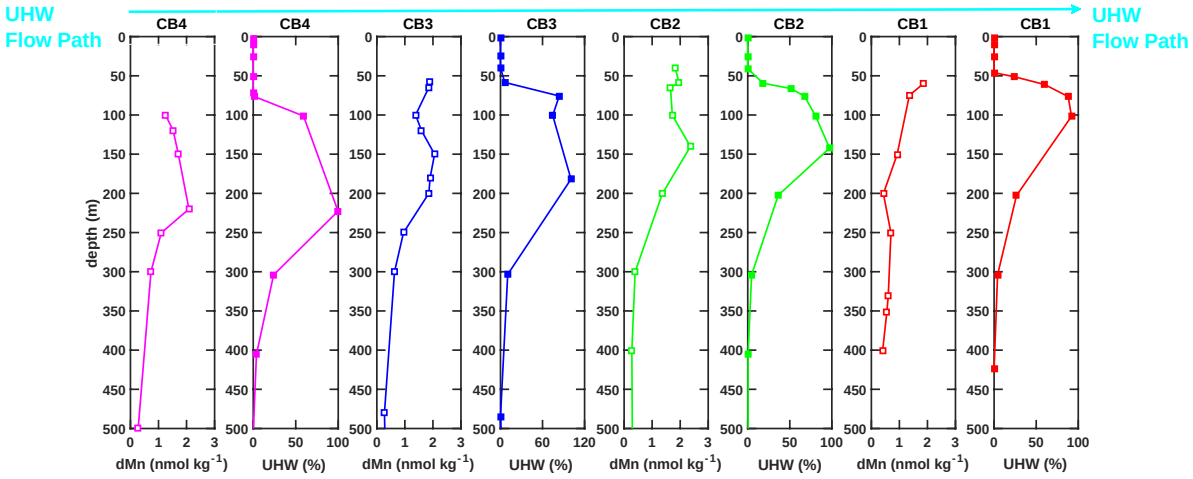

Figure 2.15: Depth profiles of dissolved Mn in the Canada Basin (a, c, e, g, data from M. Colombo), along depth profiles of the fraction of Upper Halocline Water (b, d, f, h, data from A. Beaupré-Laperriere). Only data from upper 500 m of water column are shown.

Although Mn oxidation is thermodynamically favorable, there is no unequivocal evidence asserting that Mn-oxidizing bacteria are chemoautotrophic (Tebo et al., 2005). The fact that pMn concentrations in the oligotrophic Canada Basin are comparable to other Canadian Arctic Ocean regions investigated, suggests that Mn-oxidizing bacteria might be chemoautotrophic.

Bottom enrichment of pMn due to sediment re-suspension and redox mobilization

Some stations (K1, BB1, BB3, CAA7 and CB4) show a bottom enrichment of pMn, as indicated by Figure 2.16. Two mechanisms could potentially account for this bottom enrichment, namely sediment re-suspension and redox mobilization. The former is often associated with

benthic nepheloid layers (elevated numbers of particles), which provide the water column with particulate Al, Fe, Mn, etc. For example, Lam et al. (2015) reported MnO_2 concentration up to 2.1 µg L^{-1} (or 25 nM, 0.8-51 µm in size) within nepheloid layers in the North Atlantic Ocean. MnO_x could be reduced biotically in the sediments (Stone, 1987; Loveley and Phillips, 1988; Myers and Nealson, 1988). The redox mobilization of Mn is mediated by bacteria and archaea in sediments, which could anaerobically oxidize carbon, using MnO_x as a terminal electron acceptor (reviewed by Hansel, 2017). Once MnO_x are reduced, the product (Mn^{2+}) may diffuse upward, to be re-oxidized and precipitated upon contact with O_2-rich bottom waters (Brujevicz, 1938).

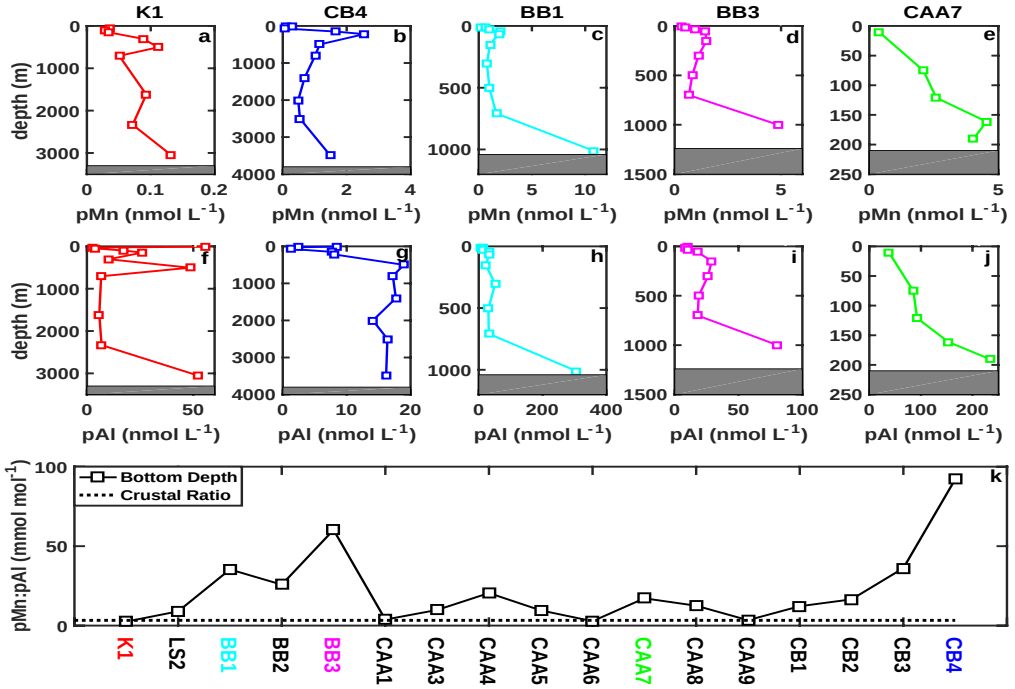

Figure 2.16: Depth profiles of pMn at stations where bottom input is evident (a-e), supplemented by depth profiles of pAl (f-j). Grey boxes indicate marine sediments. pMn:pAl ratio at the deepest depth of each station (k); the continental surface Precambrian Canadian shield composition (Shaw et al., 1976) is indicated with a dotted horizontal line.

To examine sediment re-suspension, we plotted the vertical profiles of pAl (a proxy of crustal material) at stations characterized by bottom enrichment of pMn. To investigate Mn redox mobilization, we calculated the ratio of pMn:pAl in the deepest sample of each station, and compared the results with the Precambrian shield composition in Canada (Figure 2.16). In the

absence of redox mobilization, a bottom sample is expected to display a pMn:pAl value similar to that of the continental crust, regardless of the extent of sediment re-suspension. In contrast, a pMn:pAl value higher than crustal ratio indicates redox mobilization, the signal of which could be superimposed on that of sediment re-suspension.

For example, at station K1, the bottom sample is enriched in pMn, as well as pAl, suggesting the presence of sediment re-suspension (Figure 2.16). Furthermore, the pMn:pAl ratio of the bottom sample is analogous to crustal materials, indicating the absence of Mn redox mobilization. In contrast, at CB4, the bottom sample is not enriched in pAl, suggesting the absence of sediment re-suspension. However, a spike of pMn and a high pMn:pAl ratio at the bottom sample suggest the presence of Mn redox mobilization. Bottom enrichment of pMn is also identified at BB1, BB3 and CAA7, due to collectively sediment re-suspension and Mn redox mobilization (Figure 2.16).

In anoxic marine sediments, before MnO_x is utilized to oxidize organic matter, denitrification may occur, reducing nitrate to nitrous oxide (N_2O) and ultimately N_2 gas (energy yield per mol of organic C is 453 KJ for denitrification and 349 KJ for Mn reduction; Jorgensen, 2000). As an intermediate product in denitrification, N_2O is often released from anoxic marine sediments (Naqvi et al., 2010). During our cruise, Fenwick et al. (2016) measured N_2O concentration in the water column, reporting a bottom enrichment of N_2O at CAA7. This bottom N_2O input indicates the occurrence of denitrification in the sediments, and suggests high probability of Mn redox mobilization, which is confirmed in Figure 2.16.

In anoxic marine sediments, after MnO_x is utilized to oxidize organic matter, Fe(III) oxides could be used consequently (energy yield per mol of organic C is 114 KJ for Fe reduction; Jorgensen, 2000). We calculated the ratio of pFe:pAl in the deepest sample of each station, and compared the results with the Precambrian shield composition in Canada (data not shown). The pFe:pAl ratios at the bottom depths of BB1, BB3 and CAA7 largely exceed crustal ratio, indicating Fe redox mobilization, thus confirming that of Mn (Figure 2.16). The presence of Mn—but absence of Fe—redox mobilization at BB2 (central basin, Figure 2.1) might be due to lower organic matter input, compared to Baffin Bay shelf regions (Algora et al., 2013). The latter include BB1 and BB3, where progressive oxidation of organic matter is apparent, resulting in bottom inputs of N_2O, Mn and Fe.

2.3.4 Canada Basin: connections among pBa, pMn, pCo and pCu

This section is a detailed study of the Canada Basin, suggesting that manganese oxidizing bacteria could mediate the distributions and behaviors or Co, Cu and Ba. When calculating metal stoichiometry in this section, lithogenic correction is not conducted unless specified, as its contribution to pMn, pCo, pCu and pBa is negligible in the Canada Basin (Figure 2.7).

Maxima of pBa at 100-200 m coincide with maxima in AOU, indicating barite production during organic matter degradation

The depth profiles of pBa display a peak at ~100-200 m in CB2, CB3 and CB4, accompanied by a concurrent peak of AOU (Figure 2.17b-d). Particulate Ba in seawater is dominated by barite (Dehairs et al., 1980), which is largely under-saturated throughout the entire water column. Formation of barite in seawater is considered to occur mainly in micro-environments, where dBa released during organic matter decay and oxygen consumption causes super-saturation with respect to barite, inducing *in situ* precipitation (Bishop, 1988). In the mesopelagic zone, a correlation between pBa and AOU is well-documented, making pBa a proxy for bacterial remineralization rates (Dehairs et al., 2008). Therefore, concomitant peaks of pBa and AOU at ~100-200 m in the Canada Basin suggest intensive remineralization of organic matter.

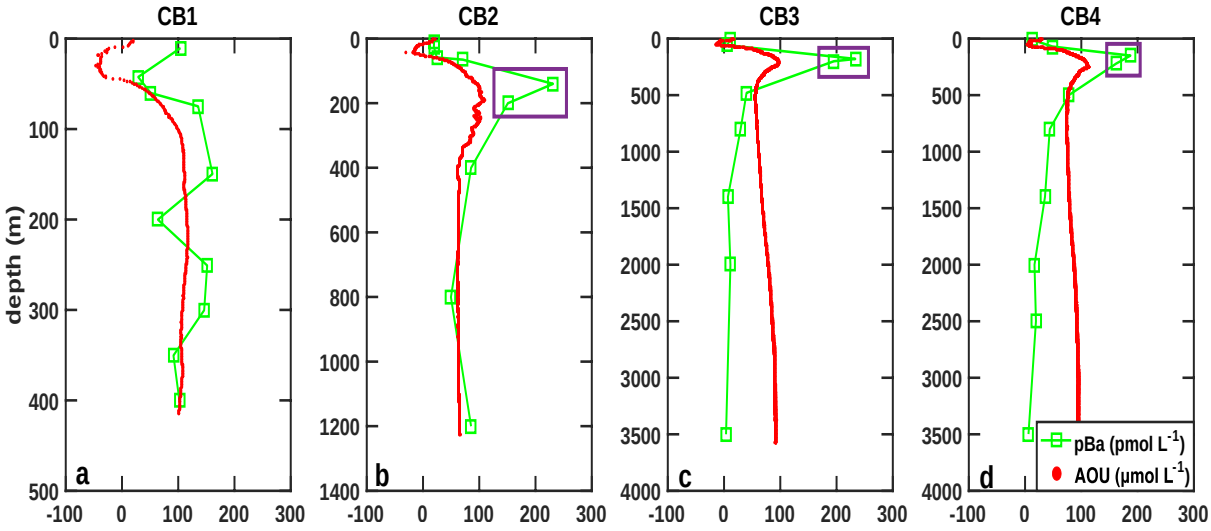

Figure 2.17: Depth profiles of pBa (green squares) and AOU (red dots) at 4 stations in the Canada Basin (a-d); At CB2, CB3 and CB4, samples at 100-200 m depth with maxima values of pBa are enclosed in purple boxes, which include concomitant AOU peaks.

Constant P-Mn-Co-Cu-Ba stoichiometry due to Mn oxidizing bacteria, that co-oxidize Co, and contain numerous multi-Cu oxidases

Interestingly, this 100-200 m depth interval in the Canada Basin is suggested to host abundant manganese oxidizing bacteria (see discussion above). Therefore, we calculated the metal molar stoichiometry of those six high-pBa samples from CB2, CB3 and CB4 (Figure 2.17, in purple box). The calculated stoichiometry, $P_{1000}Mn_{542\pm223}Co_{8\pm2}Cu_{11\pm2}Ba_{34\pm6}$, is extremely different from the average quota of 15 phytoplankton species grown under non-limiting conditions ($P_{1000}Mn_{3.8}Co_{0.21}Cu_{0.38}$, Ho et al., 2003). In essence, the particulate Mn, Co and Cu to P ratios in these six samples are approximately 140, 40 and 30 times higher than those of phytoplankton, respectively. Furthermore, these samples show high Ba content, which is rarely measured in phytoplankton stoichiometry studies (see discussion below).

Given the orders-of-magnitude difference in metal quotas between phytoplankton and those six samples, the standard deviations associated with the latter are considered to be small. Thus, the six samples in which manganese oxidizing bacteria is inferred possess a constant P-Mn-Co-Cu-Ba stoichiometry. In the ocean, manganese oxidizing bacteria are known to co-oxidize cobalt during manganese oxidation (Lee and Tebo, 1994; Moffett and Ho, 1996), the latter involving multi-Cu oxidases (Tebo et al., 2005). Therefore, we suggest that the high Mn and Co content in these six samples are due to biotic production of Mn oxides and Co oxides, while elevated Cu content indicates high activity of multi-Cu oxidase in Mn oxidizing bacteria.

The Mn-Co stoichiometry is further compared to literature value, where manganese oxidizing bacteria could be inferred. Noble et al. (2013) published pMn profiles in McMurdo Sound, Ross Sea. At two out of their three stations, pMn display a spike at ~150-300 m. At both stations, the pMn spike is accompanied by a pCo spike, with a pMn:pCo ratio of ~125. Dulaquais et al. (2017) reported the concentration of pCo in the Mediterranean Sea. A strong positive correlation between pCo and pMn (R^2=0.9; n=43) was recorded between 50 m and the bottom depth, which was attributed by removal of dCo onto MnO_x, mediated by manganese oxidizing bacteria. Interestingly, the pMn:pCo ratio derived from the correlation is 90. For those six samples in Canada Basin, our calculated pMn:pCo ratio averages at 68, close enough to 125 or 90, inferred from the two studies above. This agreement implies a pMn:pCo ratio of ~100 for oceanic manganese oxidizing bacteria among global ocean.

Biogenic barite is protected from dissolution at depth due to intracellular storage or MnO_x coating

At 100-200 m of CB2, CB3 and CB4, abundant dMn entrained by Pacific water presumably fuels manganese oxidizing bacteria (see discussion above). This depth coincides with the depth where intensive organic matter remineralization occurs, resulting in maxima of pBa and AOU. Was the formation and maximum of pBa mediated by manganese oxidizing bacteria?

When pBa was plotted versus pCu in the Canada Basin (Figure 2.18), a robust correlation was observed below 100 m down to the bottom. This is counter-intuitive, as we have suggested that pCu is presumably associated with the multi-Cu containing oxidases; while barite should dissolve during particle sinking—due to prevalent barite under-saturation in seawater (Dehairs et al., 1980; Bishop, 1988; Bishop and Wood, 2008). Therefore, pCu and pBa in the water column are expected to be controlled by distinct processes, which should have decoupled their particulate depth profiles.

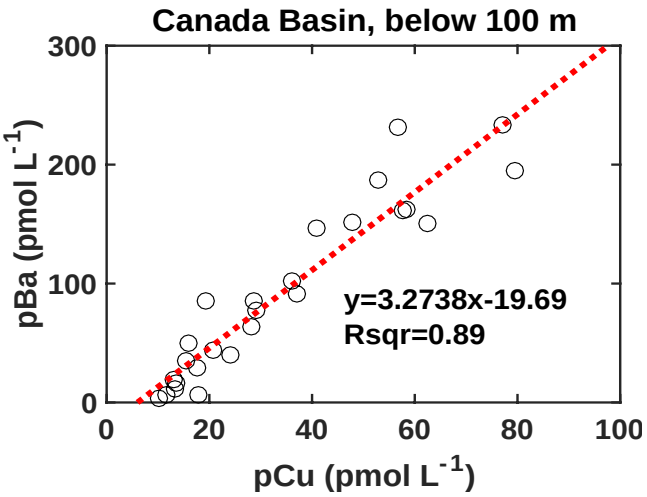

Figure 2.18: Correlation between pBa and pCu in the Canada Basin for samples collected between 100 m and the bottom depths. Data above 100 m are excluded due to photo-reduction of pMn.

Aiming to estimate the loss of pBa due to barite dissolution during particle sinking, we used an average depth-weighted dissolution flux (0.4 µg cm^{-2} yr^{-1}) from barite to dBa at two stations in the Atlantic Ocean (flux of 0.42 and 0.36 µg cm^{-2} yr^{-1} for 151-5304 m, and 105-3267 m, respectively; Dehairs et al., 1980). Assuming Stokes settling for barite particles (diameter of 5 µm, Griffith and Paytan, 2012; density of 4.5 g cm^{-3}, Deharis et al., 1980), and the following

physical properties of seawater, temperature of 0ºC and salinity of 35, we calculated a sinking rate of barite of 80000 cm yr^{-1}. Dividing dissolution flux (μg cm^{-2} yr^{-1}) by sinking rate (cm yr^{-1}) yields a loss of barite concentration during particle sinking of 40 pmol L^{-1}. This barite dissolution should be able to substantially draw down pBa during particle sinking, whereas pCu is likely remineralized by a different process. Therefore, the robust pBa-pCu correlation below the photic zone leads to the hypothesis that, biogenic barite was protected from dissolution, by preservation inside a microbial cell, or in manganese oxide shell.

So far, we have suggested that, manganese oxidizing bacteria co-oxidize cobalt, creating peaks in depth profiles of pMn and pCo. These organisms have a high Cu demand and possibly also mediate the precipitation of barite, resulting in high pCu and pBa where they occur. Furthermore, biogenic barite may either be stored intracellularly, or within MnO_x, both mechanisms protecting barite from dissolution during particle sinking.

Evidence for barite precipitation by Mn oxidizing bacteria: wherever MnO_x are present, pMn:pBa ratio is relatively constant

It is worth noting that we have no direct evidence to support that manganese oxidizing bacteria precipitate barite. Undeniably, barite formation is considered to occur during organic matter degradation, which also releases other dissolved metals. Specifically, dMn and dCo are used by manganese oxidizing bacteria for production of metal oxides. Thus, one could argue that barite is produced by other organisms, and that the concomitant maximum of pBa, pMn and pCo is a coincidence. To examine the importance of manganese oxidizing bacteria to pBa, we tested the pMn-pBa relationship among entire Canadian Arctic Ocean. First, data from the top 100 m and bottom depths were excluded due to Mn photo-reduction and Mn redox mobilization, respectively. Second, data of pMn:pP ratios larger than 50 mmol Mn (mol P)$^{-1}$ were selected, with 49 samples meeting this criteria. This pMn:pP threshold was chosen because this is an order of magnitude higher than the average phytoplankton Mn quota (3.8 mmol Mn (mol P)$^{-1}$; Ho et al., 2003), thus suggesting the presence of manganese oxidizing bacteria. Lithogenic corrections were then conducted, as trace elements in the CAA are strongly influenced by terrestrial materials (in contrast to the Canada Basin, data not shown). For the 49 samples across the Canadian Arctic Ocean, non-lithogenic pMn:pBa was 16±12 mol Mn (mol Ba)$^{-1}$. For the 6 samples in the Canada Basin, non-lithogenic pMn:pBa was similar—17±7 mol Mn (mol Ba)$^{-1}$. It

thus appears that wherever MnO_x are present, the ratio of non-lithogenic pMn:pBa is relatively stable, suggesting the coupling between MnO_x and $BaSO_4$ production.

Although barium-rich waters favoring the formation of romanechite over todorokite (Feng et al., 1998; Manceau et al, 2007), these two Mn minerals have analogous Mn:Ba ratios of 6:1 and 5:1, respectively. These values are similar to the non-lithogenic pMn:pBa value of 17±7, calculated from 49 high-pMn samples across entire Canadian Arctic Ocean. This agreement indicates that the pBa is more likely to be found within manganese oxides shell, rather than inside microbial cells.

2.3.5 Canadian Arctic Archipelago: pTM behaviors under strong lithogenic input

pCd distribution is dominated by biological processes, and pCd:pP ratios are lower at the surface than at depth

The CAA receives abundant input of terrestrial materials (Figure 2.8), contributing largely to particulate Mn, Cu and Zn. In contrast, pCd and pP are negligibly influenced by lithogenic particles in the CAA. As discussed in section 2.3.2, strong correlation between dCd and phosphate is often observed in seawater, suggesting similar biogeochemical behaviors (Boyle et al., 1976; Bruland et al., 1978). In the CAA, below 100 m (Figure 2.19a), a robust correlation between pCd and pP is observed, indicating that the distribution of pCd is dominated by biological processes. The slope of the regression equals 0.4 mmol Cd (mol P)$^{-1}$, similar to the average stoichiometry of 15 phytoplankton species grown under non-limiting conditions, $P_{1000}Cd_{0.21}$ (Ho et al., 2003). Interestingly, pCd:pP ratios within mixed layer depth (~10 m) average at 0.11±0.04 mmol Cd (mol P)$^{-1}$ (n=10 for CAA, or n=22 for all four basins investigated), which is lower than that below 100 m [0.4 mmol Cd (mol P)$^{-1}$, regression line in Figure 2.19a].

The mechanism leading to consistently low pCd:pP in the surface samples across the Canadian Arctic Ocean remains unknown. Diatoms are believed to be the greatest players in carbon export out of surface waters (Jin et al., 2006). Therefore, diatom-derived particles possibly dominate pP and pCd below 100 m, while other phytoplankton might dominate the community at the surface. Oceanic diatoms, such as *T. oceanica* and *P. inermis*, display higher Cd:P ratios (0.87 mmol Cd (mol P)$^{-1}$, Lane et al., 2009) relative to other ecologically important phytoplankton (0.4 mmol Cd (mol P)$^{-1}$, Ho et al., 2003). Therefore, the low pCd:pP ratios at the surface might be attributed to the presence of non-diatom phytoplankton.

Alternatively, the low pCd:pP ratios at the surface could be attributed to passive adsorption of phosphorus onto cell surfaces. Sanudo-Wilhelmy et al. (2004) reported that in field-collected phytoplankton, surface-adsorbed P could rival or exceed intracellular P. The existence of the surface-adsorbed P suggests that phytoplankton P uptake could be a two-step kinetic process, including adsorption and internalization, similar to Fe uptake. They also demonstrate that phytoplankton have developed mechanisms to access at least part of the surface-adsorbed P pool. In summer and fall, the CAA is characterized by low productivity and biomass of large phytoplankton cells (>5 μm) and relatively high abundance of eukaryotic picophytoplankton (<2 μm) (Ardyna et al., 2011). The large surface area-to-volume ratio of small phytoplankton could facilitate P adsorption, thus lowering pCd:pP in particles in the mixed layer. Therefore, this extracellular P pool potentially accounts for the several-fold difference in pCd:pP between samples at surface and at depth, where P adsorbed onto cell surface has been efficiently recycled.

MnO_x in the CAA presumably reflects its capacity to adsorb Al

When pMn is plotted versus pAl for samples below 100 m (to rule out Mn photo-reduction in upper waters), no significant correlation is observed. However, a linear regression with a slope of 28 mmol Mn (mol Al)$^{-1}$ describes half of the data (Figure 2.19b). Considering that the literature crustal ratio is only 3-6 mmol Mn (mol Al)$^{-1}$, data falling onto the line probably indicate the presence of MnO_x. Manganese oxides have negative surface charges near neutral pH (Yao and Millero, 1996), and have been reported to adsorb cations such as Co, Cu and Cd (Murray and Dillard, 1979; Fu et al., 1991). Thus, the pMn-pAl covariance with a slope of 28 mmol Mn (mol Al)$^{-1}$ might reflect the capacity of authigenic MnO_x to adsorb Al. The other half of the data in Figure 2.19b, which have lower pMn:pAl ratios, may indicate pAl contribution by lithogenic particles.

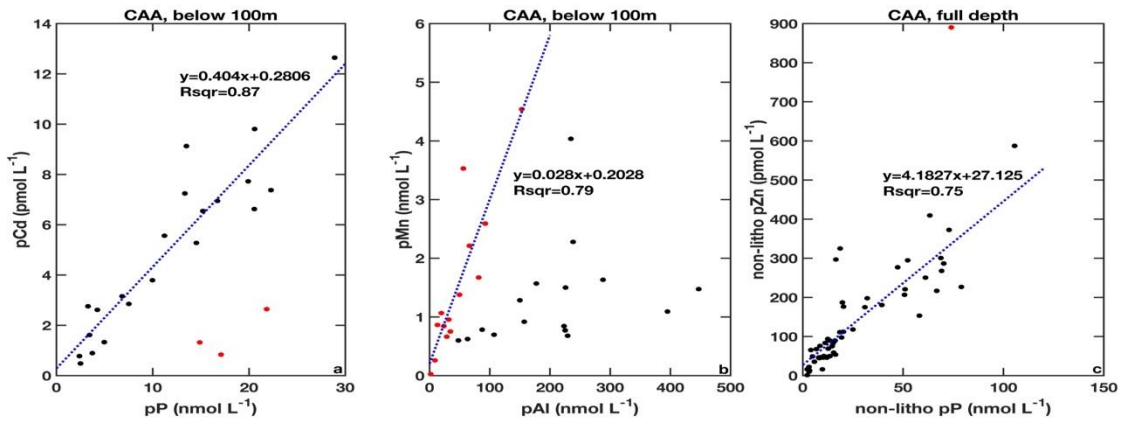

Figure 2.19: Trace metal correlations in the CAA, where lithogenic inputs are significant, between pCd-pP below 100 m (a), between pMn-pAl below 100 m (b), and between non-lithogenic pZn-pP at all depths (c). In panel a and c, potential outliers are in red, and are excluded from the regression; In panel b, the dotted line describes data in red, presumably indicating the influence by MnO_x; samples above 100 m are excluded, due to photo-reduction of pMn.

High pCu:pP ratios at surface correspond to high dissolved Cu concentration, resulting from anthropogenic Cu input

In the CAA, non-lithogenic pCu:pP ratios in the top 10 m average at 1.4±0.4 mmol Cu (mol P)$^{-1}$ (n=10, Table SI3). Intracellular Cu quotas of phytoplankton at steady-state, non-toxic conditions vary between 0.36 and 9.93 µmol Cu (mol C)$^{-1}$ (Sunda and Huntsman, 1995; Ho et al., 2003; Annett et al., 2008; Guo et al., 2012). This corresponds to 0.04 to 1.1 mmol Cu (mol P)$^{-1}$, if Redfield C:P stoichiometry is applied. Our non-lithogenic pCu:pP at the surface is slightly higher than the upper bound of these non-toxic-Cu cultured phytoplankton quotas, but lower than published quotas under Cu toxicity (15 to 150 mmol Cu (mol C)$^{-1}$, or 1.6 to 16 mmol Cu (mol P)$^{-1}$; Sunda and Huntsman, 1995; Chang and Reinfelder, 2000). Thus, in contrast to pCd which shows a surface depletion relative to pP, pCu displays a surface enrichment relative to pP.

Surface enrichments in pCu in the CAA might be associated with high anthropogenic Cu inputs and subsequent phytoplankton Cu uptake. Measurements by other researchers in the same Arctic expedition provide some evidence for this hypothesis. Firstly, profiles of dCu often show a peak at the surface (Jackson et al., in prep.), contradicting one's expectation of a depletion in dCu due to phytoplankton uptake. This finding suggests that the distribution of dCu in the CAA is not dominated by phytoplankton uptake and remineralization. Secondly, Colombo and Orians (in prep.) observed an enhancement of pCu relative to pAl in some CAA rivers, and attributed this enrichment to anthropogenic input from nearby mines. Sholkovitz et al. (2010) reported high

Cu solubility in anthropogenic aerosols from non-Saharan sources (10-100%), implying the potential of anthropogenic pCu to dissolve and release dCu. The elevated dCu concentration at the surface in CAA waters corresponds to high Cu quota within the mixed layer (1.4±0.4 mmol Cu (mol P)$^{-1}$). Guo et al. (2012) found a significant positive effect of non-toxic dCu concentrations in the growth media (ranging from 1.96 to 10.2 nM) on phytoplankton Cu quotas, regardless of algal class. Therefore, it appears that the high non-lithogenic pCu:pP ratios in surface samples from the CAA was caused by enhanced levels of dCu in surface waters, which originated from soluble anthropogenic Cu, and ultimately resulted in enhanced Cu quota in phytoplankton.

pZn is strongly dominated by both lithogenic and biogenic materials, phytoplankton with high Zn quotas deplete dissolved Zn at surface

When studying pZn in the CAA, lithogenic correction is also required due to its substantial contribution to total pZn (Figure 2.8). Non-lithogenic pZn and pP display a robust correlation in the entire water column (Figure 2.19c). The regression slope, 4.2 mmol Zn (mol P)$^{-1}$, should represent phytoplankton Zn stoichiometry. Zn quota of field-collected phytoplankton are up to 5.1 and 8.1 mmol Zn (mol P)$^{-1}$, in the Equatorial Pacific and the Southern Ocean, respectively (Twining et al., 2004; Twining et al., 2011). For cyanobacteria, in the Sargasso Sea, *Synechococcus* Zn quota are up to 25 mmol Zn (mol P)$^{-1}$ (Twining et al., 2010), while cultured cyanobacteria *Cyanophora paradoxa* and *Chlorarachnion reptans* exhibit Zn quotas of 5±0.8 and 4.7±0.1 mmol Zn (mol P)$^{-1}$, respectively (Quigg et al., 2011). Our Zn quota agrees well with previous studies, though are significantly higher than the average stoichiometry of 15 phytoplankton species grown under non-limiting Zn conditions, $P_{1000}Zn_{0.80}$ (Ho et al., 2003). The low value in the latter study was attributed to low dZn in growth medium and extensive substitution of Cd for Zn within the cells. In the CAA, dZn profiles often show a depletion at the surface (Jackson et al., in prep.), which is typical for algal nutrients. We suggest that the depletion of dZn in surface samples is due to uptake by phytoplankton, which have high Zn quota.

As a summary for this section, trace metals display distinct biogeochemical behaviors in the CAA. Most pTM were substantially influenced by lithogenic materials, except for pCd, for which lithogenic contribution was negligible. Phytoplankton within the mixed layer display an

enrichment of pP relative to pCd, which might be due to phosphorus adsorbed onto cell surface. This process might be especially significant in the CAA, where the phytoplankton community is dominated by small cells with high surface area-to volume ratios. Below 100 m, once this adsorbed pP is regenerated, a robust correlation between pCd and pP is observed. Surface phytoplankton show higher Cu quota than literature Cu stoichiometry under optimal conditions, presumably due to high levels of dCu concentration resulting from anthropogenic input. After lithogenic correction, pZn strongly correlates with pP throughout the entire water column, indicating that pZn is controlled by both lithogenic and biogenic particles. Furthermore, MnO_x seem prevalent in the CAA, adsorbing higher content of Al, and leading to a lower pMn:pAl ratio in this basin relative to those in the Canada Basin.

2.4 Summary

The present study reports for the first time spatial and vertical distributions of eleven particulate elements in the Canadian Arctic Ocean (Al, Cd, Pb, P, V, Mn, Fe, Co, Cu, Zn and Ba). The dataset described herein includes samples collected between 10 and 3500 m (near bottom), at 17 stations located in the Labrador Sea, Baffin Bay, CAA and Canada Basin. Our results indicate that particulate elements in the CAA were strongly influenced by lithogenic materials, with the exception of P and Cd. In contrast, the contribution of lithogenic particles to total particulate element concentration (except for Al, Fe and V, see below) was negligible in all other basins. The concentrations of particulate Al, Fe and V strongly correlated with each other in all basins, with their relative abundances similar to those in the continental crust. Trace elements displayed various types of depth profiles. For example, elements with a strong lithogenic component (Al, Fe and V) were characterized by a maximum at the surface. Elements with a significant biogenic component (Cd and Cu) were characterized by a decrease in concentration with depth. Furthermore, the preferential remineralization of P over Cd at shallow depth is reported. In some stations across the entire Canadian Arctic Ocean, the molar ratio between particulate Cu and P approached a plateau in the meso- or bathy-pelagic zone. The plateau represents a fixed stoichiometry of 5 mmol Cu $(\text{mol P})^{-1}$, which is 2.4-25 times higher than cellular Cu quota of phytoplankton. This high quota is attributed to the presence of ammonium oxidizing archaea, which require numerous Cu-dependent enzymes. In addition, Mn, a trace element with a predominant redox cycle, showed maximum concentrations between 100-200 m

across the entire Canadian Arctic Ocean, and an enrichment at depth, the latter due to sediment re-suspension and/or redox mobilization. We examined data from Canada Basin (low lithogenic inputs, low productivity) and CAA (high lithogenic inputs, high productivity) for case studies. In the Canada Basin, complementary data from collaborators suggest that Mn-oxidizing bacteria are fueled by excess dMn input, during the transition of Pacific water into the Canada Basin along 100-200 m depth. In addition, we propose interactions between biogenic production of manganese oxide, cobalt oxide and barite. In addition, the robust pBa-pCu correlation throughout the aphotic zone leads to the hypothesis that, biogenic barite is protected from dissolution, most likely by entrainment into the manganese oxides shell. In the CAA, bioactive pTM displayed distinct biogeochemical behaviors. For example, pCu in the mixed layer was elevated relative to pP, presumably due to high dCu at surface, resulting from anthropogenic input. In contrast, pCd in the mixed layer was lower relative to pP, likely caused by phosphorus adsorbed onto the cell surfaces of small phytoplankton that thrive there.

Chapter 3: Physiological Response on Iron Uptake by Subarctic and Arctic Phytoplankton Assemblages under Ocean Acidification and High Irradiance

3.1 Introduction

The Arctic Ocean, currently accounting for 5 to 14% of the total ocean CO_2 uptake (Bates and Mathis, 2009), is undergoing rapid climate-driven changes, including acidification and sea ice cover decline (Pachauri et al., 2014). Increasing seawater CO_2 concentrations and subsequent ocean acidification (OA) are particularly severe in the Arctic ocean relative to other regions. Low surface seawater temperature facilitates CO_2 uptake from the atmosphere, thereby enhancing the Arctic ocean′s sensitivity to increasing atmospheric CO_2. Furthermore, large freshwater inputs and sea ice melting cause surface water alkalinity to decrease, rendering the Arctic Ocean particularly prone to OA (Yamamoto-Kawai et al., 2009). Elevated CO_2 concentrations have been shown to enhance photosynthesis or growth of phytoplankton (Gao et al., 2012). In lab studies, three species of cultured diatom displayed higher growth rates under 1000 ppm than under 390 ppm CO_2, when the photosynthetic active irradiance (PAR) was below 200 µmol photon m^{-2} s^{-1} (Gao et al., 2012). In field studies, when CO_2 levels are enhanced, 10% increases in primary productivity and growth rates have been observed in natural assemblage in the Southern Ocean (Tortell et al., 2008).

In addition to high CO_2, Arctic phytoplankton are also likely to experience increasing irradiance. The maximal extent, duration and thickness of the Arctic sea ice have been decreasing in the last few decades (Comiso et al., 2008; Perovich et al., 2008), allowing more light penetration and longer growing seasons (Nicolaus et al., 2012). Stronger freshwater input and enhanced sea ice melting under global warming are predicted to enhance stratification and shoal the upper mixed layer (Doney, 2006), thus leading to additional light for Arctic phytoplankton. Due mainly to enhanced light availability, net primary productivity over the Arctic Ocean has been reported to increase by 20% between 1998 and 2009 (Arrigo and Dijken, 2011). Model projections indicate that once summer minimum sea ice cover decreases to zero, the net primary productivity of the Arctic Ocean would almost double compared to the present-day value (Arrigo et al., 2008; Pabi et al., 2008) even though macro nutrient limitation may reduce the potential for an increase in annual primary productivity (Trembley et al. 2015).

Both high CO_2 and high light can impact aqueous seawater Fe chemistry, and thereby modulate the bioavailability of Fe to marine phytoplankton (Sunda and Huntsman, 2003; Shi et al., 2010). The most bioavailable Fe species is dissolved inorganic iron (Fe´), comprising primarily of $Fe(OH)_x$ complexes (Gledhill and Buck, 2012). Given that more than 99.9% of dissolved Fe in natural seawater is complexed by organic ligands (Gledhill and van den Berg, 1994; Rue and Bruland, 1995; Hassler and Schoemann 2009), OA may influence Fe´ concentrations ([Fe´]), by altering the extent of organic Fe chelation. For example, under OA, [Fe´] might decrease in the presence of organic Fe complexes that release protons during dissociation (e.g., aminocarboxylic acids, such as Fe bound to ethylenediamine tetraacetic acid; EDTA), while [Fe´] might remain practically unchanged in the presence of organic Fe complexes that hardly release any protons upon dissociation (e.g., catecholates, such as Fe-azotochelin; Shi et al., 2010). In addition, Fe bound to some organic ligands is subject to photo-reduction (Gledhill and Buck, 2012 and references therein), and [Fe´] can be enhanced under elevated light intensities in the presence of both synthetic (Sunda and Huntsman, 2003) and natural organic ligands (Kuma et al., 1992; Waite et al., 1995).

Knowledge on Fe physiology of Arctic phytoplankton remains lacking. Taylor et al., (2013) argued that in addition to nitrate and light, Fe availability might control primary productivity in late summer of the Beaufort Sea. Thus, changes in [Fe´], mediated by OA or enhanced light, may trigger physiological responses in Arctic phytoplankton communities.

Phytoplankton acclimate to low Fe availability by increasing the number of cell surface Fe transporters, thereby controlling the maximum Fe uptake rates in short-term uptake assays (Harrison and Morel, 1986). If cells continue to experience Fe stress, after maximizing Fe transporter density (which is ultimately set by physical constraints at the cell surface), then phytoplankton may also access Fe bound to organic ligands by up-regulating a high-affinity Fe transport system (Maldonado and Price, 2001; Shaked et al., 2005, Maldonado et al., 2006).

The goal of this study was to, for the first time, examine Fe acquisition by *in situ* Arctic phytoplankton acclimated to different CO_2 concentrations and irradiances. Two incubation experiments were performed (in Subarctic and Arctic waters) in order to allow the *in situ* phytoplankton populations to adapt to high CO_2 and/or high light. After one week of acclimation, short-term Fe uptake rates by the phytoplankton communities were determined at various Fe concentrations chelated by the model ligand EDTA.

3.2 Materials and methods

3.2.1 Experimental setup

During the 2015 Canadian GEOTRACES Arctic Expedition aboard the *C.C.G.S. Amundsen*, two incubation experiments with natural plankton assemblages were conducted (OA1 and OA2). OA1 was initiated on July 19th in the Davis Strait (Subarctic waters; 63° 57.857′ N, 60° 7.552′ W), and OA2 was initiated on August 6th in Baffin Bay (Arctic waters; 71° 24.327′ N, 68° 36.057′ W).

Details on hydrological parameters, experimental setup and incubation conditions are described in Hoppe et al. (under review a and b). Briefly, phytoplankton assemblages were sampled from the bottom of the SCM (~50 m), using a trace metal clean rosette equipped with 12-L Teflon-coated GO-FLO bottles (General Oceanics, FL, USA). Seawater was sampled into acid-cleaned 50-L carboys; pre-screened through acid-cleaned 100 µm mesh to exclude large grazers; enriched with abundant macronutrients; and then dispensed into acid-cleaned 8-L polycarbonate (PC) bottles.

In both OA1 and OA2, triplicate bottles were exposed to a matrix of two CO_2 levels and two light levels, resulting in four treatments. The 8-L PC bottles were kept in on-deck incubators and continuously bubbled with commercially prepared air mixtures that contained 380 or 1000 ppm CO_2 (LC and HC, respectively), mimicking present-day and future atmospheric levels. Light amendments were 15 and 35% of surface PAR (LL and HL, respectively), representing distinct light conditions due to promoted stratification and light penetration. Light intensity and spectral distribution (400-700 nM) within the incubators were maintained by neutral density screening in combination with blue screens (#209 CT blue, Lee filters). During both OA1 and OA2, continuously flowing seawater pumped from surface maintained temperature within the incubators ~6 °C warmer than sea surface temperature.

3.2.2 Short-term Fe uptake assays

In both incubations, size-fractionated Fe uptake rates were examined on day 5 to 7 (depending on the rate of biomass buildup in the different treatments), using ^{55}Fe (7.3 mCi mg^{-1}, PerkinElmer). One liter of seawater was transferred from each 8-L PC bottle into 5 trace metal clean bottles (~200 mL each). In order to generate a Michaelis-Menten curve for Fe uptake, each bottle was spiked with one of a series of Fe concentrations (0.4, 4, 20, 100 and 200 nM) that was

pre-complexed to 10 μM EDTA. The pH of the Fe stock solution (35.8 μM Fe in 0.009 M HCl) used to prepare the Fe complexes was 2.0, to ensure that all of the Fe was truly dissolved (Maldonado and Price, 1999). Complete complexation was ensured by allowing the EDTA to react with the Fe for at least 2 hours in an aliquot of seawater, before the mixture was added to seawater in the Fe uptake bottles. The Fe additions included both ^{55}Fe and cold Fe (Taylor et al., 2013), and EDTA was chosen to be in large excess in order to buffer a relatively constant [Fe´] in each bottle and mask the effect of natural ligands on Fe speciation. After spiking, a 1 mL aliquot was taken from each bottle to inspect the final concentration of the tracer added. Bottles were then capped, sealed with Parafilm, and placed in incubators alongside the 8-L PC bottles.

The short-term Fe uptake experiments spanned 8 hours, and the time periods of the day for all treatments were similar, in order to eliminate any potential diurnal effects. After 8 hours, the content of each bottle was filtered sequentially onto 5 (large size fraction, LSF) and 0.6 μm (small size fraction, SSF) porosity PC filters, separated by nylon drain disks. Before running dry, filters were soaked in a 0.2 μm filtered Ti(III) citrate EDTA reagent for 5 min to remove any extracellular Fe (Hudson and Morel, 1989), and then rinsed with 10 mL of 0.2 μm filtered seawater to remove any loosely associated Fe. The vacuum was stopped just as the filters went dry, and each filter was placed in a 7-mL scintillation vial. Upon return to the University of British Columbia two months later, the filters were saturated with scintillation cocktail (ScintiSafe Plus 50%, Fisher), and particulate ^{55}Fe activity was determined with a scintillation counter (Beckman Coulter LS 6500 Multi-Purpose). Sample activities were corrected for tracer decay during the 2 months of archiving. Volumetric Fe uptake rates were calculated as previously described (Taylor et al., 2013).

3.2.3 Calculations and statistics

In OA1, *Pseudo-nitzschia* cf. *delicatissima* and *Fragilariopsis* cf. *cylindrus* were the predominant LSF phytoplankton species in all treatments. In OA2, *Chaetoceros socialis* dominated LSF phytoplankton in all treatments (see discussion). The sizes of these three phytoplankton cells are listed in Table SI5), and their surface area (SA) and volume are calculated based on Hillebrand et al., (1999). The conversion from cell volume (μm^3) to carbon quota (pg C $cell^{-1}$) was based on Strathmann (1966).

In the short-term assays, we calculated an operationally defined Fe uptake rate constant 'k_{in}' (for rationale, see discussion; k_{in}=measured Fe uptake rates/calculated [Fe´]) to evaluate phytoplankton Fe uptake physiology. For the k_{in} calculations, several assumptions were made. First, we assumed that the amount of Fe consumed by the phytoplankton during the one-week incubations was negligible. Thus, we used a single value of background Fe concentration for all treatments in each experiment (0.95 nM for OA1 and 0.81 nM for OA2, J. Cullen, in prep.). Second, we assumed that in the lowest Fe addition (0.4 nM), *in situ* Fe-binding ligands in excess of the total dissolved Fe were a strong determinant of Fe speciation, and the effect of EDTA was negligible. Thus, we estimated that [Fe´] equaled 0.5% of the total dissolved Fe concentration, namely background Fe concentration plus Fe addition (1.35 nM for OA1 and 1.21 nM for OA2). This proportion is greater than the typical *in situ* 0.1% (Gledhill and Buck, 2012), in order to account for our Fe addition. Third, in the remaining Fe additions, *in situ* strong Fe-binding ligands (1-2 nM; unpublished data) were ignored in [Fe´] calculations. Each of these three assumptions led to overestimations of [Fe´], rendering our calculated k_{in} a conservative upper estimate.

The conditional stability constant of the FeEDTA complex is strongly influenced by light, temperature, and pH (Sunda and Huntsman, 2003). Therefore, for the 4, 20,100 and 200 nM Fe additions, [Fe´] was calculated for the unique condition in each treatment on the day that the uptake assays were performed (Table 3.1). We report the calculated dissociation constants for the Fe additions, as well as representative [Fe´] in the 0.4 and 200 nM additions. To compare treatments, two-way analyses of variance (ANOVA) with additional Kolmogorov-Smirnov normality test were performed for k_{in}, using IBM SPSS Statistics 2015.

Table 3.1: Average pH on the total scale and temperature (±SD of triplicates), as well as irradiance during the short-term assays in OA1 (Davis Strait, Subarctic) and OA2 (Baffin Bay, Arctic). Irradiance was calculated based on surface PAR and percentage of penetration, indicating light experienced by phytoplankton, standard deviation of irradiance during the short-term assays are also reported. K_d'(dark), K_{hv}, and K_d' are the FeEDTA dissociation constants used for the Fe´ calculations in various environmental conditions. The Fe´ concentrations under these specific incubation conditions were calculated using 0.4 nM and 200 nM Fe additions as examples. Fe´ concentrations under 0.4 nM Fe addition were calculated as 0.5% of dissolved Fe after addition. These illustrate the range of [Fe´] in a given CO_2/light condition during short-term assays. LL and HL denote 15% and 35% of surface PAR, respectively, while LC and HC denote 380 ppm and 1000 ppm of CO_2.

Treatment	pH_{total}	T (°C)	Irradiance (µmol photon m^{-2} s^{-1})	K_d'(dark) (10^{-9} M)	K_{hv} (10^{-9} M)	K_d' (10^{-9} M)	[Fe´] (pM) at 0.4 nM Fe	[Fe´] (pM) at 200 nM Fe
OA1								
LL LC	8.10 ± 0.04	5.7 ± 0.1	83 ± 28	65.9	165.6	231.5	7	4673
LL HC	7.64±0.01	5.7 ± 0.1	83 ± 28	7.0	83.0	90.0	7	1810
HL LC	8.12± 0.01	5.4 ± 0.2	239 ± 86	65.9	478.8	544.7	7	11164
HL HC	7.71 ± 0.03	5.4 ± 0.2	239 ± 86	7.0	240.0	247.0	7	4901
OA2								
LL LC	8.12 ± 0.02	10.7 ± 0.5	155 ± 22	65.9	195.3	261.2	6	5284
LL HC	7.68 ± 0.03	10.7 ± 0.5	155 ± 22	7.0	97.9	105.0	6	2114
HL LC	8.09 ± 0.01	10.7 ± 0.5	286 ± 91	65.9	361.3	427.2	6	8731
HL HC	7.66 ± 0.01	10.7 ± 0.5	286 ± 91	7.0	181.1	188.1	6	1902

K_d'(dark): dark dissociation constant of FeEDTA; K_{hv}: photo-dissociation constant of FeEDTA; K_d': dissociation constant of FeEDTA; $K_d'=K_d'(dark)+K_{hv}=[Fe']\times[EDTA']/[FeEDTA]$, Sunda and Huntsman (2003).

3.3 Results

The Arctic Ocean is experiencing the greatest decrease in seawater pH in the global ocean. Concomitantly, sea ice melting is promoting higher light availability in surface waters. Though the productivity in the Arctic is mainly limited by nitrate and light (Tremblay et al., 2008; Tremblay and Gagnon, 2009), a recent study highlighted the importance of Fe nutrition for phytoplankton in this region (Taylor et al., 2013). In the present study, we examined the effects of high CO_2 (1000 ppm) and high light (~250 µmol photon m^{-2} s^{-1}) on Fe acquisition by phytoplankton in two size fractions (SSF, 0.6-5 µm; and LSF, >5 µm). Two ~1-week incubation experiments were conducted (OA1 in Subarctic and OA2 in Arctic waters). After 5-7 days of these incubations, we performed Fe uptake assays to investigate Fe uptake physiology of phytoplankton acclimated to different incubation treatments, and from these data we infer differences in bioavailability under distinct CO_2 and light conditions.

3.3.1 Phytoplankton community Chl *a* and composition during incubations

This section summarizes some results of our two incubation experiments, without introducing Fe uptake data. Chlorophyll a (Chl *a*) concentrations and size fractionation of phytoplankton assemblages are listed in Table SI6, more details are provided and discussed in Hoppe et al. (under review a and b).

Briefly, in OA1, the initial Chl *a* concentration was 0.41µg L^{-1}, with 41% of total Chl *a* in the >5 µm size fraction. By the end of incubation, Chl *a* concentrations ranged from 5.9 to 11.5 µg L^{-1}, depending on the treatments. In OA2, initial Chl *a* concentration was 0.56 µg L^{-1}, similar to the initial value of OA1, with 55% of the total Chl *a* in the >5 µm size fraction. By the end of the OA2 incubation, Chl *a* concentrations ranged from 11.7 to 13.6 µg L^{-1}. Faster biomass accumulation in OA2 was believed to be mediated by a prevalent higher incubation temperature (7±1°C) than that in OA1 (10±1°C). For the SSF phytoplankton a single picoeukaryote population, most probably *Micromonas pusilla* (based on flow cytometric comparison with cultures), was the most abundant species irrespective of incubation experiments or treatments. For the LSF phytoplankton, the pennate diatoms *Pseudo-nitzschia* cf. *delicatissima* and *Fragilariopsis* cf. *cylindrus* were the most abundant species during the Fe uptake assays of the OA1 incubation in all treatments. In contrast, the centric diatom *Chaetoceros socialis* dominated LSF phytoplankton in the OA2 incubation, regardless of treatment. Thus, for a given size fraction, any potential CO_2 or light effect on phytoplankton Fe uptake physiology would not have been mediated by a shift in phytoplankton community composition.

3.3.2 Fe uptake rate constants in short-term assays

In order to assess phytoplankton Fe uptake physiology, we originally aimed to generate Michaelis-Menten curves for Fe uptake, with Fe addition spanning from 0.4 to 200 nM. From these kinetic curves, we expected to derive maximum uptake rates (ρ_{max}) and half-saturation constants (K_ρ), and compare these parameters among incubation treatments. However, surprisingly, only 10 out of the 16 generated curves exhibited saturation kinetics, and only two became fully saturated. Thus, we were unable to calculate half-saturation constants for Fe uptake in all the incubation treatments. Instead, we examined alternative options to compare Fe physiology and bioavailability in the incubation treatments.

To compare Fe bioavailability to marine phytoplankton, Lis et al. (2015) proposed Fe uptake rate constants (k_{in}=Fe uptake rate/substrate concentration). This index allows for comparisons of Fe uptake among multiple Fe substrates (e.g., [Fe´] or FeL) and by different organisms. Furthermore, the authors proposed an empirical relationship between phytoplankton SA and the k_{in} for exclusive Fe´ uptake. This relationship implies that the k_{in} (with regard to Fe´ uptake) can be estimated for a given organism, as long as its size is known. We assumed that the substrate for phytoplankton Fe uptake was Fe´ in all treatments during both incubation experiments. By the end of both incubation experiments, no Fe limitation was inferred in any treatments, according to the consistently high F_v/F_m (>0.55, Hoppe et al., under review a and b). Since Fe uptake from FeL complexes is a characteristic of Fe-limited eukaryotic phytoplankton (for a review see Marchetti and Maldonado, 2016), our assumption of exclusive Fe´ uptake seems reasonable. Based on this assumption, we calculated the k_{in} for various Fe additions (k_{in}=measured Fe uptake rates/calculated [Fe´], Figure 3.1 and 3.2).

In both incubations, the SSF community was dominated by a picoeukaryote species, (most likely *Micromonas pusilla*; Hoppe et al., under review a and b), with an SA of 8 μm^2 (Reynolds, 2006). The empirical k_{in} for a phytoplankton cell in the SSF was estimated following Lis et al. (2015) (dashed line, Figure 3.1). This empirical k_{in} indicates the inherently maximum capability of phytoplankton to transport Fe´. For the SSF phytoplankton in both incubations, at the lowest Fe addition (0.4 nM), the calculated k_{in} were 1 to 17-fold higher the empirical k_{in}, and the calculated k_{in} often decreased with increasing Fe addition. In most cases, the calculated k_{in} eventually approached a plateau value that was in agreement (within a factor of two) with the empirical k_{in} determined for a cell with a SA like that of *Micromonas pusilla*.

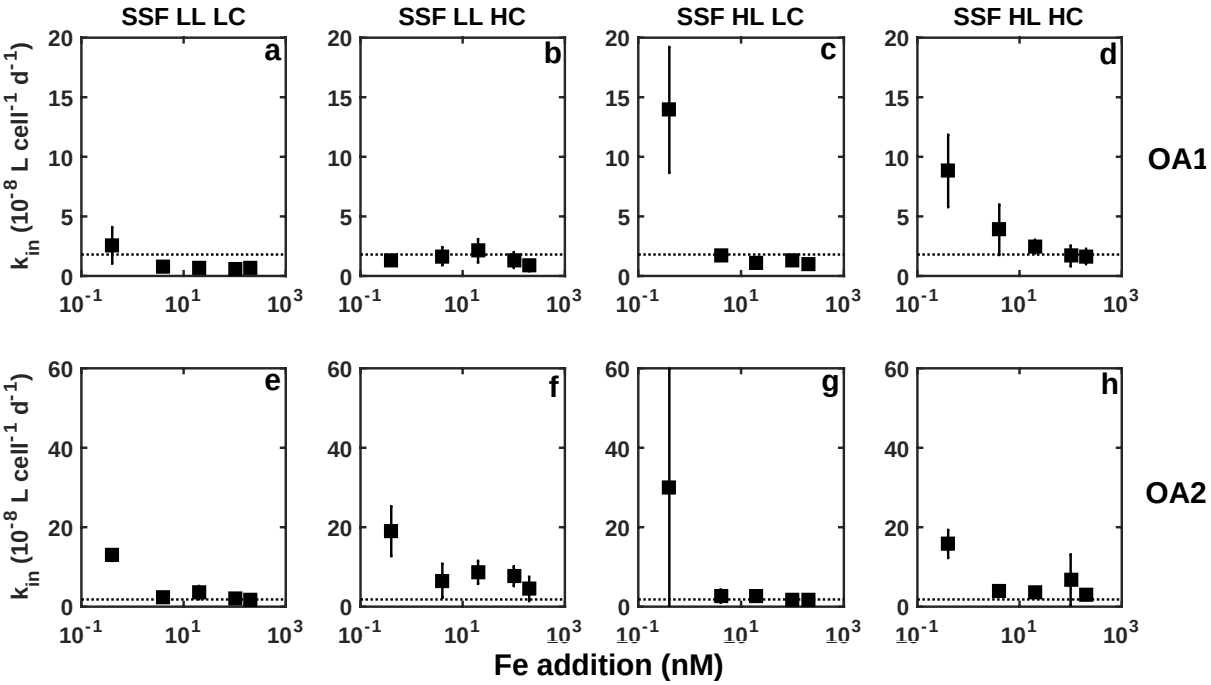

Figure 3.1: Fe uptake rate constants (mean ± SD) in short-term Fe uptake assays for the small size fraction of the phytoplankton (SSF; 0.6-5 µm) in the incubation treatments of OA1 (a-d) and OA2 (e-h). LL and HL denote 15% and 35% of surface PAR, respectively, while LC and HC denote 380 ppm and 1000 ppm of CO_2. The dashed line denotes the empirical k_{in} calculated for Fe´ uptake of *Micromonas pusilla*-like cells (which dominated SSF community in both OA1 and OA2), with a cell radium of 0.8 µm.

For the LSF phytoplankton, we observed the same trend across treatments as that for the SSF phytoplankton, showing that the calculated k_{in} for exclusive Fe´ uptake decreased with increasing Fe concentration (Figure 3.2). Notably, cell volume and SA are required in calculations of cell density (thus k_{in}), and empirical k_{in}, respectively. We averaged the SA of *P. delicatissima* and *F. cylindrus*, and utilized the mean to represent LSF phytoplankton in OA1. In OA2, the SA of *C. socialis* was applied when calculating the empirical k_{in} (Figure 3.2, represented by the horizontal bar). As observed for SSF phytoplankton, under high Fe additions, the calculated k_{in} approached to the empirical k_{in} value.

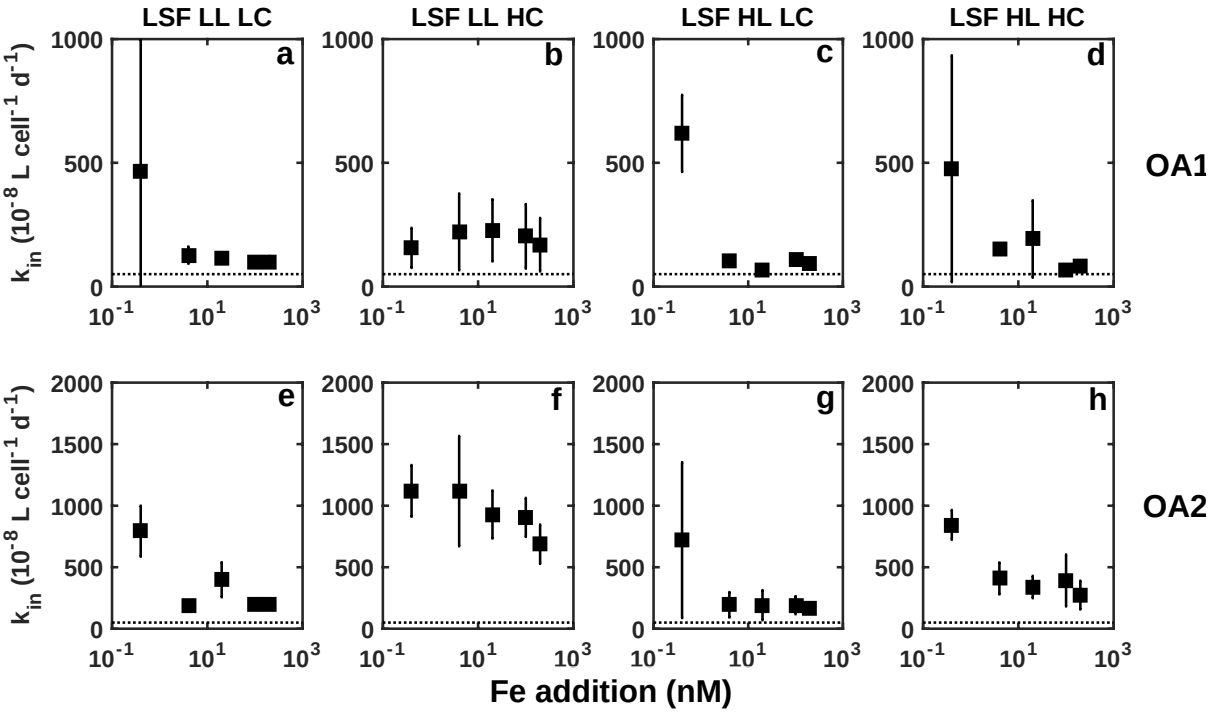

Figure 3.2: Fe uptake rate constants (mean ± SD) in short-term Fe uptake assays for the large size fraction of the phytoplankton (LSF; >5 µm) in the incubation treatments of OA1 (a-d) and OA2 (e-h). LL and HL denote 15% and 35% of surface PAR, respectively, while LC and HC denote 380 ppm and 1000 ppm of CO_2. The dashed line denotes the empirical k_{in} for Fe´ uptake of those representative diatom species. In OA1, volume and SA are represented by averaging those of *Pseudo-nitzschia* cf. *delicatissima* and *Fragilariopsis* cf. *cylindrus*, which dominated the LSF phytoplankton in all treatments. In OA2, volume and SA applied are those of *Chaetoceros socialis*, which dominated the LSF phytoplankton in all treatments.

3.3.3 An index of Fe uptake physiology for comparison among treatments

After the cells were acclimated to a specific CO_2/light treatment, their Fe uptake rates were determined under 0.4, 4, 20, 100 and 200 nM Fe additions. To evaluate the effects of CO_2 and light levels on phytoplankton Fe uptake physiology among incubation treatments, we chose to compare the Fe uptake rate constant (k_{in}) at the 20 nM Fe addition in the short-term assays, by dividing Fe uptake rates by estimated [Fe´] in each treatment. This specific k_{in} (with [Fe´]<1 nM), was chosen as an index, because this [Fe´] was below the average half-saturation constant for Fe uptake in marine phytoplankton ([Fe´]~3 nM). Thus, the Fe´ transporters are expected to be sub-saturated, which is a prerequisite condition for appropriate k_{in} calculations (see discussion). To confirm that Fe′ transporters were sub-saturated under 20 nM Fe additions, we calculated the ratio of Fe uptake rates between 100 nM Fe addition and 20 nM Fe addition ($Uptake_{100/20}$) for

each size fraction. If [Fe´] under 20 nM Fe addition was larger than the half-saturation constant, the maximum uptake rate could not exceed two times the Fe uptake rate under 20 nM Fe addition. Therefore, for a specific size fraction in a given treatment, an $Uptake_{100/20}$ larger than two indicates sub-saturation for Fe′ transporters under 20 nM Fe addition. According to Table 3.2, no treatment showed $Uptake_{100/20}$ lower than two, meaning that Fe′ transporters were consistently sub-saturated under 20 nM Fe addition. Furthermore, our estimated [Fe´] in this 20 nM Fe uptake assay is reasonably accurate, given that it contained large excess of Fe and EDTA relative to the background Fe and class one ligands L_1 (20 nM Fe:10 µM EDTA addition to ~1 nM Fe:1-2 nM L_1 *in situ*, unpublished data by J. Cullen and M. Maldonado). In this section, k_{in}^{20} refers to k_{in} under 20 nM Fe addition.

Table 3.2: $Uptake_{100/20}$=(Fe uptake rates under 100 nM Fe addition)/(Fe uptake rates under 20 nM Fe addition) for the two phytoplankton size fractions SSF (0.6-5 µm) and LSF (>5 µm). LL and HL denote 15% and 35% of surface PAR, respectively, while LC and HC denote 380 ppm and 1000 ppm of CO_2. Mean ± SD is derived from triplicates, except for 1) OA2 low light/high CO_2, where both SSF and LSF data are derived from duplicates; and 2) OA2 low light/high CO_2, where one of the SSF replicates is a potential outlier, the value in brackets is derived after excluding the putative outlier.

Treatment	SSF, $Uptake_{100/20}$	LSF, $Uptake_{100/20}$
OA1 LL LC	4.2±0.4	4.4±1.2
OA1 LL HC	3.0±0.3	4.4±3.0
OA1 HL LC	5.8±0.6	8.3±2.3
OA1 HL HC	3.6±2.5	2.5±1.7
OA2 LL LC	2.9±1.0	2.7±1.6
OA2 LL HC	3.7±0.0	5.0±0.0
OA2 HL LC	3.5±1.0	5.6±2.2
OA2 HL HC	8.5±7.1 (4.4±1.3)	5.8±3.2

In OA1, CO_2 had a significant ($p<0.05$) positive effect on k_{in}^{20} (high CO_2 increases k_{in}^{20}) of phytoplankton (Figure 3.3 and Table 3.3), regardless of size fraction. Also in OA2, CO_2 tended to exert a positive effect on k_{in}^{20} (high CO_2 increases k_{in}^{20}) for both SSF and LSF phytoplankton. Furthermore, a negative light effect on k_{in}^{20} (high light decreases k_{in}^{20}) was observed for LSF phytoplankton in OA1, as well as both SSF and LSF phytoplankton in OA2 (Figure 3.3 and Table 3.3).

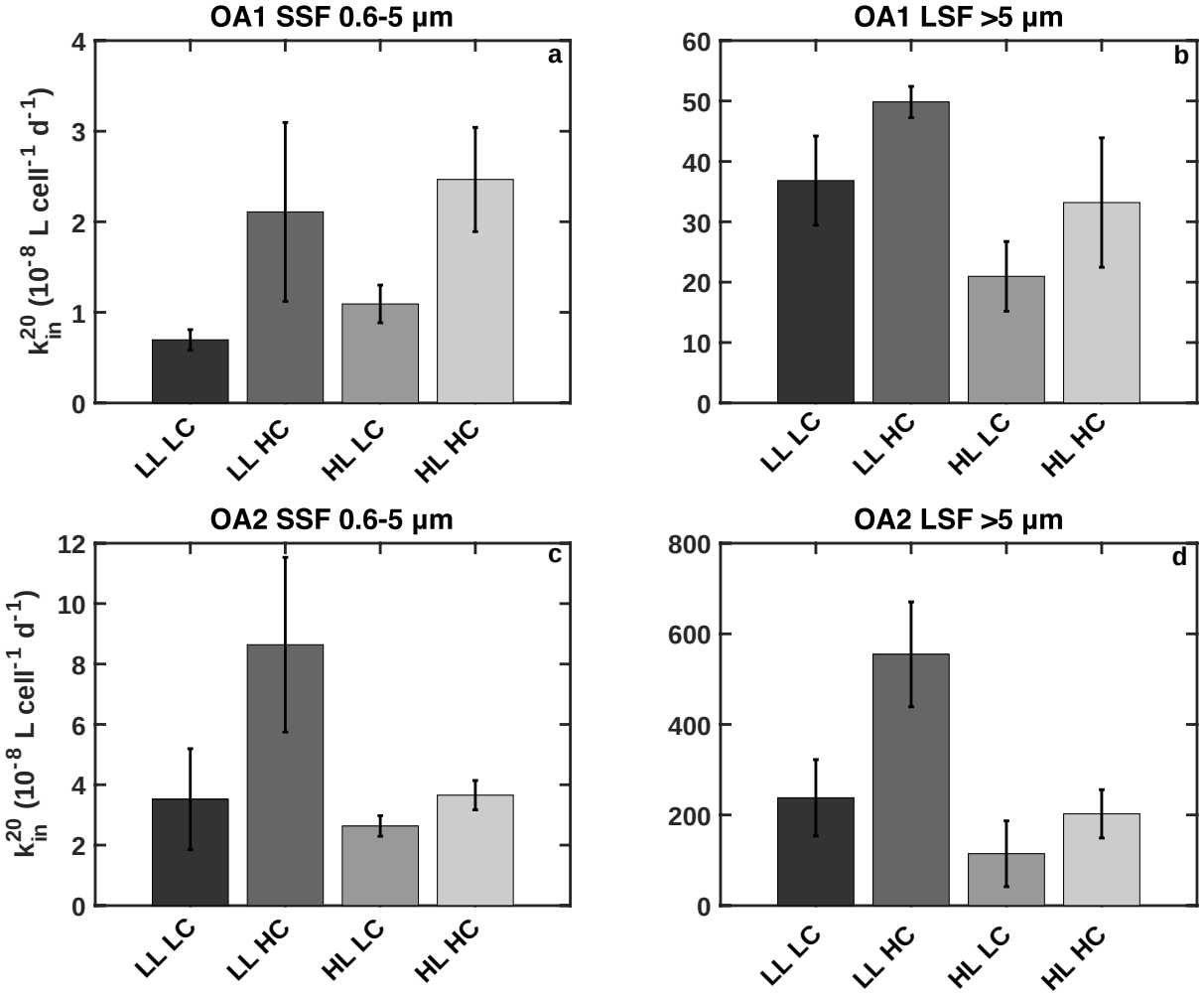

Figure 3.3: Fe uptake rate constants k_{in}^{20} (mean ± SD) from short-term assays (20 nM Fe:10 µM EDTA addition) for OA1 (a, b) and OA2 (c, d), under different CO_2 and light levels for the two phytoplankton size fractions SSF (0.6-5 µm) and LSF (>5 µm). LL and HL denote 15% and 35% of surface PAR, respectively, while LC and HC denote 380 ppm and 1000 ppm of CO_2.

Table 3.3: Results from two-way ANOVAs of Fe uptake rate constants k_{in}^{20} (20 nM Fe:10 µM EDTA addition) for OA1 and OA2 for the two phytoplankton size fractions SSF (0.6-5 µm) and LSF (>5 µm). LL and HL denote 15% and 35% of surface PAR, respectively, while LC and HC denote 380 ppm and 1000 ppm of CO_2. Kolmogorov-Smirnov normality tests were performed and passed prior to ANOVA. Significance level was set to p=0.05, significant effects are bolded, and NA denotes not applicable. The statistical results are then interpreted in combination with Figure 3.3.

Exp. and SF	Factor of ANOVA	ANOVA p-value	Interpretation of light effect	Interpretation of CO_2 effect
OA1 SSF	Light	0.296	*Not Significant*	*Positive*
	CO_2	**0.003**		
	Interaction	0.955		
OA1 LSF	Light	**0.012**	*Negative*	*Positive*
	CO_2	**0.032**		
	Interaction	0.933		
OA2 SSF	Light	**0.013**	*Negative*	*Positive*
	CO_2	**0.011**		
	Interaction	0.054		
OA2 LSF	Light	**0.002**	*Negative*	*Positive*
	CO_2	**0.004**		
	Interaction	0.051		

Note: For LSF phytoplankton in OA1, normality test failed due to two potential outliers (one of triplicates in LL/HC and HL/HC, respectively). After excluding these two data, the dataset passed the normality test, ANOVA was performed, and the results are presented.

3.4 Discussion

3.4.1 What was the substrate for uptake during short-term Fe uptake assays?

In many cases, we observed a declining k_{in} with increasing Fe concentration (Figure 3.1 and 2). Furthermore, the k_{in} largely exceeded the empirical k_{in} at the lowest Fe addition (0.4 nM) in most treatments. Notably, three conditions must be satisfied when calculating k_{in}. Firstly, the Fe substrate accessed by phytoplankton needs to be identified, either as Fe´ or organically bound Fe (e.g., FeDFB). Secondly, the concentration of the Fe substrate has to be sub-saturating. Thirdly, the assayed phytoplankton are expected to be Fe-limited, thereby ensuring maximum density of surface Fe transporters. We initially assume that the uptake substrate was Fe´ in all treatments of both incubation experiments, and examine the other two conditions.

The second condition was met, as [Fe´] in the 0.4, 4 and 20 nM Fe additions were below the half-saturation constant for phytoplankton Fe´ uptake (~3 nM [Fe´], reviewed by Marchetti and Maldonado, 2016), and were thus sub-saturating. This sub-saturation was confirmed by a $Uptake_{100/20}$ larger than two in all treatments across incubations (Table 3.2, see above). However, the third condition (Fe-limited phytoplankton) might not have been met, according to the

consistently high F_v/F_m (>0.55 by the end of all incubation treatments, Hoppe et al., under review a and b). Assuming that Fe´ was the substrate for uptake, if this third condition was not met in our experiments, this would imply that the Fe transporters might not have been maximized. However, this unsatisfied condition would result in a lower k_{in} relative to the empirical k_{in}, instead of the higher k_{in} we observed under low Fe additions (Figure 3.1 and 3.2). The large calculated k_{in} under 0.4 nM Fe addition could thus be due to an erroneous estimate of the [Fe´] (0.5% of dissolved Fe) or an erroneous assumption that Fe´ was the only substrate for uptake. We are unable to determine whether our [Fe´] value under 0.4 nM Fe addition is correct, but we believe it is an overestimation (see section 3.2.3), if incorrect. This overestimation could not explain our calculated high k_{in} under 0.4 nM Fe addition. Thus, we conclude that our initial assumption that Fe´ was the only substrate for Fe uptake is unlikely correct. Instead, we hypothesize that the phytoplankton were accessing Fe bound to *in situ* ligands (FeL). This hypothesis is supported by the convergence of calculated k_{in} and empirical k_{in} at high Fe additions, showing the increasing importance of [Fe´] to the total dissolved Fe pool (Fe´+FeL) as the Fe addition was increased. In summary, although we were unable to identify the Fe nutritional status for phytoplankton (as limited, stressed or replete) during the incubation, we show that phytoplankton are capable of taking up Fe from FeL complexes, regardless of size fractions or experiments. This finding might question the concurrence between phytoplankton Fe-limitation and Fe uptake from FeL complexes.

3.4.2 CO_2 and light effects on phytoplankton Fe uptake capability

For phytoplankton in any given size fraction (SSF or LSF) across experiments (OA1 or OA2), CO_2 had a significant positive effect on k_{in}^{20} (Figure 3.3 and Table 3.3). Given that k_{in}^{20} was calculated by normalizing measured Fe uptake rates to estimated [Fe´] for each treatment, larger k_{in}^{20} suggests higher capability of phytoplankton to access Fe, a physiological characteristic normally observed when phytoplankton experience Fe stress. This implies that in the one-week incubations exposed to 1000 ppm CO_2, Fe bioavailability to phytoplankton was lower than those exposed to 380 ppm CO_2. Shi et al. (2010) showed that high CO_2 lowered Fe bioavailability in the presence of organic complexes that release protons either during dissociation (e.g., FeEDTA) or during the enzymatic reduction at the cell surface (e.g., FeDFB). Thus, the CO_2 effect we observed suggests that the *in situ* organic Fe complexes in the

incubation also released protons prior to Fe assimilation. This lowered Fe bioavailability and the phytoplankton responded by increasing their Fe uptake capability (k_{in}^{20}). Shi et al. (2010) examined phytoplankton Fe transport under OA, and found no difference in Fe uptake physiology under various CO_2/pH levels. However, their experimental design was such that in the high CO_2 treatments, cells were exposed to consistently higher concentrations of dissolved Fe (Figure 1, Shi et al., 2010). This higher dissolved Fe could potentially compensate for the high CO_2-induced Fe′ loss, thus resulting in similar Fe bioavailability among treatments. Therefore, identical Fe uptake physiology was not unexpected in their treatments.

In the present study, a significant light effect on k_{in}^{20} was observed in OA1 for LSF phytoplankton, as well as in OA2 for both SSF and LSF phytoplankton (Figure 3.3 and Table 3.3). The light effect was negative, as expected, given that high light increases the photo-reduction of Fe within organic complexes (Sunda and Huntsman, 2003), and should ultimately result in higher Fe bioavailability and lower k_{in}^{20}. In conclusion, the light effect on k_{in}^{20} across size fractions and experiments suggests that high light triggered lower Fe uptake capability by phytoplankton. We attribute this physiological response to higher Fe bioavailability, induced by high light during incubations.

Interestingly for SSF phytoplankton in OA1, no significant light effect on k_{in}^{20} was found (Figure 3.3 and Table 3.3), which was unexpected based on discussion above. At the end of OA1 incubation, in the low light treatments the LSF phytoplankton accounted for ~35% of total Chl *a* (Table SI6), while in the high light treatments they accounted for ~70% of total Chl *a*. Hoppe et al. (under review a) argued that under high light treatments, SSF phytoplankton were photo-inhibited and thus outcompeted by LSF diatoms. For SSF phytoplankton in OA1, when light was increased, [Fe´] was enhanced, which would encourage phytoplankton to lower their Fe uptake capability. Simultaneously, high light might have caused photo-inhibition of SSF phytoplankton, resulting in high cellular Fe demand. This extra Fe might be required to deal with oxidative stress, by synthesizing SOD (Lesser, 2006). These antagonistic light effects eventually resulted in similar Fe uptake capability between low light and high light treatments. The fact that light effect was still significant for LSF phytoplankton in OA1 is attributed to higher photo-protective capabilities of diatoms compared to small phytoplankton (Raven, 1998, Wagner et al. 2006). When light was increased, LSF phytoplankton in OA1 benefited from enhanced [Fe´], without

suffering from photo-inhibition. This was supported by the dominance of LSF phytoplankton in the high light treatments.

3.4.3 Present-day vs. future Arctic waters

Surface waters of the Arctic are experiencing increasing CO_2 and light levels concomitantly (Pachauri et al., 2014). As Fe could be a co-limiting factor—in addition to nitrate and light—for primary productivity in some regions of the Arctic Ocean (Taylor et al., 2013), the combined effect of changes in CO_2 and light on Fe bioavailability and phytoplankton Fe uptake physiology is of interest. For LSF phytoplankton in OA1, as well as both SSF and LSF phytoplankton in OA2, a negative light effect on k_{in}^{20} was observed, indicating high Fe bioavailability due to high light during incubations (Figure 3.3 and Table 3.3). In addition, a positive CO_2 effect on on k_{in}^{20} suggests low Fe bioavailability induced by high CO_2. To examine Fe uptake physiology of phytoplankton in present versus future conditions in surface waters, we compared POC-normalized Fe uptake rates versus calculated [Fe´], for low light/low CO_2 treatment (mimicking present-day conditions), and high light/high CO_2 treatment (mimicking a future scenario) (Figure 3.4). For LSF phytoplankton in OA1, as well as SSF and LSF phytoplankton in OA2, all the data from both treatments closely follow a single line, suggesting that phytoplankton Fe uptake physiology were similar between these two scenarios. This is attributed to the opposing effects of high light and high CO_2 on Fe bioavailability. We thus infer that, in a future scenario where both atmospheric CO_2 and underwater irradiance are elevated (Arrigo and Dijken, 2011), Fe bioavailability to Arctic phytoplankton during spring bloom might be similar to present-day values (see Figure 3.5 for an illustration). For SSF phytoplankton in OA1, high CO_2 decreased Fe bioavailability thus increasing Fe uptake capability (Figure 3.3 and Table 3.3). However, as high light failed to significantly affect—in a negative manner—Fe uptake capability (which was expected to counteract the high CO_2 effect, see discussion above), scenarios of today and future display different Fe uptake physiology (Figure 3.4). Furthermore, for the SCM community which hypothetically persists through summer (Martin et al., 2010), as light enhancement is less drastic than at surface, Fe bioavailability might be lowered by OA.

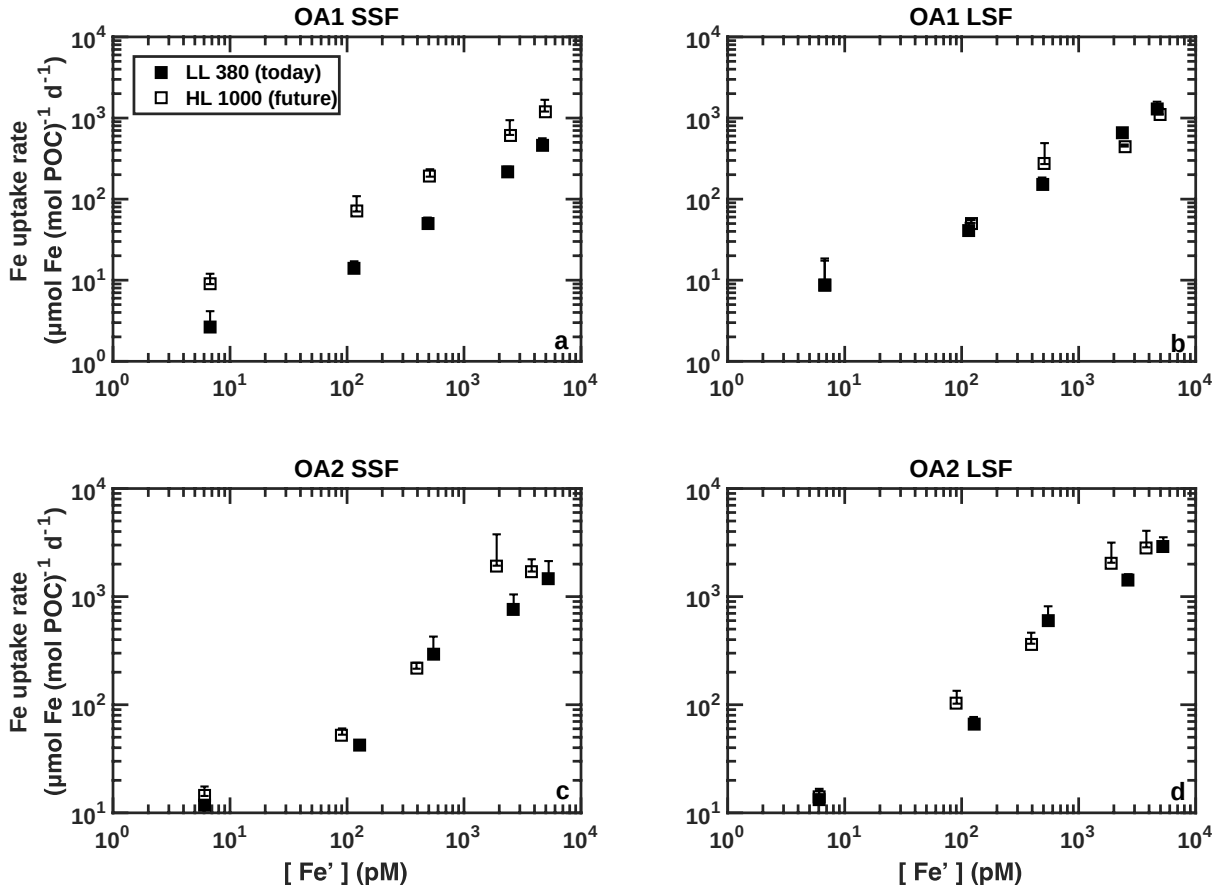

Figure 3.4: POC-normalized Fe uptake rates of the size-fractionated phytoplankton assemblage, versus calculated Fe´ concentrations for two treatments in each experiment. The two treatments mimic present-day (15% of surface PAR, 380 ppm CO_2), and future conditions (35% of surface PAR, 1000 ppm CO_2) in surface Arctic waters. Mean + SD of triplicates is reported.

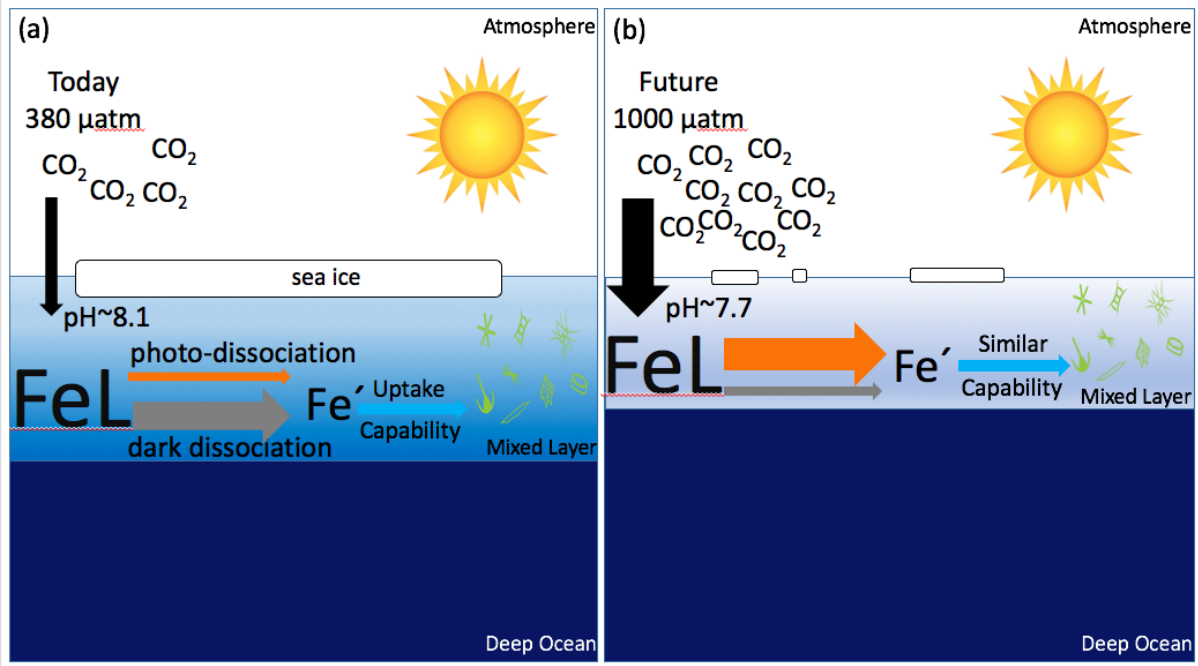

Figure 3.5: In the present-day scenario (a), atmospheric CO_2 level is 380 µatm, resulting in a surface seawater pH of ~8.1. Fe´ is produced by both photo-dissociation and dark dissociation of FeL. In the future scenario (b), atmospheric CO_2 level is 1000 µatm, resulting in a surface seawater pH of ~7.7. This pH decline impacts the dark dissociation of FeL, thus decreasing Fe´ concentration. In addition, the ice melting leads to a shallower mixed layer and enhanced light penetration, hence promoting photo-dissociation of FeL and increasing Fe´ concentration. Consequently, Fe´ concentration in future Arctic Ocean could remain similar as that of present-day value, and phytoplankton might not show obvious physiological response in Fe uptake.

3.5 Summary

The Arctic Ocean is experiencing the greatest decrease in seawater pH, as well as rapid ice melting, which can increase surface stratification and boost light intensity in surface waters. These changes can potentially alter the bioavailability of iron (Fe), an important limiting nutrient for phytoplankton productivity in vast open ocean regions. To examine phytoplankton Fe uptake physiology and infer Fe bioavailability under low pH and high light, two incubation experiments were performed in the Canadian Arctic during summer 2015. After natural assemblage acclimated to different CO_2/light treatments for one week, short-term Fe uptake assays were conducted under 0.4, 4, 20, 100 and 200 nM Fe bound to 10 µM EDTA. We first identified the substrate for phytoplankton Fe uptake under various Fe additions, and observed that Fe´ (soluble inorganic Fe) was not the only substrate for uptake when the Fe addition was low. Instead, we hypothesize that phytoplankton were accessing Fe bound to *in situ* ligands (FeL). In both

experiments, phytoplankton acclimated to all CO_2/light treatments appeared to be able to access FeL, while the importance of Fe´ for Fe uptake increased as the Fe addition was enhanced. The present study also shows—for the first time—that high CO_2 has a significant positive effect on Fe uptake capability of phytoplankton, while light has a negative effect. We attribute these physiological responses to high-CO_2-induced low Fe bioavailability and high-light-induced high Fe bioavailability during the one-week incubation. Compared to the present-day scenario, the future scenario for the Arctic waters predicts higher atmospheric CO_2 and higher light levels in the surface layer. Consequently, these opposing effects on phytoplankton Fe uptake physiology could lead to similar Fe bioavailability to phytoplankton during spring bloom as that of today.

Chapter 4: Conclusion

4.1 Significance and major findings

In Chapter 2, I report full-depth profiles of eleven particulate elements in the Canada Basin, Canadian Arctic Archipelago (CAA), Baffin Bay, and Labrador Sea, which cover distinct oceanic regimes in the Canadian Arctic Ocean. In Chapter 3, I present the results from two incubation experiments in the Canadian Arctic, to examine phytoplankton Fe uptake physiology and infer Fe bioavailability under low pH and high light. Together, these two chapters help fill in the existing knowledge gap on the distributions and concentrations of particulate trace metals in the Arctic Ocean, their bioavailability under drastic climate change, and how phytoplankton respond to varying metal bioavailability.

In Chapter 2, some general trends were evident. Particulate elements (except for P and Cd) in the CAA were strongly influenced by lithogenic materials, whereas the contribution of lithogenic particles to particulate element concentrations (except for Al, Fe and V, see below) was negligible in all other basins. The concentrations of particulate Al, Fe and V were strongly correlated to each other across the entire Canadian Arctic Ocean, with their relative abundances similar to those in local continental crust. Vertical distributions of elements with a strong lithogenic component (Al, Fe and V), were characterized by an enrichment at the surface, due to sediment released from melting sea ice. In addition, vertical distributions of elements with a significant biogenic component (Cd and Cu), showed a downward decrease in concentration due to POM decay. The preferential remineralization of P over Cd at shallow depths was reported. In numerous stations across the entire Canadian Arctic Ocean, the molar ratio between particulate Cu and P approached a plateau at depth. This plateau represented a fixed value of 5 mmol Cu $(\text{mol P})^{-1}$, which is 2.4-25 times higher than the average cellular Cu demand of phytoplankton. I propose that the high and constant pCu:pP ratio at depth suggests the occurrence of ammonium oxidizing archaea (AOA), which have high cellular Cu requirement. Manganese, an element with a predominant redox cycle, displayed a maximum between 100-200 m across the entire Canadian Arctic Ocean, as well as a bottom enrichment in various stations. In the Canada Basin, complementary data from collaborators suggest that Mn-oxidizing bacteria are fueled by a dMn input, during the transition of Pacific water along 100-200 m depth. I also propose interactions among the biogenic production of manganese oxide, cobalt oxide and barite. Furthermore, the robust pBa-pCu correlation below the photic zone in the Canada Basin indicates that biogenic

barite is protected from dissolution.

In Chapter 3, I first identify the substrate for phytoplankton Fe transport during short-term uptake assays, and suggest that Fe´ was not the sole substrate for uptake. Instead, under low Fe concentrations, phytoplankton were accessing Fe bound to *in situ* ligands (FeL), regardless of previous incubation conditions or their cell size. However, the relative importance of the Fe´ pool in the total Fe uptake rates increased as Fe addition was enhanced. I propose an index, k_{in}^{20} (Fe uptake rate constant under 20 nM Fe addition), for direct comparison of phytoplankton's Fe uptake capability among treatments. The Fe uptake capability was influenced positively and negatively by CO_2 level and light level during their one-week acclimation period, respectively. Under OA, the changes in phytoplankton Fe uptake rates have been attributed to altered medium Fe chemistry (Shi et al., 2010). The present study shows for the first time that phytoplankton adjust their Fe uptake physiology under varying light/CO_2 levels. These responses imply that high CO_2 exerts a significant negative effect on Fe bioavailability, thus triggering an enhancement in their Fe uptake capability. In contrast, high light has a positive effect on Fe bioavailability. Compared to the present-day scenario, a future scenario of higher atmospheric CO_2 and underwater irradiance appear to show analogous phytoplankton Fe uptake physiology, suggesting similar Fe bioavailability to phytoplankton as that of today.

4.2 Caveats and limitations

In Chapter 2, our pCo dataset is largely incomplete. We determined our pTM by ICP-MS, relying on a standard curve spanning 0.1-90 ppb in concentration for each element. Unfortunately, the difference in concentration between Co and Al (the most abundant element) in our particulate samples frequently exceeded a factor of 900. Consequently, often the detection of Co had to be compromised under a given dilution level. However, a full pCo dataset would enable us to investigate the pCo-pMn relationship, as well as the interactions between biogenic production of Mn/Co oxides and barite. As samples have been digested and stored in a trace metal clean manner, repeat measurements with a lower dilution levels are recommended for future pCo determinations.

In Chapter 3, in order to assess phytoplankton Fe uptake physiology, we originally aimed to generate Michaelis-Menten curves for Fe uptake, with Fe addition spanning from 0.4 to 200 nM. From these kinetic curves, we expected to derive maximum uptake rates (ρ_{max}) and half-

saturation constants (K_ρ), and compare these parameters among incubation treatments. However, only 10 out of the 16 generated curves exhibited saturation kinetics, rendering the curve fitting problematic. To address this issue, we introduced k_{in}^{20} and demonstrated its potential as an index for the capability of phytoplankton Fe uptake. Although this alternative index is useful in evaluating Fe uptake physiology, the parameters derived from Michaelis-Menten curves (ρ_{max} and K_ρ) are extremely useful to global ocean carbon modelers, as Fe uptake rates can thus be calculated for a broad range of Fe concentrations in the ocean. Furthermore, to generate these curves, Fe uptake rates under 5 distinct Fe additions are required. This larger dataset would lower the caveats of applying k_{in}^{20}, for which only uptake rates under a 20 nM Fe addition were considered and significant trends could be strongly driven by a few outliers. Indeed, the calculated Fe´ concentration under our highest Fe addition (200 nM Fe) ranged from 1 to 6 nM, depending on treatment conditions. Given that the average half-saturation constant for phytoplankton Fe´ uptake falls between 1 to 6 nM (~3 nM [Fe´], reviewed by Marchetti and Maldonado, 2016), the ten under-saturated Fe uptake Michaelis-Menten curves we encountered should not be completely unexpected. In order to generate saturated Michaelis-Menten curves, higher Fe additions are recommended.

4.3 Future outlook

In Chapter 2, I propose some hypotheses to explain the observed particulate element distributions. Some of them are highly speculative, and raise new questions regarding the biogeochemical behaviors of particulate trace elements. Firstly, it would be interesting to examine the pCu-pBa relationship throughout the aphotic zone, where Mn-oxidizing bacteria are common and presumably play an important role in the cycling of both elements. Since these Mn-oxidizing bacteria have been successfully cultured (Tebo et al., 2005), and synchrotron-based X-ray fluorescence techniques have been used to determine the elemental composition of single plankton cells (Twining et al., 2004), determining the elemental composition of these bacteria appears possible. Secondly, the fixed Cu-P stoichiometry of particles at depth merits further study. Given the cosmopolitan and high abundance of AOA at depth (Delong et al., 1994; Stein and Simon, 1996; Karner et al., 2001), as well as their high cellular Cu requirements (Amin et al., 2013), AOA have the potential to control the depth profiles of particulate Cu below the photic zone, where nitrification is not light-inhibited. Furthermore, in the North Sea, amoA (ammonia

monooxygenase alfa subunit) copy numbers of archaea *Crenarchaeotal* were 1-3 orders of magnitude higher than those of bacterial amoA, suggesting a major role of archaea in oceanic nitrification (Wuchter et al., 2006). Thus, in turn, Cu might exert an unrecognized role on the distribution of AOA, and the marine nitrogen cycle. Thirdly, the high PON:pP ratios, and putative N-fixation in upper Labrador Sea is worth examining. Blais et al. (2012) reported substantial N-fixation rates in Mackenzie River plume, suggesting that the process should not be dismissed in the Arctic and surrounding seas. Given the presence of Pacific-delivered water (Jones et al., 2003), which has excess phosphorus (Yamamoto-Kawai et al., 2006), in the Labrador Sea, information on N-fixation would refine our understanding on the global N cycle. Even a small contribution of N-fixation in the Arctic Ocean could have a strong impact in the oceanic nitrogen balance and, ultimately the global carbon cycle (Falkowski, 1997).

Bibliography

Algora, Camelia, et al. "Geochemistry and microbial populations in sediments of the Northern Baffin Bay, Arctic." Geomicrobiology Journal 30.8 (2013): 690-705.

Amin, Shady A., et al. "Copper requirements of the ammonia-oxidizing archaeon Nitrosopumilus maritimus SCM1 and implications for nitrification in the marine environment." Limnology and Oceanography 58.6 (2013): 2037-2045.

Annett, Amber L., et al. "The effects of Cu and Fe availability on the growth and Cu: C ratios of marine diatoms." Limnology and Oceanography 53.6 (2008): 2451.

Ardini, Francisco, et al. "Trace elements in marine particulate and surface sediments of Kongsfjorden, Svalbard Islands." Rendiconti Lincei 27.1 (2016): 183-190.

Ardyna, Mathieu, et al. "Environmental forcing of phytoplankton community structure and function in the Canadian High Arctic: contrasting oligotrophic and eutrophic regions." Marine Ecology Progress Series 442 (2011): 37-57.

Arrigo, Kevin R., and Gert L. van Dijken. "Secular trends in Arctic Ocean net primary production." Journal of Geophysical Research: Oceans 116.C9 (2011).

Arrigo, Kevin R., et al. "Massive phytoplankton blooms under Arctic sea ice." Science 336.6087 (2012): 1408-1408.

Arrigo, Kevin R., Gert van Dijken, and Sudeshna Pabi. "Impact of a shrinking Arctic ice cover on marine primary production." Geophysical Research Letters 35.19 (2008).

BANCHETTI, R., R. NOBILI, and F. ESPOSITO. "An experimentally determined carbon: volume ratio for marine “oligotrichous” ciliates from estuarine and coastal waters." (1989).

Bates, N. R., and J. T. Mathis. "The Arctic Ocean marine carbon cycle: evaluation of air-sea CO 2 exchanges, ocean acidification impacts and potential feedbacks." Biogeosciences 6.11 (2009): 2433-2459.

Bender, Michael L., Teh-Lung Ku, and Wallace S. Broecker. "Manganese nodules: their evolution." Science 151.3708 (1966): 325-328.

BeszczynskA-Möller, AgnieszkA, et al. "A synthesis of exchanges through the main oceanic gateways to the Arctic Ocean." in: The Changing Arctic Ocean: Special Issue on the International Polar Year (20072009), Oceanography, 24 (3) 99. 82 (2011).

Bishop, James KB, and T. J. Wood. "Particulate matter chemistry and dynamics in the twilight zone at VERTIGO ALOHA and K2 sites." Deep Sea Research Part I: Oceanographic Research Papers 55.12 (2008): 1684-1706.

Bishop, James KB. "The barite-opal-organic carbon association in oceanic particulate matter." Nature 332.6162 (1988): 341-343.

Blais, Marjolaine, et al. "Nitrogen fixation and identification of potential diazotrophs in the Canadian Arctic." Global Biogeochemical Cycles 26.3 (2012).

Bonatti, E. N. R. I. C. O., and G. Arrhenius. "Eolian sedimentation in the Pacific off northern Mexico." Marine Geology 3.5 (1965): 337-348.

Boyd, P. W., and M. J. Ellwood. "The biogeochemical cycle of iron in the ocean." Nature Geoscience 3.10 (2010): 675-682.

Boyle, E. A_, F. Sclater, and J. M. Edmond. "On the marine geochemistry of cadmium." Nature 263.5572 (1976): 42-44.

Boyle, Edward A. "Cadmium, zinc, copper, and barium in foraminifera tests." Earth and Planetary Science Letters 53.1 (1981): 11-35.

Boyle, Edward A., et al. "Anthropogenic lead emissions in the ocean." Oceanography 69 (2014).

Brand, Larry E., William G. Sunda, and Robert RL Guillard. "Reduction of marine phytoplankton reproduction rates by copper and cadmium." Journal of Experimental Marine Biology and Ecology 96.3 (1986): 225-250.

Bratbak, Gunnar. "Bacterial biovolume and biomass estimations." Applied and environmental microbiology 49.6 (1985): 1488-1493.

Breitbarth, E., et al. "Ocean acidification affects iron speciation during a coastal seawater mesocosm experiment." *Biogeosciences (BG)* 7.3 (2010): 1065-1073.

Brewer, P. G., et al. "Sediment trap experiments in the deep North Atlantic: isotopic and elemental fluxes." J. Mar. Res.;(United States) 38.4 (1980).

Brown, Kristina A., et al. "Determination of particulate organic carbon sources to the surface mixed layer of the Canada Basin, Arctic Ocean." *Journal of Geophysical Research: Oceans* 119.2 (2014): 1084-1102.

Brujevicz, S. W. "Oxidation reduction potential andthe pH of sediments of the Barentz and Kara seas." Dokl. Akad. Nauk. SSSR. Vol. 19. 1938.

Bruland, K. W., M. C. Lohan, and H. Elderfield. "The oceans and marine geochemistry." Treatise on Geochemistry 6 (2003): 23-47.

Bruland, Kenneth W., George A. Knauer, and John H. Martin. "Cadmium in northeast Pacific waters." Limnology and Oceanography 23.4 (1978): 618-625.

Bruland, Kenneth W., Kristin J. Orians, and James P. Cowen. "Reactive trace metals in the stratified central North Pacific." Geochimica et Cosmochimica Acta 58.15 (1994): 3171-3182.

Buat-Menard, P., and R. Chesselet. "Variable influence of the atmospheric flux on the trace metal chemistry of oceanic suspended matter." Earth and Planetary Science Letters 42.3 (1979): 399-411.

Campbell, J. A., and P. A. Yeats. "The distribution of manganese, iron, nickel, copper and cadmium in the waters of Baffin-Bay and the Canadian arctic archipelago." Oceanologica Acta 5.2 (1982): 161-168.

Chang, Sung Il, and John R. Reinfelder. "Bioaccumulation, subcellular distribution, and trophic transfer of copper in a coastal marine diatom." Environmental science & technology 34.23 (2000): 4931-4935.

Christopher, I., et al. "A commercially available rosette system for trace metal–clean sampling." *Limnol. Oceanogr.: Methods* 6 (2008): 384-394.

Cid, Abigail Parcasio, et al. "Stoichiometry among bioactive trace metals in seawater on the Bering Sea shelf." Journal of oceanography 67.6 (2011): 747-764.

Cid, Abigail Parcasio, Seiji Nakatsuka, and Yoshiki Sohrin. "Stoichiometry among bioactive trace metals in the Chukchi and Beaufort Seas." Journal of oceanography 68.6 (2012): 985-1001.

Clark, Lauren Lisa, Ellery D. Ingall, and Ronald Benner. "Marine phosphorus is selectively remineralized." Nature 393.6684 (1998): 426-426.

Comiso JC, Parkinson CL, Gersten R, Stock L (2008) Accelerated decline in the Arctic sea ice cover. Geophysical Research Letters 35:L01703

Crawford, David W., et al. "Low particulate carbon to nitrogen ratios in marine surface waters of the Arctic." Global Biogeochemical Cycles 29.12 (2015): 2021-2033.

Cullen, Jay T. "On the nonlinear relationship between dissolved cadmium and phosphate in the modern global ocean: Could chronic iron limitation of phytoplankton growth cause the kink?." Limnology and oceanography 51.3 (2006): 1369-1380.

Cullen, Jay T., et al. "Modulation of cadmium uptake in phytoplankton by seawater CO2 concentration." Nature 402.6758 (1999): 165-167.

Cutter, G., et al. "Sampling and Sample-handling Protocols for GEOTRACES Cruises, Cookbook, htt p." (2010).

Dehairs, Frank, et al. "Barium in twilight zone suspended matter as a potential proxy for particulate organic carbon remineralization: Results for the North Pacific." Deep Sea Research Part II: Topical Studies in Oceanography 55.14 (2008): 1673-1683.

Dehairs, Frank, Roger Chesselet, and Jacques Jedwab. "Discrete suspended particles of barite and the barium cycle in the open ocean." Earth and Planetary Science Letters 49.2 (1980): 528-550.

DeLong, Edward F., et al. "High abundance of Archaea in Antarctic marine picoplankton." Nature 371.6499 (1994): 695-697.

Déry, Stephen J., and E. F. Wood. "Decreasing river discharge in northern Canada." Geophysical Research Letters 32.10 (2005).

Díez, Beatriz, et al. "High cyanobacterial nifH gene diversity in Arctic seawater and sea ice brine." Environmental microbiology reports 4.3 (2012): 360-366.

Doney, Scott C. "Oceanography: Plankton in a warmer world." Nature 444.7120 (2006): 695-696.

Duce, Robert A., and Gerald L. Hoffman. "Atmospheric vanadium transport to the ocean." Atmospheric Environment (1967) 10.11 (1976): 989-996.

Dulaquais, Gabriel, et al. "The biogeochemistry of cobalt in the Mediterranean Sea." *Global Biogeochemical Cycles* 31.2 (2017): 377-399.

Elderfield, H., and R. E. M. Rickaby. "Oceanic Cd/P ratio and nutrient utilization in the glacial Southern Ocean." Nature 405.6784 (2000): 305-310.

Falkowski, Paul G. "Evolution of the nitrogen cycle and its influence on the biological sequestration of CO2 in the ocean." Nature 387.6630 (1997): 272.

Feng, Q. I., Kazumichi Yanagisawa, and Nakamichi Yamasaki. "Hydrothermal soft chemical process for synthesis of manganese oxides with tunnel structures." *Journal of Porous Materials* 5.2 (1998): 153-162.

Fenwick, Lindsay Alexandra. Methane and nitrous oxide distributions across the North American Arctic Ocean during summer, 2015. Diss. University of British Columbia, 2016.

Field, Christopher B., et al. "Primary production of the biosphere: integrating terrestrial and oceanic components." Science 281.5374 (1998): 237-240.

Finkel, Zoe V., et al. "Phytoplankton in a changing world: cell size and elemental stoichiometry." Journal of plankton research (2009): fbp098.

Fitzsimmons, Jessica N., et al. "Iron persistence in a distal hydrothermal plume supported by dissolved-particulate exchange." *Nature Geoscience* 10.3 (2017): 195-201.

Francois, Roger, et al. "Biogenic barium fluxes to the deep sea: Implications for paleoproductivity reconstruction." Global Biogeochemical Cycles 9.2 (1995): 289-303.

Frew, Russell D. "Influence of Southern Ocean waters on the cadmium—phosphate properties of the global ocean." Nature 360 (1992).

Fu, Gongmin, Herbert E. Allen, and Christina E. Cowan. "Adsorption of cadmium and copper by manganese oxide." Soil Science 152.2 (1991): 72-81.

Gao, Kunshan, et al. "Rising CO2 and increased light exposure synergistically reduce marine primary productivity." Nature climate change 2.7 (2012): 519-523.

Geider, Richard, and Julie La Roche. "Redfield revisited: variability of C: N: P in marine microalgae and its biochemical basis." *European Journal of Phycology* 37.1 (2002): 1-17.

Giesbrecht, Timothy, et al. "The distribution of dissolved and total dissolvable aluminum in the Beaufort Sea and Canada Basin region of the Arctic Ocean." Journal of Geophysical Research: Oceans 118.12 (2013): 6824-6837.

Gledhill, Martha, and Constant MG van den Berg. "Determination of complexation of iron (III) with natural organic complexing ligands in seawater using cathodic stripping voltammetry." Marine Chemistry 47.1 (1994): 41-54.

Gledhill, Martha, et al. "Influence of ocean acidification on the complexation of iron and copper by organic ligands in estuarine waters." *Marine Chemistry* 177 (2015): 421-433.

Gledhill, Martha, and Kristen N. Buck. "The organic complexation of iron in the marine environment: a review." The microbial ferrous wheel: iron cycling in terrestrial, freshwater, and marine environments 29 (2012).

González-Munoz, Maria Teresa, et al. "Precipitation of barite by Myxococcus xanthus: possible implications for the biogeochemical cycle of barium." Applied and Environmental Microbiology 69.9 (2003): 5722-5725.

Gooday, A. J., and J. A. Nott. "Intracellular barite crystals in two xenophyophores, Aschemonella ramuliformis and Galatheammina sp.(Protozoa: Rhizopoda) with comments on the taxonomy of A. ramuliformis." Journal of the Marine Biological Association of the United Kingdom 62.03 (1982): 595-605.

Griffith, Elizabeth M., and Adina Paytan. "Barite in the ocean–occurrence, geochemistry and palaeoceanographic applications." Sedimentology 59.6 (2012): 1817-1835.

Grill, Erwin, Ernst-L. Winnacker, and Meinhart H. Zenk. "Phytochelatins, a class of heavy-metal-binding peptides from plants, are functionally analogous to metallothioneins." *Proceedings of the National Academy of Sciences* 84.2 (1987): 439-443.

Guerrero, Maria A., and Ronald D. Jones. "Photoinhibition of marine nitrifying bacteria. I. Wavelength-dependent response." Marine Ecology Progress Series 141 (1996): 183-192.

Guo, Jian, et al. "COPPER-UPTAKE KINETICS OF COASTAL AND OCEANIC DIATOMS1." Journal of Phycology 46.6 (2010): 1218-1228.

Guo, Jian, et al. "THE EFFECTS OF IRON AND COPPER AVAILABILITY ON THE COPPER STOICHIOMETRY OF MARINE PHYTOPLANKTON1." Journal of phycology 48.2 (2012): 312-325.

Hansel CM. "Manganese in Marine Microbiology." Advances in Microbial Physiology. 70 (2017): 37–83.

Harrison, Gail I., and F. M. M. Morel. "Response of the marine diatom Thalassiosira weissflogii to iron stress." Limnology and Oceanography 31.3 (1986): 989-997.

Hassler, Christel, and V. Schoemann. "Bioavailability of organically bound Fe to model phytoplankton of the Southern Ocean." *Biogeosciences* 6.10 (2009): 2281-2296.

Hatzenpichler, Roland. "Diversity, physiology, and niche differentiation of ammonia-oxidizing archaea." Applied and Environmental Microbiology 78.21 (2012): 7501-7510.

Hillebrand, Helmut, et al. "Biovolume calculation for pelagic and benthic microalgae." *Journal of phycology* 35.2 (1999): 403-424.

Ho, Tung-Yuan, et al. "The trace metal composition of size-fractionated plankton in the South China Sea: Biotic versus abiotic sources." Limnology and Oceanography 52.5 (2007): 1776-1788.

Ho, Tung-Yuan, et al. "The Elemental composition of some marine phytoplankton1." Journal of Phycology 39.6 (2003): 1145-1159.

Honjo, Susumu, et al. "Particulate organic carbon fluxes to the ocean interior and factors controlling the biological pump: A synthesis of global sediment trap programs since 1983." *Progress in Oceanography* 76.3 (2008): 217-285.

Hoppe et al. "Resistance of Arctic phytoplankton to ocean acidification and high irradiance." *Polar Biology* (2017). in review.

Hoppe et al. "Functional redundancy facilitates resilience of Subarctic phytoplankton assemblages towards Ocean Acidification and high irradiance." *Frontiers in Marine Science* (2017). in review.

Horner, Tristan J., et al. "Nonspecific uptake and homeostasis drive the oceanic cadmium cycle." *Proceedings of the National Academy of Sciences* 110.7 (2013): 2500-2505.

Hudson, Robert JM, and Francois MM Morel. "Distinguishing between extra-and intracellular iron in marine phytoplankton." Limnology and Oceanography 34.6 (1989): 1113-1120.

Hudson, Robert JM, Fraqois MM Morel, and F. M. M. Morel. "Iron transport in marine phytoplankton: Kinetics of cellular and medium coordination reactions." Limnol. Oceanogr 35.5 (1990): 1002-1020.

Hurst, Matthew P., Ana M. Aguilar-Islas, and Kenneth W. Bruland. "Iron in the southeastern Bering Sea: elevated leachable particulate Fe in shelf bottom waters as an important source for surface waters." Continental Shelf Research 30.5 (2010): 467-480.

Jeandel, C., M. Caisso, and J. F. Minster. "Vanadium behaviour in the global ocean and in the Mediterranean Sea." Marine Chemistry 21.1 (1987): 51-74.

Jickells, T. D., et al. "Global iron connections between desert dust, ocean biogeochemistry, and climate." science 308.5718 (2005): 67-71.

Jin, X., et al. "Diagnosing the contribution of phytoplankton functional groups to the production and export of particulate organic carbon, CaCO3, and opal from global nutrient and alkalinity distributions." *Global Biogeochemical Cycles* 20.2 (2006).

Johnson, Kenneth S., Francisco P. Chavez, and Gernot E. Friederich. "Continental-shelf sediment as a primary source of iron for coastal phytoplankton." Nature 398.6729 (1999): 697-700.

Jones, E. P., et al. "Tracing Pacific water in the North Atlantic ocean." Journal of Geophysical Research: Oceans 108.C4 (2003).

Jørgensen, Bo Barker. "Bacteria and marine biogeochemistry." Marine geochemistry. Springer Berlin Heidelberg, 2000. 173-207.

Kalanetra, Karen M., Nasreen Bano, and James T. Hollibaugh. "Ammonia-oxidizing Archaea in the Arctic Ocean and Antarctic coastal waters." Environmental microbiology 11.9 (2009): 2434-2445.

Karl, David M., et al. "Trichodesmium blooms and new nitrogen in the North Pacific gyre." Marine pelagic cyanobacteria: Trichodesmium and other diazotrophs. Springer Netherlands, 1992. 219-237.

Karner, Markus B., Edward F. DeLong, and David M. Karl. "Archaeal dominance in the mesopelagic zone of the Pacific Ocean." Nature 409.6819 (2001): 507-510.

Kerou, Melina, et al. "Proteomics and comparative genomics of Nitrososphaera viennensis reveal the core genome and adaptations of archaeal ammonia oxidizers." Proceedings of the National Academy of Sciences (2016): 201601212.

Kirchman, David L., et al. "Standing stocks, production, and respiration of phytoplankton and heterotrophic bacteria in the western Arctic Ocean." Deep Sea Research Part II: Topical Studies in Oceanography 56.17 (2009): 1237-1248.

Könneke, Martin, et al. "Isolation of an autotrophic ammonia-oxidizing marine archaeon." Nature 437.7058 (2005): 543-546.

Kuma, Kenshi, et al. "Photo-reduction of Fe (III) by dissolved organic substances and existence of Fe (II) in seawater during spring blooms." Marine Chemistry 37.1-2 (1992): 15-27.

Lam, Phoebe J., and James KB Bishop. "The continental margin is a key source of iron to the HNLC North Pacific Ocean." Geophysical Research Letters 35.7 (2008).

Lam, Phoebe J., Daniel C. Ohnemus, and Maureen E. Auro. "Size-fractionated major particle composition and concentrations from the US GEOTRACES north Atlantic zonal transect." Deep Sea Research Part II: Topical Studies in Oceanography 116 (2015): 303-320.

Lam, Phoebe J., et al. "Wintertime phytoplankton bloom in the subarctic Pacific supported by continental margin iron." Global Biogeochemical Cycles 20.1 (2006).

Landing, William M., and Kenneth W. Bruland. "The contrasting biogeochemistry of iron and manganese in the Pacific Ocean." Geochimica et Cosmochimica Acta 51.1 (1987): 29-43.

Lane, Erin S., et al. "Effects of iron limitation on intracellular cadmium of cultured phytoplankton: implications for surface dissolved cadmium to phosphate ratios." *Marine Chemistry* 115.3 (2009): 155-162.

Lee, Jennifer G., Beth A. Ahner, and François MM Morel. "Export of cadmium and phytochelatin by the marine diatom Thalassiosira weissflogii." *Environmental science & technology* 30.6 (1996): 1814-1821.

Lee, Sanghoon, and Jed A. Fuhrman. "Relationships between biovolume and biomass of naturally derived marine bacterioplankton." Applied and environmental microbiology 53.6 (1987): 1298-1303.

Lee, Yoon, and Bradley M. Tebo. "Cobalt (II) oxidation by the marine manganese (II)-oxidizing Bacillus sp. strain SG-1." Applied and environmental microbiology 60.8 (1994): 2949-2957.

Lesser, Michael P. "Oxidative stress in marine environments: biochemistry and physiological ecology." *Annu. Rev. Physiol.* 68 (2006): 253-278.

Letelier, Ricardo M., and David M. Karl. "Role of Trichodesmium spp. in the productivity of the subtropical North Pacific Ocean." (1996).

Li, Yuan-Hui, James Bischoff, and Guy Mathieu. "The migration of manganese in the Arctic Basin sediment." Earth and Planetary Science Letters 7.3 (1969): 265-270.

Lippsett, Lonny. "Is global warming changing the Arctic?." *Oceanus* 44.3 (2005): 24.

Lis, Hagar, et al. "Iron bioavailability to phytoplankton: an empirical approach." The ISME journal 9.4 (2015): 1003-1013.

Liu, W. X., et al. "Multivariate statistical study of heavy metal enrichment in sediments of the Pearl River Estuary." Environmental Pollution 121.3 (2003): 377-388.

Loring, D. H. "Trace-metal geochemistry of sediments from Baffin Bay." Canadian Journal of Earth Sciences 21.12 (1984): 1368-1378.

Löscher, B. M., J. T. M. De Jong, and H. J. W. De Baar. "The distribution and preferential biological uptake of cadmium at 6 W in the Southern Ocean." Marine Chemistry 62.3 (1998): 259-286.

Lovely, D. R., Elizabeth JP Phillips, and Debra J. Lonergan. "Enzymatic versus nonenzymatic mechanisms for Fe (III) reduction in aquatic sediments." Environmental Science and Technology;(United States) 25.6 (1991).

Loveley, Derek R., and Elizabeth JP Phillips. "Novel mode of microbial energy metabolism: organic carbon oxidation coupled to dissimilatory reduction of iron or manganese." Applied and environmental microbiology 54.6 (1988): 1472-1480.

Luo, Y-W., et al. "Database of diazotrophs in global ocean: abundance, biomass and nitrogen fixation rates." Earth System Science Data 4.1 (2012): 47-73.

Maldonado, M. T., and N. M. Price. "Influence of N substrate on Fe requirements of marine centric diatoms." Marine Ecology Progress Series 141 (1996): 161-172.

Maldonado, Maria T., and Neil M. Price. "Reduction and transport of organically bound iron by Thalassiosira oceanica (Bacillariophyceae)." Journal of Phycology 37.2 (2001): 298-310.

Maldonado, Maria T., and Neil M. Price. "Utilization of iron bound to strong organic ligands by plankton communities in the subarctic Pacific Ocean." Deep Sea Research Part II: Topical Studies in Oceanography 46.11 (1999): 2447-2473.

Maldonado, Maria T., et al. "Copper-dependent iron transport in coastal and oceanic diatoms." Limnology and oceanography 51.4 (2006): 1729-1743.

Manceau, Alain, et al. "Ba and Ni speciation in a nodule of binary Mn oxide phase composition from Lake Baikal." *Geochimica et Cosmochimica Acta* 71.8 (2007): 1967-1981.

Marchetti A and Maldonado MT. (2016) Iron, In: Borowitzka MA, Beardell J and Raven J (ed.) The Physiology of Microalgae. Springer Publishing. 233-279.

Martens-Habbena, Willm, et al. "Ammonia oxidation kinetics determine niche separation of nitrifying Archaea and Bacteria." Nature 461.7266 (2009): 976-979.

Martin, Johannie, et al. "Prevalence, structure and properties of subsurface chlorophyll maxima in Canadian Arctic waters." *Marine Ecology Progress Series* 412 (2010): 69-84.

Martin, J. M., et al. "Preliminary assessment of the distributions of some trace elements (As, Cd, Cu, Fe, Ni, Pb and Zn) in a pristine aquatic environment: the Lena River estuary (Russia)." Marine Chemistry 43.1-4 (1993): 185-199.

Martinez-Perez, Clara, et al. "The small unicellular diazotrophic symbiont, UCYN-A, is a key player in the marine nitrogen cycle." Nature Microbiology 1 (2016): 16163.

Martiny, Adam C., Jasper A. Vrugt, and Michael W. Lomas. "Concentrations and ratios of particulate organic carbon, nitrogen, and phosphorus in the global ocean." *Scientific data* 1 (2014).

McLaughlin, Fiona A., and Eddy C. Carmack. "Deepening of the nutricline and chlorophyll maximum in the Canada Basin interior, 2003–2009." Geophysical Research Letters 37.24 (2010).

McLaughlin, Fiona, et al. "The hydrography of the southern Canada Basin, 2002." Polar Biology 28.3 (2005): 182-189.

Measures, C. I. "The role of entrained sediments in sea ice in the distribution of aluminium and iron in the surface waters of the Arctic Ocean." Marine chemistry 68.1 (1999): 59-70.

Michel, Christine, et al. "Arctic Ocean outflow shelves in the changing Arctic: A review and perspectives." Progress in Oceanography 139 (2015): 66-88.

Millero, Frank J., Sara Sotolongo, and Miguel Izaguirre. "The oxidation kinetics of Fe (II) in seawater." Geochimica et Cosmochimica Acta 51.4 (1987): 793-801.

Mills, Matthew M., et al. "Iron and phosphorus co-limit nitrogen fixation in the eastern tropical North Atlantic." Nature 429.6989 (2004): 292-294.

Moffett, James W., and Jackson Ho. "Oxidation of cobalt and manganese in seawater via a common microbially catalyzed pathway." Geochimica et Cosmochimica Acta 60.18 (1996): 3415-3424.

Montoya, Joseph P., et al. "High rates of N2 fixation by unicellular diazotrophs in the oligotrophic Pacific Ocean." Nature 430.7003 (2004): 1027-1032.

Moran, S. B., and J. N. Smith. "234Th as a tracer of scavenging and particle export in the Beaufort Sea." Continental Shelf Research 20.2 (2000): 153-167.

Morel, F. M. M., et al. "Zinc and carbon co-limitation of marine phytoplankton." Nature 369.6483 (1994): 740-742.

Murozumi, M., Tsaihwa J. Chow, and Claire Patterson. "Chemical concentrations of pollutant lead aerosols, terrestrial dusts and sea salts in Greenland and Antarctic snow strata." Geochimica et Cosmochimica Acta 33.10 (1969): 1247-1294.

Murray, James W., and John G. Dillard. "The oxidation of cobalt (II) adsorbed on manganese dioxide." Geochimica et Cosmochimica Acta 43.5 (1979): 781-787.

Myers, Charles R., and Kenneth H. Nealson. "Bacterial manganese reduction and growth with manganese oxide as the sole electron acceptor." Science 240.4857 (1988): 1319.

Nair, R. R., and V. Ittekkot. "Enhanced particle fluxes in Bay of Bengal induced by injection of fresh water." Nature 351.6325 (1991): 385.

Naqvi, S. W. A., et al. "Marine hypoxia/anoxia as a source of CH4 and N2O." (2010).

Nealson, Kenneth H., Bradley M. Tebo, and Reinhardt A. Rosson. "Occurrence and mechanisms of microbial oxidation of manganese." *Advances in Applied Microbiology* 33 (1988): 279-318.

Nicolaus M, Katlein C, Maslanik J, Hendricks S (2012) Changes in Arctic sea ice result in increasing light transmittance and absorption. Geophysical Research Letters 39:L24501

Noble, Abigail E., et al. "Dissolved and particulate trace metal micronutrients under the McMurdo Sound seasonal sea ice: basal sea ice communities as a capacitor for iron." Frontiers in chemistry 1 (2013): 25.

Ohnemus, Daniel Chester. *The biogeochemistry of marine particulate trace metals*. Diss. Massachusetts Institute of Technology, 2014.

Ohnemus, Daniel C., and Phoebe J. Lam. "Cycling of lithogenic marine particles in the US GEOTRACES North Atlantic transect." Deep Sea Research Part II: Topical Studies in Oceanography 116 (2015): 283-302.

Ohnemus, Daniel C., et al. "Laboratory intercomparison of marine particulate digestions including Piranha: a novel chemical method for dissolution of polyethersulfone filters." Liminol. Oceanogr. Methods 12 (2014): 530-547.

Orians, Kristin J., and Kenneth W. Bruland. "The biogeochemistry of aluminum in the Pacific Ocean." Earth and planetary science letters 78.4 (1986): 397-410.

Pabi, Sudeshna, Gert L. van Dijken, and Kevin R. Arrigo. "Primary production in the Arctic Ocean, 1998–2006." Journal of Geophysical Research: Oceans 113.C8 (2008).

Peers, Graham, and Neil M. Price. "Copper-containing plastocyanin used for electron transport by an oceanic diatom." Nature 441.7091 (2006): 341-344.

Pachauri, Rajendra K., et al. Climate change 2014: synthesis report. Contribution of Working Groups I, II and III to the fifth assessment report of the Intergovernmental Panel on Climate Change. IPCC, 2014.

Peers, Graham, Sarah-Ann Quesnel, and Neil M. Price. "Copper requirements for iron acquisition and growth of coastal and oceanic diatoms." Limnology and oceanography 50.4 (2005): 1149-1158.

Perovich, Donald K., et al. "Sunlight, water, and ice: Extreme Arctic sea ice melt during the summer of 2007." Geophysical Research Letters 35.11 (2008).

Planquette, Hélène, et al. "Particulate iron delivery to the water column of the Amundsen Sea, Antarctica." Marine Chemistry 153 (2013): 15-30.

Quigg, Antonietta, Andrew J. Irwin, and Zoe V. Finkel. "Evolutionary inheritance of elemental stoichiometry in phytoplankton." Proceedings of the Royal Society of London B: Biological Sciences 278.1705 (2011): 526-534.

Rachold, Volker, et al. "Sediment transport to the Laptev Sea–hydrology and geochemistry of the Lena River." Polar Research 15.2 (1996): 183-196.

Raven, J. (1998). The twelfth Tansley lecture. Small is beautiful: The picophytoplankton. Functinal Ecology 12, 503-513.

Raven, John A., Michael CW Evans, and Rebecca E. Korb. "The role of trace metals in photosynthetic electron transport in O2-evolving organisms." Photosynthesis Research 60.2-3 (1999): 111-150.

Revels, Brandi N., et al. "The isotopic signature and distribution of particulate iron in the North Atlantic Ocean." Deep Sea Research Part II: Topical Studies in Oceanography 116 (2015): 321-331.

Reynolds, Colin S. The ecology of phytoplankton. Cambridge University Press, 2006.

Rosen, Julia. "AFTER THE ICE GOES." (2017): 152-154.

Rosman, K. J. R., et al. "Isotopic evidence for the source of lead in Greenland snows since the late 1960s." Nature 362.6418 (1993): 333-335.

Rudels, Bert, et al. "Atlantic sources of the Arctic Ocean surface and halocline waters." *Polar Research* 23.2 (2004): 181-208.

Rue, Eden L., and Kenneth W. Bruland. "Complexation of iron (III) by natural organic ligands in the Central North Pacific as determined by a new competitive ligand equilibration/adsorptive cathodic stripping voltammetric method." Marine chemistry 50.1-4 (1995): 117-138.

Rueter, John G., James J. McCarthy, and Edward J. Carpenter. "The toxic effect of copper on Oscillatoria (Trichodesmium) theibautii." Limnology and Oceanography 24.3 (1979): 558-562.

Run, Zhang, et al. "Insights into the coupling of upper ocean-benthic carbon dynamics in the western Arctic Ocean from an isotopic (13C, 234Th) perspective." Acta Oceanologica Sinica 34.6 (2015): 26-33.

Saager, Paul M., Johan Schijf, and Hein JW de Baar. "Trace-metal distributions in seawater and anoxic brines in the eastern Mediterranean Sea." Geochimica et cosmochimica acta 57.7 (1993): 1419-1432.

Saito, Mak A., et al. "Cobalt limitation and uptake in Prochlorococcus." Limnology and Oceanography 47.6 (2002): 1629-1636.

Sañudo-Wilhelmy, Sergio A., et al. "The impact of surface-adsorbed phosphorus on phytoplankton Redfield stoichiometry." Nature 432.7019 (2004): 897-901.

Segovia, María, et al. "Iron availability modulates the effects of future CO2 levels within the marine planktonic food web." *Marine Ecology Progress Series* 565 (2017): 17-33.

Semeniuk, David M., et al. "Iron–copper interactions in iron-limited phytoplankton in the northeast subarctic Pacific Ocean." Limnology and Oceanography 61.1 (2016): 279-297.

Shaked, Yeala, Adam B. Kustka, and François MM Morel. "A general kinetic model for iron acquisition by eukaryotic phytoplankton." Limnol. Oceanogr 50.3 (2005): 872-882.

Shaw, Denis M., Jaroslav Dostal, and Reid R. Keays. "Additional estimates of continental surface Precambrian shield composition in Canada." Geochimica et Cosmochimica Acta 40.1 (1976): 73-83.

Sherrell, Robert M., and Edward A. Boyle. "The trace metal composition of suspended particles in the oceanic water column near Bermuda." Earth and Planetary Science Letters 111.1 (1992): 155-174.

Sherrell, Robert M., M. Paul Field, and Greg Ravizza. "Uptake and fractionation of rare earth elements on hydrothermal plume particles at 9 45′ N, East Pacific Rise." *Geochimica et Cosmochimica Acta* 63.11 (1999): 1709-1722.

Shi, Dalin, et al. "Effect of ocean acidification on iron availability to marine phytoplankton." Science 327.5966 (2010): 676-679.

Sholkovitz, Edward R., Peter N. Sedwick, and Thomas M. Church. "On the fractional solubility of copper in marine aerosols: Toxicity of aeolian copper revisited." Geophysical Research Letters 37.20 (2010).

Silver, Simon, and le T. Phung. "A bacterial view of the periodic table: genes and proteins for toxic inorganic ions." *Journal of Industrial Microbiology and Biotechnology* 32.11-12 (2005): 587-605.

Smith, Kenneth L., et al. "Free-drifting icebergs: hot spots of chemical and biological enrichment in the Weddell Sea." science 317.5837 (2007): 478-482.

Stein, Jeffrey L., and Melvin I. Simon. "Archaeal ubiquity." Proceedings of the National Academy of Sciences 93.13 (1996): 6228-6230.

Stone, Alan T. "Microbial metabolites and the reductive dissolution of manganese oxides: oxalate and pyruvate." Geochimica et Cosmochimica Acta 51.4 (1987): 919-925.

CEL, PHYTOPLANKTON FROM, and L. VOLUME OR. "Richard R. Strathmann." *CELL* 2400.2600 (1966): 2800.

Sugie, Koji, et al. "Synergistic effects of pCO2 and iron availability on nutrient consumption ratio of the Bering Sea phytoplankton community." *Biogeosciences* 10.10 (2013): 6309-6321.

Sunda, W. G., S. A. Huntsman, and G. R. Harvey. "Photoreduction of manganese oxides in seawater and its geochemical and biological implications." (1983): 234-236.

Sunda, William G., and Susan A. Huntsman. "Interactive effects of external manganese, the toxic metals copper and zinc, and light in controlling cellular manganese and growth in a coastal diatom." Limnology and Oceanography 43.7 (1998): 1467-1475.

Sunda, William G., and Susan A. Huntsman. "Interrelated influence of iron, light and cell size on marine phytoplankton growth." Nature 390.6658 (1997): 389-392.

Sunda, William G., and Susan A. Huntsman. "Regulation of copper concentration in the oceanic nutricline by phytoplankton uptake and regeneration cycles." Limnology and oceanography 40.1 (1995): 132-137.

Sunda, William, and Susan Huntsman. "Effect of pH, light, and temperature on Fe–EDTA chelation and Fe hydrolysis in seawater." Marine Chemistry 84.1 (2003): 35-47.

Swinbanks, David D., and Yoshihisa Shirayama. "High levels of natural radionuclides in a deep-sea infaunal xenophyophore." (1986): 354-358.

Taylor, Kevin G., and Joe HS Macquaker. "Iron minerals in marine sediments record chemical environments." Elements 7.2 (2011): 113-118.

Taylor, Rebecca L., et al. "Colimitation by light, nitrate, and iron in the Beaufort Sea in late summer." Journal of Geophysical Research: Oceans 118.7 (2013): 3260-3277.

Taylor, S. R. "Abundance of chemical elements in the continental crust: a new table." Geochimica et cosmochimica acta 28.8 (1964): 1273-1285.

Taylor, Stuart Ross, and Scott M. McLennan. "The geochemical evolution of the continental crust." Reviews of Geophysics 33.2 (1995): 241-265.

Tebo, Bradley M. "Manganese (II) oxidation in the suboxic zone of the Black Sea." *Deep Sea Research Part A. Oceanographic Research Papers* 38 (1991): S883-S905.

Tebo, Bradley M., et al. "Geomicrobiology of manganese (II) oxidation." TRENDS in Microbiology 13.9 (2005): 421-428.

Tendal, Ole Secher. A monograph of the xenophyophoria:(Rhizopodea, Protozoa). Danish Science Press, 1972.

Thamdrup, Bo. "Bacterial manganese and iron reduction in aquatic sediments." Advances in microbial ecology. Springer US, 2000. 41-84.

Tortell, Philippe D., et al. "CO2 sensitivity of Southern Ocean phytoplankton." *Geophysical Research Letters* 35.4 (2008).

Tremblay, Jean-Éric, et al. "Global and regional drivers of nutrient supply, primary production and CO 2 drawdown in the changing Arctic Ocean." *Progress in Oceanography* 139 (2015): 171-196.

Tremblay, Jean-Éric, and Jonathan Gagnon. "The effects of irradiance and nutrient supply on the productivity of Arctic waters: a perspective on climate change." Influence of climate change on the changing arctic and sub-arctic conditions. Springer Netherlands, 2009. 73-93.

Tremblay, Jean-Éric, et al. "Vertical stability and the annual dynamics of nutrients and chlorophyll fluorescence in the coastal, southeast Beaufort Sea." Journal of Geophysical Research: Oceans 113.C7 (2008).

Trimble, S. M., and M. Baskaran. "The role of suspended particulate matter in 234 Th scavenging and 234 Th-derived export fluxes of POC in the Canada Basin of the Arctic Ocean." Marine Chemistry 96.1 (2005): 1-19.

Twining, Benjamin S., et al. "Metal quotas of plankton in the equatorial Pacific Ocean." Deep Sea Research Part II: Topical Studies in Oceanography 58.3 (2011): 325-341.

Twining, Benjamin S., et al. "Variations in Synechococcus cell quotas of phosphorus, sulfur, manganese, iron, nickel, and zinc within mesoscale eddies in the Sargasso Sea." Limnology and Oceanography 55.2 (2010): 492-506.

Twining, Benjamin S., Stephen B. Baines, and Nicholas S. Fisher. "Element stoichiometries of individual plankton cells collected during the Southern Ocean Iron Experiment(SOFeX)." Limnology and oceanography 49.6 (2004): 2115-2128.

Twining, Benjamin S., and Stephen B. Baines. "The trace metal composition of marine phytoplankton." *Annual review of marine science* 5 (2013): 191-215.

Varela, Diana E., et al. "Pelagic primary productivity and upper ocean nutrient dynamics across Subarctic and Arctic Seas." Journal of Geophysical Research: Oceans 118.12 (2013): 7132-7152.

Waeles, Matthieu, et al. "Cadmium in the waters off South Morocco: Nature of particles hosting Cd and insights into the mechanisms fractionating Cd from phosphate." Journal of Geophysical Research: Oceans 121.5 (2016): 3106-3120.

Wagner, H., Jakob, T., Wilhelm, C. (2006). Balancing the energy flow from captured light to biomass under fluctuating light conditions. New Phytologist 169, 95-108.

Waite, T. D., et al. "Diel variations in iron speciation in northern Australian shelf waters." Marine Chemistry 50.1-4 (1995): 79-91.

Wedepohl, K. Hans. "The composition of the continental crust." Geochimica et cosmochimica Acta 59.7 (1995): 1217-1232.

Westerlund, Stig, and Peder Öhman. "Iron in the water column of the Weddell Sea." Marine Chemistry 35.1-4 (1991): 199-217.

Wilson, Samuel T., et al. "Dissolved hydrogen and nitrogen fixation in the oligotrophic North Pacific Subtropical Gyre." *Environmental microbiology reports* 5.5 (2013): 697-704.

Wuchter, Cornelia, et al. "Archaeal nitrification in the ocean." Proceedings of the National Academy of Sciences 103.33 (2006): 12317-12322.

Xu, Yan, et al. "Structure and metal exchange in the cadmium carbonic anhydrase of marine diatoms." Nature 452.7183 (2008): 56-61.

Yamamoto-Kawai M, McLaughlin FA, Carmack EC, Nishino S, Shimada K (2009) Aragonite undersaturation in the Arctic Ocean: Effects of ocean acidification and sea ice melt. Science 326:1098-1100.

Yamamoto-Kawai, Michiyo, Eddy Carmack, and Fiona McLaughlin. "Nitrogen balance and Arctic throughflow." Nature 443.7107 (2006): 43-43.

Yang, Jiayan. "Seasonal and interannual variability of downwelling in the Beaufort Sea." *Journal of Geophysical Research: Oceans* 114.C1 (2009).

Yao, Wensheng, and Frank J. Millero. "Oxidation of hydrogen sulfide by hydrous Fe (III) oxides in seawater." *Marine Chemistry* 52.1 (1996): 1-16.

Yoshimura, Takeshi, et al. "Impacts of elevated CO2 on particulate and dissolved organic matter production: microcosm experiments using iron-deficient plankton communities in open subarctic waters." *Journal of oceanography* 69.5 (2013): 601-618.

Zehr, Jonathan P., et al. "Unicellular cyanobacteria fix N2 in the subtropical North Pacific Ocean." *Nature* 412.6847 (2001): 635-638.

Appendices (Supplementary tables)

Table SI1: Full-depth dataset of particulate trace metals, particulate phosphorus, PON and POC in the Labrador Sea. Note the units are nM for Al, P and Fe; µM for PON and POC. NS denotes not sampled; BDL denotes below detection limit.

Station	**Depth (m)**	Al (nM)	Cd (pM)	Pb (pM)	P (nM)	V (pM)	Mn (pM)	Fe (nM)	Co (pM)	Cu (pM)	Zn (pM)	Ba (pM)	PON (µM)	POC (µM)
K1	**9**	55.4	4.2	1.3	50.8	BDL	BDL	1.0	BDL	52.9	236.3	BDL	2.0	15.1
K1	**29**	2.6	5.6	0.2	35.5	BDL	BDL	BDL	BDL	29.5	63.3	BDL	1.6	9.5
K1	**50**	3.6	2.7	0.0	24.4	BDL	36.5	0.0	BDL	30.9	141.1	BDL	2.1	12.6
K1	**100**	17.4	2.6	0.3	13.2	BDL	27.4	0.2	BDL	32.6	65.3	46.5	0.7	5.6
K1	**149**	26.0	1.8	0.1	10.7	BDL	34.1	0.4	BDL	36.9	37.8	52.1	0.4	3.6
K1	**305**	10.2	1.7	0.2	8.1	BDL	88.4	1.2	BDL	28.1	135.0	29.3	0.2	2.9
K1	**504**	48.4	1.1	18.8	4.7	BDL	111.6	1.2	BDL	26.2	370.3	123.4	0.2	1.9
K1	**707**	6.7	1.0	3.5	5.3	BDL	50.7	0.7	BDL	21.4	43.0	93.9	0.3	2.4
K1	**1620**	5.8	0.5	0.4	3.3	BDL	93.0	1.3	BDL	25.2	9.5	21.7	NS	NS
K1	**2332**	6.9	BDL	5.6	1.5	BDL	71.7	1.5	BDL	11.0	23.0	12.2	0.1	1.9
K1	**3047**	51.9	BDL	17.3	5.3	BDL	131.8	2.8	BDL	27.1	102.7	2.2	0.1	1.3
LS2	**11**	4.1	8.0	12.7	81.6	50.6	59.8	0.7	BDL	74.8	226.8	7.4	2.0	11.7
LS2	**11**	3.8	10.6	10.5	81.5	52.2	82.1	0.7	BDL	66.3	257.1	18.2	2.0	11.7
LS2	**19**	4.3	6.6	2.2	49.5	44.1	87.0	0.7	BDL	63.3	181.1	23.9	2.1	11.0
LS2	**30**	2.9	7.6	BDL	55.5	35.9	96.7	0.6	BDL	59.3	366.7	34.9	1.2	7.4
LS2	**45**	5.6	4.8	4.0	18.8	BDL	164.8	0.8	BDL	53.4	65.5	28.4	0.4	2.9
LS2	**63**	5.4	5.4	1.4	17.7	11.4	285.9	1.2	BDL	65.0	146.8	48.5	0.4	2.6
LS2	**301**	15.1	BDL	48.2	4.7	17.5	182.9	3.1	BDL	36.8	71.3	81.0	0.1	1.0
LS2	**504**	20.4	3.1	2.4	12.9	16.6	158.7	3.3	BDL	53.3	76.9	267.4	0.1	0.8
LS2	**1008**	20.2	2.2	31.0	5.4	13.4	114.7	2.1	BDL	28.4	66.9	215.7	0.1	0.6
LS2	**1008**	8.0	BDL	5.2	6.7	BDL	105.1	2.1	BDL	34.8	135.8	193.2	0.1	0.6
LS2	**2028**	17.9	BDL	5.7	3.1	20.6	207.0	4.0	BDL	32.9	38.8	109.6	0.2	0.5
LS2	**2435**	23.1	3.7	6.6	8.5	24.9	207.9	4.1	BDL	46.5	166.0	396.4	0.1	0.4

Table SI2: Full-depth dataset of particulate trace metals, particulate phosphorus, PON and POC in the Baffin Bay. Note the units are nM for Al, P and Fe; µM for PON and POC. NS denotes not sampled; BDL denotes below detection limit.

Station	**Depth (m)**	Al (nM)	Cd (pM)	Pb (pM)	P (nM)	V (pM)	Mn (pM)	Fe (nM)	Co (pM)	Cu (pM)	Zn (pM)	Ba (pM)	PON (µM)	POC (µM)
BB1	**10**	6.9	7.2	1.2	64.6	12.5	219.0	1.7	BDL	78.3	189.1	57.6	1.7	8.6
BB1	**11**	11.9	9.6	2.5	72.1	22.0	621.3	2.7	BDL	120.1	186.4	98.6	1.4	7.0
BB1	**29**	14.3	10.0	7.1	46.6	27.6	965.5	3.3	BDL	96.1	106.5	110.4	1.3	7.3
BB1	**46**	34.2	9.8	4.5	26.0	50.6	1983.3	6.5	12.6	110.7	302.3	161.0	0.8	3.1
BB1	**65**	32.9	9.4	4.3	16.7	45.9	1877.7	6.5	13.8	87.9	166.5	153.8	0.4	1.9
BB1	**151**	22.5	8.7	59.3	12.4	26.7	1051.6	6.3	BDL	80.4	342.4	208.5	0.5	2.7
BB1	**303**	51.2	7.3	11.7	12.3	51.4	769.5	11.1	BDL	79.7	181.7	314.5	0.2	1.5
BB1	**505**	30.3	3.4	12.5	6.9	39.2	1015.4	7.4	BDL	63.3	157.3	207.7	0.1	1.1
BB1	**708**	31.4	3.1	3.8	10.3	60.6	1642.0	10.0	BDL	51.7	91.3	187.4	0.1	1.1
BB1	**1011**	306.2	4.1	41.9	15.2	407.1	10818.6	96.9	67.0	181.9	371.1	860.7	0.2	1.4
BB2	**10**	4.9	8.2	3.0	51.2	19.6	549.4	1.1	BDL	76.7	233.4	55.3	1.0	6.3
BB2	**16**	6.6	16.4	10.2	67.3	35.6	525.1	1.5	BDL	90.8	181.3	105.3	1.1	7.7
BB2	**36**	17.8	11.3	2.5	43.7	45.9	1788.7	4.8	BDL	112.0	180.1	123.5	1.3	7.6
BB2	**40**	21.9	13.6	14.8	34.7	54.8	2063.2	6.1	BDL	104.3	253.5	121.2	0.8	5.1
BB2	**54**	30.4	7.6	4.9	17.7	57.3	2083.7	7.1	BDL	93.5	102.2	137.7	0.9	6.9
BB2	**150**	11.3	12.7	19.3	31.7	25.2	1215.4	2.4	15.1	84.3	383.1	133.4	0.5	3.0
BB2	**302**	9.1	2.3	BDL	6.8	15.1	570.0	2.1	BDL	54.7	349.2	181.7	0.4	2.6
BB2	**604**	10.6	2.1	1.9	7.0	14.9	454.6	2.5	BDL	43.8	96.4	157.6	0.2	1.1
BB2	**1008**	14.6	BDL	42.1	5.0	19.8	570.6	3.5	BDL	41.3	17.1	137.3	0.3	0.7
BB2	**1615**	12.8	BDL	BDL	4.8	17.3	547.7	3.2	BDL	58.6	23.2	109.5	NS	NS
BB2	**2122**	42.4	BDL	2.2	4.2	41.7	1425.5	8.7	BDL	66.4	73.8	241.1	0.2	1.6
BB2	**2325**	41.0	BDL	4.5	4.6	37.5	1058.3	6.8	BDL	68.8	58.7	150.8	0.6	2.4
BB3	**10**	10.6	6.9	BDL	56.4	17.9	329.5	2.5	BDL	97.5	296.0	801.1	1.3	8.7
BB3	**15**	8.6	8.7	1.0	120.4	24.1	513.5	2.1	BDL	105.4	337.6	2045.4	3.0	15.9
BB3	**30**	10.5	9.4	3.1	86.2	32.9	979.3	2.6	BDL	119.6	413.7	402.6	1.4	8.4
BB3	**55**	17.5	4.5	5.6	13.0	36.5	1436.8	4.4	BDL	76.2	160.7	141.7	0.2	1.6
BB3	**150**	29.0	8.2	3.3	11.8	42.9	1494.8	6.2	BDL	100.7	1033.1	136.2	0.3	2.0
BB3	**300**	26.2	4.3	2.2	8.8	37.1	1115.2	5.8	BDL	141.6	103.8	283.1	0.4	2.1
BB3	**500**	18.9	2.8	2.0	7.6	31.0	826.4	4.8	BDL	55.7	40.5	170.2	0.2	0.6
BB3	**700**	18.0	1.8	2.1	8.1	27.1	671.3	4.3	BDL	47.2	73.2	148.1	0.1	0.8
BB3	**1000**	80.5	4.5	13.0	13.2	266.7	4849.0	44.1	16.9	76.9	191.7	278.0	0.1	0.8

Table SI3: Full-depth dataset of particulate trace metals, particulate phosphorus, PON and POC in the CAA. Note the units are nM for Al, P and Fe; µM for PON and POC. NS denotes not sampled; BDL denotes below detection limit.

Station	**Depth (m)**	Al (nM)	Cd (pM)	Pb (pM)	P (nM)	V (pM)	Mn (pM)	Fe (nM)	Co (pM)	Cu (pM)	Zn (pM)	Ba (pM)	PON (µM)	POC (µM)
CAA1	**10**	61.1	8.4	1.6	70.8	41.9	182.9	11.5	BDL	82.4	303.2	146.6	1.8	11.3
CAA1	**10**	58.8	6.3	3.3	67.3	41.2	171.9	11.0	BDL	90.1	232.7	153.5	1.8	11.3
CAA1	**20**	143.9	32.0	2.7	70.5	86.1	384.5	24.6	24.7	114.9	307.2	346.1	3.1	16.3
CAA1	**31**	261.7	58.5	2.9	107.9	159.1	679.6	46.8	51.6	167.3	659.1	181.1	2.0	14.0
CAA1	**43**	419.0	45.9	2.8	67.0	242.4	1117.0	78.1	49.0	172.7	524.5	286.3	1.8	13.8
CAA1	**44**	552.6	71.8	2.1	73.7	205.4	952.2	60.2	46.4	164.0	452.4	104.6	1.8	12.0
CAA1	**101**	447.1	12.6	3.9	28.9	259.4	1474.3	73.5	38.4	151.2	240.7	314.2	0.3	2.4
CAA1	**151**	225.9	9.8	4.7	20.6	187.0	1499.1	48.3	23.8	143.6	386.9	250.8	0.3	2.4
CAA1	**202**	288.2	2.6	2.3	21.8	178.2	1633.2	58.2	22.3	130.1	176.5	254.3	0.5	1.9
CAA1	**301**	150.0	1.3	2.3	14.9	91.9	1284.2	25.3	8.5	79.0	91.0	392.1	0.1	1.4
CAA1	**403**	1.9	BDL	BDL	1.3	BDL	24.8	0.5	BDL	BDL	BDL	BDL	0.5	3.3
CAA1	**604**	223.4	0.8	2.7	17.1	140.0	842.7	36.5	11.5	81.9	144.4	203.2	0.2	2.2
CAA3	**10**	221.1	4.8	3.0	52.7	114.4	391.0	35.1	17.7	115.4	267.3	157.2	NS	NS
CAA3	**18**	50.8	20.6	2.2	52.7	34.2	154.9	9.3	BDL	93.4	308.5	159.2	1.2	9.0
CAA3	**28**	26.8	11.8	2.1	32.3	BDL	104.0	5.2	BDL	99.3	204.9	79.2	1.1	8.7
CAA3	**40**	12.1	16.1	0.8	31.1	BDL	304.2	2.2	BDL	81.7	178.1	52.2	1.9	13.9
CAA3	**101**	66.3	6.5	3.8	15.2	87.5	2212.4	13.0	BDL	74.0	93.2	145.6	NS	NS
CAA3	**150**	49.8	BDL	2.3	10.7	55.7	1377.7	10.6	BDL	74.7	59.5	134.5	NS	NS
CAA3	**201**	56.2	7.2	3.4	13.3	86.0	3529.6	12.7	13.6	78.2	64.3	186.6	NS	NS
CAA3	**300**	8.9	BDL	0.5	5.9	BDL	258.3	1.7	BDL	40.0	37.8	147.4	NS	NS
CAA3	**401**	28.5	BDL	0.9	8.3	BDL	662.1	5.4	BDL	46.1	52.8	176.2	NS	NS
CAA3	**604**	63.1	BDL	2.3	10.3	62.6	623.2	10.7	BDL	52.4	33.3	114.0	NS	NS
CAA4	**9**	39.5	6.9	1.9	51.3	42.0	288.9	8.9	BDL	83.5	231.4	267.4	1.5	12.4
CAA4	**34**	11.1	13.6	0.8	39.5	BDL	139.8	2.0	BDL	82.7	183.5	199.1	1.8	15.8
CAA4	**47**	8.4	42.7	0.6	73.0	BDL	135.1	1.6	BDL	112.5	374.8	58.4	1.2	10.8
CAA4	**150**	81.6	5.6	2.9	11.2	81.3	1671.2	16.0	BDL	65.3	72.3	154.9	0.5	2.7
CAA5	**12**	42.7	6.5	1.0	61.5	39.3	164.4	9.5	BDL	84.4	262.2	122.9	1.1	8.5
CAA5	**20**	40.4	7.2	2.6	58.5	BDL	154.0	8.1	BDL	90.9	164.2	122.3	1.7	12.5
CAA5	**35**	4.0	2.7	0.6	20.4	BDL	36.3	0.9	BDL	65.8	177.3	8.6	0.3	2.2
CAA5	**101**	177.4	BDL	5.3	12.8	173.3	1569.2	34.2	BDL	105.7	132.1	335.2	0.2	2.0
CAA5	**221**	238.3	6.6	4.1	20.6	212.7	2278.5	47.1	16.9	144.4	176.3	346.4	0.5	2.9
CAA6	**10**	59.9	9.6	3.1	47.8	66.0	172.7	11.4	BDL	72.5	293.2	537.0	1.6	19.2
CAA6	**32**	38.6	96.2	12.5	74.4	46.9	276.5	7.5	32.0	130.2	900.8	276.7	3.3	27.8
CAA6	**75**	62.6	22.9	2.1	20.3	68.0	304.3	11.7	BDL	74.7	204.0	163.9	1.4	11.2
CAA6	**151**	229.4	7.4	6.0	22.3	245.7	678.8	42.8	BDL	130.0	175.1	451.4	0.3	2.6

Station	**Depth (m)**	Al (nM)	Cd (pM)	Pb (pM)	P (nM)	V (pM)	Mn (pM)	Fe (nM)	Co (pM)	Cu (pM)	Zn (pM)	Ba (pM)	PON (µM)	POC (µM)
CAA6	**242**	395.3	7.7	8.6	19.9	442.7	1091.1	79.0	22.9	172.2	405.2	835.0	0.4	3.4
CAA7	**10**	38.0	9.2	3.3	79.4	37.0	378.7	8.5	BDL	73.1	237.0	479.2	1.0	7.9
CAA7	**76**	85.4	12.5	4.2	14.4	79.1	2102.4	17.5	BDL	63.7	112.7	161.0	0.2	2.1
CAA7	**121**	92.5	9.1	3.2	13.5	82.4	2591.2	17.2	BDL	62.2	94.2	243.8	0.2	1.9
CAA7	**161**	153.1	6.9	5.8	16.7	146.7	4540.1	28.8	BDL	73.4	100.8	339.0	0.1	1.5
CAA7	**191**	234.7	5.3	5.1	14.5	223.1	4035.5	51.5	22.4	83.1	158.2	297.8	0.3	1.9
CAA8	**10**	30.4	1.1	1.5	16.4	29.1	743.5	5.3	4.4	64.1	97.7	577.9	0.4	2.9
CAA8	**15**	9.5	0.8	0.0	8.1	BDL	529.9	1.4	BDL	51.1	49.1	11.9	0.3	2.2
CAA8	**45**	10.6	3.0	0.5	16.4	15.2	252.5	1.7	BDL	64.1	56.5	30.0	0.4	3.2
CAA8	**90**	8.3	1.4	0.4	3.5	16.1	545.3	1.7	2.9	31.4	15.3	68.3	0.2	1.4
CAA8	**120**	13.1	2.6	0.9	4.2	23.1	862.5	2.6	BDL	40.8	1.2	96.7	0.1	0.9
CAA8	**150**	19.5	2.8	0.8	3.3	32.0	1064.4	3.6	5.0	36.3	27.6	116.3	0.1	1.0
CAA8	**200**	23.7	0.8	0.2	2.4	25.2	842.8	4.2	3.6	33.1	7.6	84.3	0.1	1.1
CAA8	**250**	31.7	1.6	0.7	3.4	31.0	954.7	5.5	4.2	30.0	18.9	104.8	0.3	1.0
CAA8	**350**	34.5	0.5	0.3	2.5	31.0	751.0	5.4	3.7	27.3	25.4	69.1	0.4	0.8
CAA8	**450**	47.9	0.9	0.3	3.7	36.9	598.5	6.5	4.4	28.8	11.0	77.1	0.2	0.8
CAA9	**11**	18.7	1.3	0.2	12.2	18.4	167.5	2.7	BDL	32.7	50.7	4.6	NS	NS
CAA9	**70**	62.4	3.3	0.5	8.9	63.8	586.7	9.8	3.8	53.7	61.7	6.0	NS	NS
CAA9	**90**	78.6	4.2	0.5	9.3	76.4	711.1	12.1	4.6	60.3	97.4	46.4	NS	NS
CAA9	**121**	87.4	2.8	1.2	7.5	85.5	782.8	13.4	4.5	52.8	91.5	11.8	NS	NS
CAA9	**150**	107.2	1.3	1.6	5.0	84.3	696.1	13.3	4.7	50.4	94.8	106.7	NS	NS
CAA9	**200**	157.2	3.8	1.7	10.0	136.6	917.3	23.4	7.8	71.0	90.0	117.2	NS	NS
CAA9	**250**	225.2	3.2	2.7	6.8	113.5	770.9	18.2	6.8	58.8	110.8	90.9	NS	NS

Table SI4: Full-depth dataset of particulate trace metals, particulate phosphorus, PON and POC in the Canada Basin. Note the units are nM for Al, P and Fe; µM for PON and POC. NS denotes not sampled; BDL denotes below detection limit.

Station	**Depth (m)**	Al (nM)	Cd (pM)	Pb (pM)	P (nM)	V (pM)	Mn (pM)	Fe (nM)	Co (pM)	Cu (pM)	Zn (pM)	Ba (pM)	PON (µM)	POC (µM)
CB1	**11**	99.1	1.5	4.0	25.3	141.9	2151.1	16.6	14.0	89.8	76.6	104.0	0.4	2.8
CB1	**14**	5.3	0.9	2.1	14.7	6.1	59.5	0.4	BDL	39.2	156.6	BDL	0.1	2.0
CB1	**43**	6.3	3.2	BDL	22.3	7.9	88.9	0.9	2.7	65.4	117.6	28.7	0.4	3.3
CB1	**60**	9.3	1.5	0.6	11.6	19.6	546.3	1.5	4.1	50.2	45.3	50.9	NS	NS
CB1	**75**	19.8	2.0	2.2	10.7	39.0	862.5	4.0	8.3	55.3	169.9	135.3	0.6	2.0
CB1	**150**	37.3	2.8	1.5	9.1	57.7	1070.6	6.1	8.1	57.7	25.9	160.9	0.2	0.6
CB1	**200**	18.1	0.4	0.7	3.1	29.3	446.4	2.8	3.6	28.2	46.5	63.7	BDL	0.8
CB1	**251**	43.8	2.3	2.9	7.6	77.4	1091.3	9.2	7.2	47.9	132.2	151.4	0.1	0.9
CB1	**300**	52.8	1.8	4.2	6.5	76.2	984.3	8.3	6.4	40.8	70.8	146.1	0.1	0.9
CB1	**350**	42.4	1.2	1.8	5.2	62.6	785.4	6.6	5.5	37.0	39.1	91.4	BDL	1.4
CB1	**400**	54.8	0.9	1.4	5.2	76.0	667.8	9.1	6.5	36.0	28.2	102.0	0.9	1.8
CB2	**10**	6.8	0.8	1.0	13.8	16.5	317.1	0.9	3.0	86.0	19.0	19.6	0.1	2.5
CB2	**25**	2.0	1.5	2.2	10.0	9.3	285.1	0.3	3.7	56.0	10.7	19.3	0.1	1.4
CB2	**59**	1.4	3.2	BDL	14.1	9.4	144.2	0.5	3.9	73.0	39.7	24.4	0.3	2.7
CB2	**65**	2.2	1.7	7.9	6.3	9.5	454.4	0.3	9.6	462.3	1508.5	71.0	0.2	1.9
CB2	**140**	4.6	2.1	0.7	5.2	40.2	2868.9	0.9	39.6	56.8	23.2	231.1	0.1	0.8
CB2	**200**	10.7	0.9	1.4	5.6	32.4	1851.9	1.7	32.2	62.5	16.1	150.8	0.1	0.7
CB2	**400**	19.7	BDL	0.9	4.6	38.9	982.2	2.7	15.6	28.6	11.1	85.3	BDL	0.6
CB2	**800**	39.6	BDL	1.0	2.4	61.0	878.8	4.8	6.3	16.0	423.3	49.5	BDL	0.7
CB2	**1200**	63.7	BDL	1.7	3.6	83.9	1052.5	7.7	8.6	19.4	26.6	85.4	BDL	0.7
CB3	**10**	4.8	1.9	1.7	13.7	14.4	674.1	0.8	5.0	56.2	70.9	10.4	0.2	2.3
CB3	**25**	0.9	BDL	BDL	5.9	11.3	853.3	0.2	6.8	59.9	33.9	BDL	0.1	2.0
CB3	**58**	2.5	2.2	BDL	11.0	9.8	233.4	0.5	3.1	52.1	26.7	5.7	0.2	1.6
CB3	**180**	14.7	3.2	1.5	7.2	76.3	4841.5	2.6	70.1	77.0	26.3	233.5	BDL	0.7
CB3	**200**	8.4	1.8	1.5	5.9	64.7	5127.2	2.4	60.3	79.6	28.7	195.2	0.1	0.8
CB3	**480**	7.5	BDL	BDL	3.7	18.6	957.3	1.1	15.2	24.0	15.3	39.9	NS	NS
CB3	**800**	7.0	BDL	0.9	2.5	15.8	840.5	1.1	13.7	17.7	2.0	29.4	BDL	1.8
CB3	**1400**	5.2	BDL	BDL	2.8	11.3	363.7	0.9	6.8	11.5	7.4	6.8	BDL	1.1
CB3	**2000**	8.4	BDL	BDL	2.5	15.5	444.9	1.2	7.8	13.3	6.9	11.3	0.0	0.5
CB3	**2500**	8.4	BDL	BDL	3.3	14.0	378.2	1.1	6.3	11.4	0.3	BDL	0.2	0.5
CB3	**3500**	10.5	BDL	0.6	2.5	17.9	379.0	1.4	4.4	10.2	487.5	3.4	BDL	0.5
CB4	**10**	8.5	BDL	BDL	9.8	9.1	104.4	1.4	BDL	60.5	32.2	12.2	0.4	1.3
CB4	**25**	2.4	0.6	0.5	9.3	8.3	272.8	0.3	3.0	78.7	840.1	BDL	0.5	1.5
CB4	**71**	1.3	1.4	BDL	13.5	9.2	76.1	0.2	BDL	49.2	16.8	48.7	0.2	1.2
CB4	**150**	7.7	1.4	0.8	6.4	25.5	1636.9	1.3	30.8	52.9	8.7	187.4	0.1	0.7

Station	**Depth (m)**	Al (nM)	Cd (pM)	Pb (pM)	P (nM)	V (pM)	Mn (pM)	Fe (nM)	Co (pM)	Cu (pM)	Zn (pM)	Ba (pM)	PON (µM)	POC (µM)
CB4	**220**	8.1	1.1	1.2	4.4	39.7	2550.3	1.5	37.6	58.4	24.5	162.1	0.3	1.2
CB4	**500**	18.9	BDL	1.0	5.8	38.7	1153.7	3.1	15.4	29.1	43.2	77.9	NS	NS
CB4	**800**	17.2	BDL	1.3	3.4	42.0	1012.7	3.7	10.2	20.8	17.7	43.8	BDL	0.9
CB4	**1401**	17.7	BDL	0.8	3.5	31.4	679.6	2.7	9.3	15.5	7.2	35.3	0.2	0.8
CB4	**2000**	14.1	BDL	1.3	3.1	24.3	483.0	2.1	7.1	13.5	1.9	16.7	0.0	0.4
CB4	**2500**	16.4	BDL	0.6	2.1	24.9	537.2	2.4	8.5	13.2	7.6	19.3	0.1	0.3
CB4	**3499**	16.2	BDL	1.0	3.0	30.4	1488.5	2.5	11.9	17.8	78.3	6.1	0.1	0.3

Table SI5. Cell sizes as length of apical and pervalvar axes of the three most dominant species *Pseudo-nitzschia* cf. *delicatissima, Fragilariopsis* cf. *cylindrus* and *Chaetoceros socialis* based on representative cell measurements from light microscopy based images (n≥30; Axiovision software). Surface area and volume were calculated based on equations presented by Hillebrand et al, (1999). Data source: Hoppe et al. (under review a and b).

Species	Length apical axis (µm)	Length pervalvar axis (µm)	Surface area (μm^2)	Volume (μm^3)
Pseudo-nitzschia cf. *delicatissima*	45.0±10.0	2.5±0.5	361.4±102.3	223.9±83.9
Fragillariopsis cf. *cylindrus*	6.5±1.5	2.5±0.5	56.5±17.2	28.7±13.3
Chaetoceros socialis	8.0±2.0	6.0±1.5	232.1±60.9	270.1±99.6

Table SI6. Chl *a* concentrations, as well as composition of phytoplankton assemblages characterized by the proportion of the >5 µm size-fraction to total Chl *a*, and C-normalized picoplankton counts (*n*=3; mean ± SD). Data source: Hoppe et al. (under review a and b).

Exp.	Treatment	Chl *a* ($\mu g\ L^{-1}$)	Chl *a*>5 µm (% of total)	Picoplankton [cells $(ng\ POC)^{-1}$]
1	LL LC	6.1±0.5	37±4	730±71
	LL HC	5.9±0.2	32±2	825±108
	HL LC	11.5±0.7	75±3	249±55
	HL HC	9.3±1.0	68±3	257±48
2	LL LC	12.4±1.9	80±5	307±70
	LL HC	12.9±1.2	79±6	281±75
	HL LC	13.6±2.8	84±5	269±89
	HL HC	11.7±1.6	80±5	338±72